Politecnico di Torino

Politecnico di Torino

Master of Science in Petroleum and Mining Engineering
Academic year 2021/2023
Graduation Session November 2023

Well testing for gas reservoirs

State of the art

Supervisors:
Dario Viberti
Eloisa Salina Borello

Candidate:
Agnes Aguilar Mancilla

Abstract

As natural gas is currently playing an important role in the growing energy demand and for the support of the energy transition due to its lower carbon emissions in comparison to other fossil fuels, ensuring the gas production implies to use all the methods available for reservoir evaluation. Pressure transient analysis (PTA) is used throughout the productive life of a reservoir and provides valuable information regarding the reservoir such as flow capacity, reservoir pressure, reservoir size, and wellbore conditions. The well produces at a constant flow rate and the pressure response is recorded. Pressure transient tests can be analyzed and interpreted by using analytical methods such as the semilog approach, the log-log type curves, and the pressure derivative method, which can be sufficient to evaluate the gas reservoir performance.

Contents

List of Figures

List of Tables

Chapter 1. Introduction

1.1 General

Pressure Transient Analysis (PTA) is a well-established technique in petroleum industry for reservoir characterization and well condition assessment. It plays a key role in evaluating exploration and development prospects. It is performed by measuring the bottom-hole pressure while the well is producing at a constant rate (Escobar, 2017). Pressure transient Analysis uses the PVT properties of the fluid and the dynamic reservoir data, including production rates and pressure responses, to (Satter & Iqbal, 2016):

- determine the properties of the reservoir such as: permeability, formation transmissibility, and storativity;
- to estimate the average reservoir pressure;
- to evaluate the presence of boundaries such as sealing faults;
- to understand the conditions near the wellbore drainage area due to skin effects;
- and to predict the reservoir performance over time and deliverability of gas wells.

Conventionally, analytical PTA has been used to determine reservoir properties through well test interpretation by using analytical tools and mathematical models to match the flow rates history and flowing pressure data from buildup (Jackson, Banerjee, & Thambynayagam, 2003).

1.2 Objective of Study

The aim of this work is to study the different analytical methods and interpretation models that are used to perform the analysis of pressure transient tests of gas wells considering the characteristics of gas flow with mathematical expressions. The work is limited to:

- Dry gas and gas condensate reservoirs.
- Homogeneous, heterogeneous, and naturally fractured reservoir models.

- Vertical wells with full or partial penetration.

1.3 Organization of the work

The present work is organized into five chapters. Chapter 1 introduces the topic, the objective, and the limitations for the elaboration of this work. Chapter 2 describes the behavior of gas reservoirs, including the properties of natural gas and the properties of the reservoir rock. Chapter 3 is dedicated to explaining the fundamental concepts and the analytical methods used for the analysis of a pressure transient test. Chapter 4 describes the different interpretation models that raise as the transient response moves further into the reservoir. Finally, Chapter 5 draws some conclusions.

Chapter 2. Behavior of Gas Reservoirs

2.1 Differences between reservoir liquids and gases

The classification of a hydrocarbon system, either an oil or gas reservoir, is based on the consideration of the conditions such as pressure and temperature under which these different phases exist initially in the reservoir, as well as the chemical composition of the mixtures of hydrocarbons, and the conditions of pressure and temperature under which these fluids are produced at surface. This classification can be expressed in phase diagrams of pressure and temperature (p-T diagram) to identify the type of hydrocarbon system as seen on Figure 1. (Ahmed, 2019)

The phase diagram is composed of key points that helps to define the behavior of the hydrocarbon system. The phase envelope is the region where liquid and gas coexist in equilibrium, it is enclosed by the bubble-point curve and the dew-point curve. At the bubble point, p_b, the first bubble of gas forms in the system; hence, the bubble-point curve separates the liquid region from the two-phase envelope. At the dew point, p_d, the first drop of liquid forms; the dew-point curve then separates the gaseous phase from the two-phase region. At the critical point, p_c and T_c, the properties of gas and liquid phases are equal. The quality lines inside the envelope indicate the volume fraction of liquid at given pressure and temperature conditions. The cricondenbar and cricondentherm are the maximum pressure and temperature, respectively, where two phases can coexist. In other words, no gas can be formed above the cricondenbar (the maximum pressure regardless of temperature), and no liquid can be formed above the cricondentherm (the maximum temperature regardless of pressure). (Mohamed Mansour, El Aily, & Eldin Mohamed Desouky, 2019)

According to the location of the point on the phase diagram that represents the original pressure and temperature of the reservoir, the hydrocarbon system will be identified as an oil or a gas reservoir.

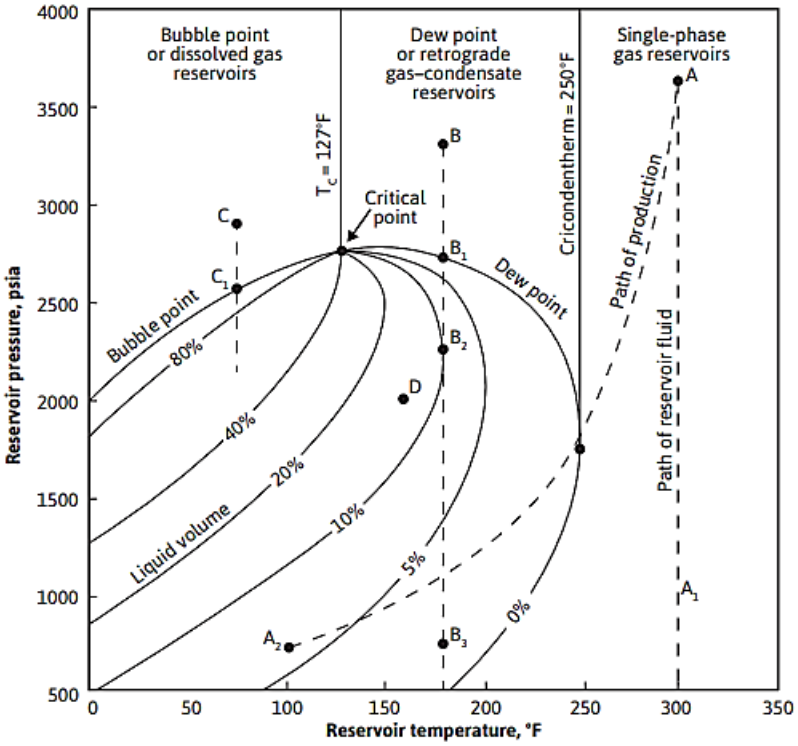

Figure 1: *p-T diagram of reservoir fluids.*

Note. Adapted from *Pressure-temperature phase diagram of a reservoir fluid* (p. 10), by Terry & Rogers, 2015, Pearson Education.

2.1.1 Oil reservoirs

Oil reservoirs fall in the region where the temperature, T, of the reservoir is lower than the critical temperature, T_c, of the hydrocarbon fluid. Depending on their initial reservoir pressure, p_i, oil reservoirs are subdivided into:

- Undersaturated reservoirs
- Saturated reservoirs
- Gas-cap reservoirs

If the initial pressure is above the bubble-point pressure of the fluid, as expressed by point C on Figure 1, the oil reservoir is undersaturated (Ahmed, 2007). Initially the oil contains natural gas in solution, and as the reservoir pressure reduces to reach the bubble-point pressure the oil

dissolves this gas (Terry & Rogers, 2015). If the reservoir is initially at the bubble-point pressure pb, then the oil reservoir is saturated, as shown by point C_1 on Figure 1. At this pressure the oil holds all the dissolved gas. Further reduction in pressure will result in gas released in the reservoir and will create a free phase of gas. Consequently, oil shrinkage will be observed (McCain Jr, 1990). An oil reservoir with a gas cap is known as a two-phase reservoir since the initial pressure, p_i, is below the bubble-point pressure, p_b, of the fluid (Ahmed, 2019).

Ahmed (2007) and Tewari et al. (2019) state that oil reservoirs can contain crude oil of low or high shrinkage. They are classified depending on their chemical composition, physical characteristics, physical properties such as API gravity, GOR, and p-T diagrams. For instance, an ordinary black oil is composed of mainly heavy hydrocarbons such as heptanes (C_{7+}), and it can be considered as a low-shrinkage oil. The quality lines that represent the liquid volume fraction are evenly spaced in the envelope, as indicated by the path $\overline{EF}$ on Figure 2. The oil at the bubble-point starts shrinking isothermally as the pressure goes below the bubble-point curve to even 50% of its liquid volume. GOR increases to values between 200 and 700 scf/STB, and the oil gravity ranges between 15° and 40° API. Volatile oils are considered as high-shrinkage oils and near-critical crude oils due to the presence of more intermediate molecules (C_{2+} to C_{6+}) than heavy molecules, and due to the small difference between the initial pressure and the bubble-point pressure. As pressure decreases below the bubble-point, a large amount of gas is liberated in the reservoir, and the oil starts shrinking immediately to even more than half of its liquid volume. A liquid fraction around 30% can be observed by the path $\overline{23}$ on Figure 3. GOR increases to such values between 2000 and 3000 scf/STB, and the oil gravity can be considered between 45° and 55° API.

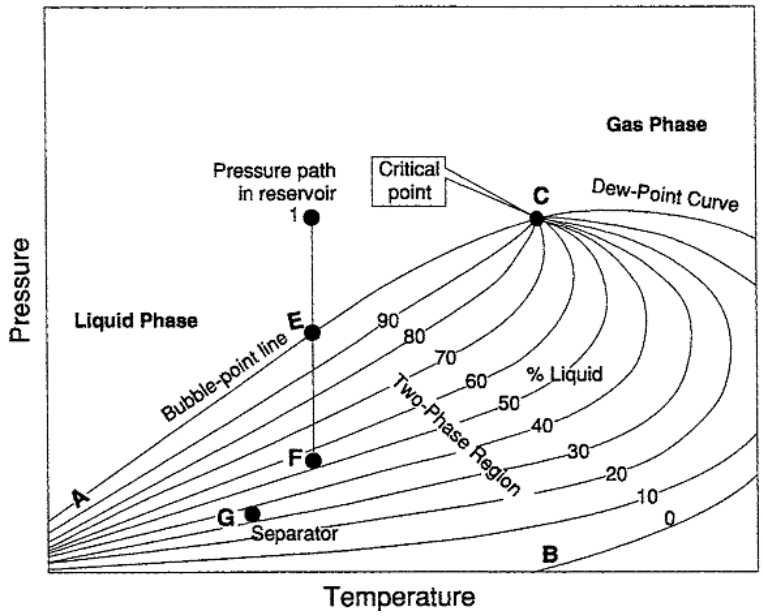

Figure 2: *p-T diagram of an ordinary black oil reservoir.*

Note. Adapted from *Typical p/T diagram for ordinary black oil* (p. 34), by Tarek Ahmed, 2007, Gulf Publishing Company.

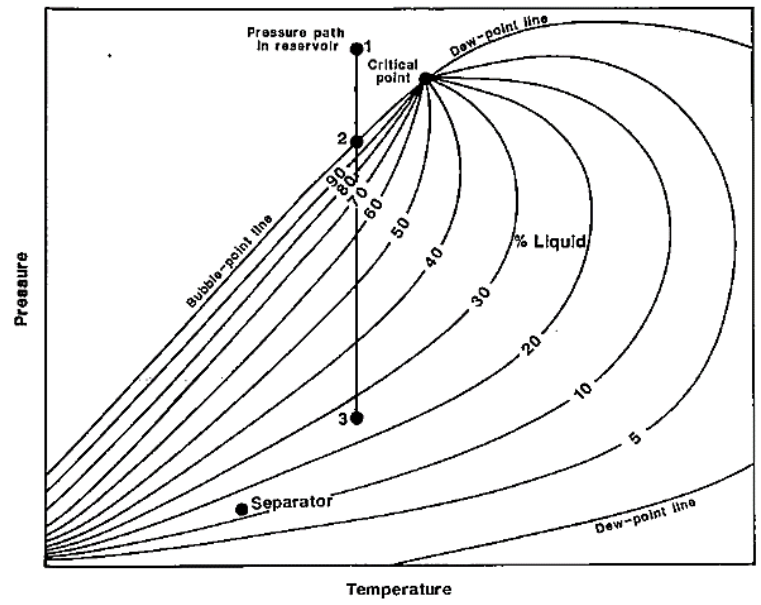

Figure 3: *p-T diagram of a volatile oil reservoir.*

Note. Adapted from *Phase diagram of a typical volatile oil of isothermal reduction of reservoir pressure,* $\overline{123}$*, and surface separator conditions* (p. 152), by William D. McCain Jr., 1990, PennWell Publishing Company.

2.1.2 Gas Reservoirs

Gas reservoirs fall in the region in which the temperature T of the reservoir is higher than the critical temperature Tc of the fluid. They are classified into:

- Dry gas reservoirs
- Wet gas reservoirs
- Condensate (retrograde gas) reservoirs

A dry gas reservoir is characterized by remaining outside the dew-point curve of the phase envelope as a single-phase fluid at reservoir conditions and through the path to reach separator conditions as shown on Figure 4. These natural gas reservoirs are composed of mainly methane (C_1) and are known as nonassociated gas reservoirs since no liquid hydrocarbons are produced at surface (Ahmed, 2019).

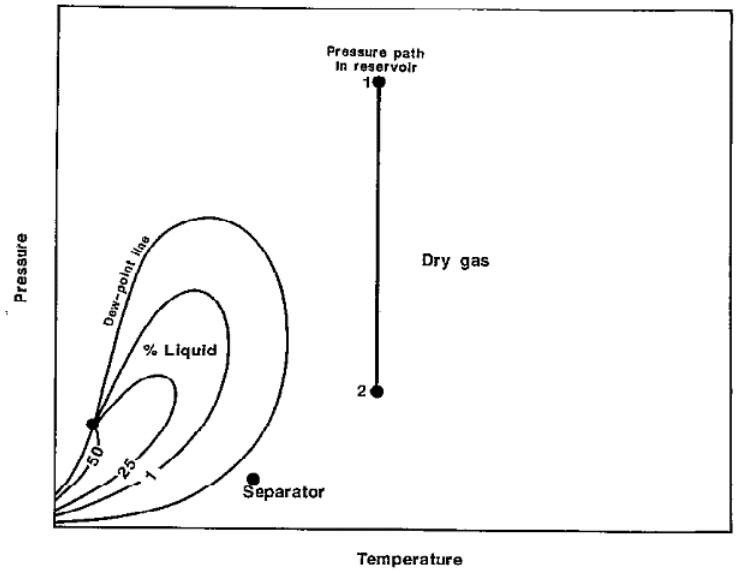

Figure 4: *p-T diagram of a dry gas reservoir.*

Note. Adapted from *Phase diagram of a typical dry gas with line of isothermal reduction of reservoir pressure,* $\overline{12}$*, and surface separator conditions* (p. 15), *by* William D. McCain Jr., 1990, PennWell Publishing Company.

Wet gas reservoirs are initially outside of the cricondentherm as a single-phase fluid at reservoir conditions. As the pressure and temperature reduces to reach the separator conditions, the fluid enters the two-phase envelope that causes the presence of hydrocarbon liquids at surface as seen on Figure 5. These reservoirs are characterized by having constant values of GOR between 60,000 and 100,000 scf/STB, and oil gravities at stock-tank conditions above 60° API (Ahmed, 2007). Wet gases are composed of light hydrocarbon molecules such as methane, ethane, propane, and butane (C_1-C_4) (Tewari, Dandekar, & Moreno Ortiz, 2019).

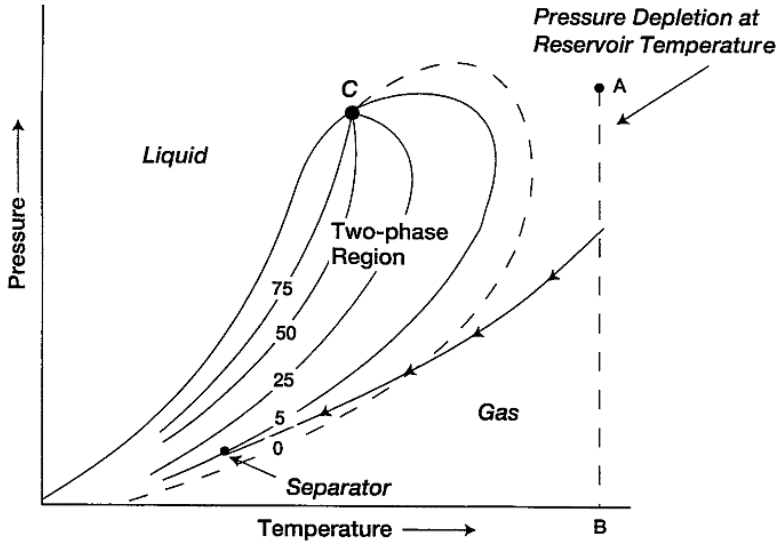

Figure 5: *p-T diagram of a wet gas reservoir.*

Note. Adapted from *Phase diagram for a wet gas* (p. 43), by Tarek Ahmed, 2007, Gulf Publishing Company.

The gas mixture of gas condensate (retrograde) reservoirs is composed of less methane than dry or wet gas reservoirs, but of heavier gases such as ethane, propane, and butane (Tewari, Dandekar, & Moreno Ortiz, 2019). Gas condensate reservoirs are characterized by having an initial temperature higher than the critical temperature, T_c, but lower than the cricondentherm. These reservoirs exist as a single vapor phase at initial conditions above the dew-point pressure (Figure 6), as the reservoir pressure reduces to the dew-point pressure, p_d, at which the first

drop of liquid forms, the heavier gases start to condense leading to a second phase formation in the reservoir (Ahmed, 2019). On Figure 6, the path from point 1 to point 2 indicates a natural condensation, in which gas and a percentage of condensates of 25 or 30% are recovered at surface. As pressure declines isothermally to point 3, a retrograde condensation is observed until reaching the maximum liquid dropout. As pressure continues decreasing to point 4, all the liquid formed re-vaporizes into the gas phase in the reservoir. These reservoirs are characterized by having condensates above 50° API and GOR between 8000 and 70,000 scf/STB, due to liquid dropout the values of GOR increase with time (Ahmed, 2007). Gas condensate reservoirs are of economic importance due to the production of condensates. During natural condensation, the production of condensates increases or is stable, whereas during retrograde condensation large volumes of condensates are not recovered at surface since the dropout of liquids takes place in the reservoir. Therefore, and injection of produced gas back into the reservoir is a solution to maintain the reservoir pressure high and increase the recovery of condensates (Schlumberger, 2006).

It should be emphasized that the initial composition of the hydrocarbon system is important for the classification of reservoir fluids. The presence of heavy components has a strong effect in determining if the hydrocarbon system is gas or liquid (Ahmed, 2019). Table 1 summarizes this information.

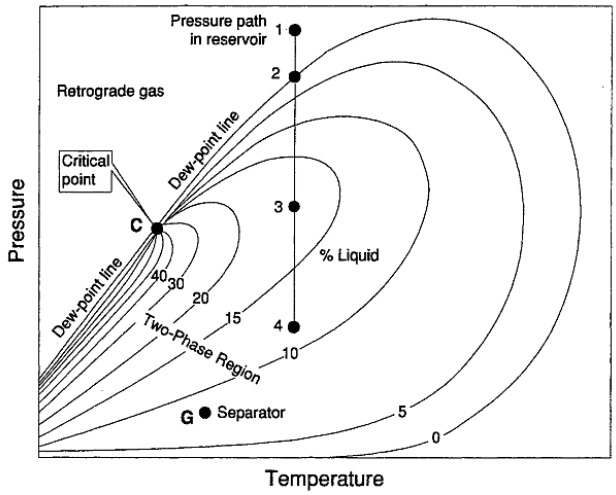

Figure 6: *p-T diagram of a condensate (retrograde) gas reservoir.*

Note. Adapted from *Typical phase diagram of a retrograde system* (p. 39) by Tarek Ahmed, 2007, Gulf Publishing Company.

Table 1: *Composition (mol% Cn) for classification of reservoir fluids.*

Note. Schlumberger (2006, p. 29)

Hydrocarbon	C_1	C_2	C_3	C_4	C_5	C_{6+}
Dry gas	88	4	4	1	1	1
Condensate	71	8	5	5	4	7
Volatile oil	60	8	5	4	3	20
Nonvolatile oil	41	3	5	5	4	42
Heavy oil	11	3	1	1	4	80
Tar/bitumen						100

2.2 Composition of Natural Gases

Natural gas has low density and viscosity values. It is a homogeneous fluid that is composed of light hydrocarbon molecules, generally lighter than heptanes (C_{7+}). However, natural gas also contains impurities such as carbon dioxide (CO_2), hydrogen sulfide (H_2S) and nitrogen (N_2) that must be removed. These impurities are called non-hydrocarbon gases (Ahmed, 2019).

Dry gas reservoirs are characterized by having more than 90 mol-% methane and fewer intermediate gases with other compounds as seen in Table 2. On the other hand, condensate gases are characterized by being composed of more intermediate gases and traces of other compounds as shown in Table 3 (Pedersen, Christensen, & Shaikh, 2014).

Table 2: *Dry gas mixture composition.*

Note. Pedersen, Christensen, & Shaikh *(2014, p. 7)*

Component	Mole Percentage
N2	0.340
CO2	0.840
C1	90.400
C2	5.199
C3	2.060
iC4	0.360
nC4	0.550
iC5	0.140
nC5	0.097
C6	0.014

Non-hydrocarbon gases such as CO_2 causes a severe impact on the environment, and it is considered an acid gas since it becomes corrosive when mixes with water generating carbonic acid. Variable CO_2 concentrations can be found in fields with clastic and carbonate formations. Sulfur is found in heavier oils and occurs in natural gas as H_2S (Tewari, Dandekar, & Moreno Ortiz, 2019). H_2S is a highly toxic and corrosive compound caused by sulfate-reducing bacteria (SRB) and formed from sulfates in aqueous environments. It contaminates fuel gas and reduces injectivity when precipitation of ferrous sulfide is deposited in injection wells (Cord-Ruwisch, 1987). H_2S affects the economic value of natural gas, since a sweet gas which by treating the H_2S content, it will have a higher economic value than a sour gas containing H_2S (Guo & Ghalambor, Natural gas engineering handbook, 2005).

Table 3: *Gas condensate mixture composition.*

Note. Adapted from Pedersen, Christensen, & Shaikh *(2014, p. 8)*

Component	Mole Percentage
N2	0.53
CO2	3.30
C1	72.98
C2	7.68
C3	4.10
iC4	0.70
nC4	1.42
iC5	0.54
nC5	0.67
C6	0.85
C7	1.33
C8	1.33
C9	0.78
C10	0.61
C11	0.42
C12	0.33
C13	0.42
C14	0.24
C15	0.30
C16	0.17
C17	0.21
C18	0.15
C19	0.15
C20+	0.80

Natural gas reserves contaminated with nitrogen have a low thermal energy content (BTU) that must be removed to be commercially exploited. This involves expensive technology for nitrogen removal. However, non-hydrocarbon gases including CO_2 and nitrogen can be an alternative to natural gas to increase the reservoir fluid saturation pressure in oil fields and for gas re-cycling in gas condensate reservoirs (Belhaj, 2016).

Water is always present in hydrocarbon reservoirs as brine or formation water with a concentration of solids such as sodium chloride, and up to 30 or 40 other ions including calcium, magnesium, potassium, barium, sulfates, iodine, and sulfur. Pressure effects are observed with gas solubility in water, as the gas pressure increases so does gas solubility. A combination of water and gas at high pressures and low temperatures forms hydrates (McCain Jr, 1990).

The physical and chemical properties of natural gas mixture can be determined from the properties of the individual pure components in the gas mixture (Lee & Wattenbarger, 1996). These properties are shown in Figure 7 and are used to develop pseudo-properties for gases.

Component	Chemical Formula	Molecular Weight (lbm/lbm-mol)	Critical Temperature (°R)	Critical Pressure (psia)	Critical Volume (ft3/lba)	Liquid Density* (lbm/ft3)	Gas Density (lbm/ft3)	Gas Viscosity (cp)
Methane	CH4	16.043	343.00	666.4	0.0988	18.710	0.04228	0.01078
Ethane	C2H6	30.070	549.59	706.5	0.0783	22.214	0.07924	0.00901
Propane	C3H8	44.097	665.73	616.0	0.0727	31.619	-	0.00788
i-Butane	C4H10	58.123	734.13	527.9	0.0714	35.104	-	0.00732
n-Butane	C4H10	58.123	765.29	550.6	0.0703	36.422	-	0.00724
i-Pentane	C5H12	72.150	828.77	490.4	0.0679	38.960	-	-
n-Pentane	C5H12	72.150	845.47	488.6	0.0675	39.360	-	-
n-Hexane	C6H14	86.177	913.27	436.9	0.0688	41.400	-	-
n-Heptane	C7H16	100.204	972.37	396.8	0.0691	42.920	-	-
n-Octane	C8H18	114.231	1023.89	360.7	0.0690	44.090	-	-
n-Nonane	C9H20	128.258	1070.35	331.8	0.0684	45.020	-	-
n-Decane	C10H22	142.285	1111.67	305.2	0.0679	45.790	-	-
Hydrogen	H2	2.109	59.36	187.5	0.5165	4.432	0.005312	0.00871
Helium	He	4.003	9.34	32.9	0.2300	7.802	0.01055	0.01927
Water	H2O	18.015	1164.85	3200.1	0.04975	62.336	-	~1.122
Carbon monoxide	CO	28.013	227.16	493.1	0.0532	50.479	0.07381	0.01725
Nitrogen	N2	28.010	239.26	507.5	0.0510	49.231	0.07382	0.01735
Oxygen	O2	31.999	278.24	731.4	0.0367	71.228	0.08432	0.02006
Hydrogen sulfide	H2S	34.08	672.35	1306.0	0.0461	49.982	0.08981	0.01240
Carbon dioxide	CO2	44.010	547.58	1071.0	0.0344	51.016	0.1160	0.01439
Air	N2+O2	28.963	238.36	546.9	0.0517	54.555	0.07632	0.01790

Figure 7: *Properties of natural gas mixture at standard conditions of 60 °F and 14.7 psi.*

Note. *Liquid densities for components that exist as liquids and for components that exist as gases at standard conditions. Adapted from *Physical properties of gases at 14.7 psia and 60 °F* (p. 2) by Lee & Wattenbarger, 1996, Society of Petroleum Engineers.

2.3 Equations of State (EOS)

2.3.1 The Ideal Gas EOS

To describe mathematically the relationship between pressure, volume, and temperature (PVT) of the gases, an equation of state should be implemented. At low pressures, such as those close to the atmospheric pressure, natural gas behaves as an ideal gas. The equation used to describe such behavior is the ideal gas law:

$$pV = nRT \quad (1)$$

Where p is absolute pressure, psia; V is volume, ft^3; n is the number of moles of gas, lbmol; R is the universal constant of gases equal to 10.73 psia·ft^3/lbmol·°R; and T is absolute temperature, °R.

The number of moles of gas can be expressed as the relationship between the weight of the gas and its molecular weight:

$$n = \frac{m}{M} \quad (2)$$

Where m is the mass of gas, lb_m; and M is the gas molecular weight, lbmol (Tiab, 2000).

2.3.2 The Real Gas EOS

At high pressures, such as those that occur in reservoirs, natural gas behaves as a nonideal gas. The application of the ideal gas law to gases at reservoir conditions gives rise to errors. Therefore, Equation 3 represents the real gas equation of state to be implemented.

$$pV = ZnRT \quad (3)$$

Where Z is the gas deviation factor in dimensionless units (Ahmed, 2019).

2.3.3 The Cubic EOS

The development of more complex and modern equations of state, such as the cubic equations of state, attempt to describe the behavior and properties of real gases at high pressures, including the condensation phenomena of pure gases as compressed isothermally, the equilibrium between vapor-liquid phases, and gas properties such as Z-factor (McCain Jr, 1990).

The Van der Waals EOS. The ideal gas equation of state is based on the assumptions that there are not forces acting between molecules and the volume of molecules is negligible. Van der Waals presented an equation of state for gases at high pressures, real gases, in which

the attractive and repulsive forces between molecules as well as the volume of the gas molecules are considered.

$$p = \frac{RT}{V_M - b} - \frac{a}{b^2} \quad (4)$$

Where p is the absolute system pressure, psia; R is the universal constant of gases equal to 10.73 psia·ft^3/lbmol·°R; T is the absolute system temperature, °R; V_m is the molar volume, ft^3/mol. The characteristic constants of the molecular properties of gases, a and b, are given by Equations 5 and 6. The constant a accounts for the intermolecular attractive forces, and the constant b for the repulsive forces and considers the volume of the molecules.

$$a = \frac{27}{64}\frac{R^2 {T_c}^2}{p_c} \quad (5)$$

$$b = \frac{1}{8}\frac{RT_c}{p_c} \quad (6)$$

Where a characteristic constant units in psia·ft^2/mol^2; and b characteristic constant with units ft/mol.

Therefore, Equation 4 can be expressed as a cubic equation of state, as indicated by Equation 7.

$${V_M}^3 - \left(b + \frac{RT}{p}\right){V_M}^2 + \left(\frac{a}{p}\right)V_M - \left(\frac{ab}{p}\right) = 0 \quad (7)$$

Equation 7 can be expressed in terms of compressibility factor Z as shown in Equation 8 and used to calculate other gas properties such as density (Ahmed, 2019).

$$Z^3 - \left(1 + \frac{bp}{RT}\right)Z^2 + \left(\frac{ap}{R^2T^2}\right)Z - \frac{abp^2}{(RT)^3} = 0 \quad (8)$$

The Soave-Redlich-Kwong EOS. This equation of state considers the effects of temperature variations of molecular attractions.

$$\left[p + \frac{a_T}{V_M(V_M + b)}\right](V_M - b) = RT \quad (9)$$

$$a_T = a_c \alpha \quad (10)$$

Where a_T is a temperature-dependent parameter and α is a temperature-dependent dimensionless parameter equal to 1 at the critical temperature T_c. The terms a_c and b are given by Equation 11 and Equation 12 (McCain Jr, 1990).

$$a_c = 0.42747 \frac{R^2 {T_c}^2}{p_c} \quad (11)$$

$$b = 0.08664 \frac{RT_c}{p_c} \quad (12)$$

When α is not at the critical temperature T_c, it can be calculated by Equation 13 which introduces the term m that considers the substance acentric factor as expressed by Equation 14.

$$\alpha = [1 + m(1 - T_r)]^2 \quad (13)$$

$$m = 0.480 + 1.574\omega - 0.176\omega^2 \quad (14)$$

Where T_r is the reduced temperature, °R; and ω is the substance acentric factor (Ahmed, 2019).

The Peng-Robinson EOS. This equation of state given by the Equation 15 presents the temperature-dependent parameter a_T with slightly different values of a_c and b from the Soave-Redlich-Kwong EOS. These terms are determined by Equation 16 and Equation 17 (McCain Jr, 1990).

$$p = \frac{RT}{V_M - b} - \frac{a_T}{V_M(V_M + b) + b(V_M - b)} \quad (15)$$

$$a_c = 0.45724 \frac{R^2 {T_c}^2}{p_c} \quad (16)$$

$$b = 0.07780\frac{RT_c}{p_c} \quad (17)$$

2.4 Properties of Natural Gases

2.4.1 Gas Deviation Factor Z

The gas deviation factor or gas compressibility factor, Z, is introduced as a correction factor to measure the deviation of the real gas from the ideal gas. This Z-factor corrects the equation of state of the ideal gas to explain the behavior of real gases. It depends on pressure, temperature, and gas composition, and is obtained from lab measurements or correlations. Z-factor is a dimensionless parameter and taken as equal to 1 at standard conditions ($T = 60$ °F and $p = 14.7$ psia). It is defined as the ratio of the real volume that a gas occupies at a given pressure and temperature to the ideal volume occupied at the same conditions as if it behaves as an ideal gas (Wang & Economides, 2009).

$$Z = \frac{V_{real\ @\ p,T}}{V_{ideal\ @\ p,T}} \quad (18)$$

Principle of Corresponding States. Substances are at corresponding states if they have the same behavior at the same reduced states. Z-factor is a gas property that is based on this law. Thus, for different gases, the real gas and the ideal gas law will show the same deviation at the same reduced pressure and reduced temperature (Tiab, 2000).

For pure compounds, the properties of liquid-vapor phases are alike at the critical temperature and critical pressure. Their reduced states are:

$$p_r = \frac{p}{p_c} \quad (19)$$

$$T_r = \frac{T}{T_c} \quad (20)$$

Where P_r is the reduced pressure, dimensionless; P is the system pressure, psia; P_c is the critical pressure, psia; T_r is the reduced temperature, dimensionless; T is the system temperature, °R;

and T_c is the critical temperature, R°. For a gas mixture, the pseudo-critical temperature and pseudo-critical pressure are not the true critical properties of the gas mixture due to their paraffinic hydrocarbons. Therefore, the properties of the liquid-vapor phase are not alike (Lee & Wattenbarger, 1996).

Pseudocritical properties are determined from the molal average and critical properties of the gas mixture compounds.

$$p_{pc} = \sum y_i p_{ci} \quad (21)$$

$$T_{pc} = \sum y_i T_{ci} \quad (22)$$

Where p_{pc} is the pseudocritical pressure of the gas mixture, psia; T_{pc} is the pseudocritical temperature of the gas mixture, °R; p_{ci} is the critical pressure of component i in the gas mixture, psia; T_{ci} is the critical temperature of component i in the gas mixture, °R; y_i is the mole fraction of component i in the gas mixture (Guo & Ghalambor, 2005).

These pseudocritical properties are used to compute the pseudoreduced pressure and pseudoreduced temperature of gas mixtures and to determine the gas compressibility factor.

$$p_{pr} = \frac{p}{p_{pc}} \quad (23)$$

$$T_{pr} = \frac{T}{T_{pc}} \quad (24)$$

Where p_{pr} and T_{pr} are pseudoreduced pressure and pseudoreduced temperature, respectively, given in dimensionless units (Tiab, 2000).

Figure 8 shows the gas deviation factor chart presented by Standing and Katz based on the pseudoreduced properties and applied to gases with a low quantity of nonhydrocarbons (Ahmed, 2019).

If the gas mixture contains non-hydrocarbon gases, the Wichert and Aziz correlation can be applied to determine the Z-factor by using the Standing and Katz chart (Figure 8). Equations 25 and 26 present the correction for the pseudo-critical properties of the gas, and the ξ term is obtained from Figure 9 as a function of the concentrations of H_2S and CO_2.

$$T'_{pc} = T_{pc} - \xi \quad (25)$$

$$p'_{pc} = \frac{p_{pc}T'_{pc}}{T_{pc} + \gamma_{H_2S}(1 - \gamma_{H_2S})\xi} \quad (26)$$

Where T'_{pc} is the corrected pseudocritical temperature for H_2S and CO_2; p'_{pc} is the corrected pseudocritical pressure for H_2S and CO_2; γ_{H_2S} is the mole fraction of hydrogen sulfide; and the term ξ represents the correction factor for H_2S and CO_2 concentrations (Wang & Economides, 2009).

Further corrections (Lee & Wattenbarger, 1996) are presented for water vapor and nitrogen impurities:

$$T_{pc,cor} = -246.1\gamma_{N_2} + 400.0\gamma_{H_2O} \quad (27)$$

$$p_{pc,cor} = -162.0\gamma_{N_2} + 1270.0\gamma_{H_2O} \quad (28)$$

The final correlations for the corrected pseudocritical properties are then indicated by equations 29 and 30.

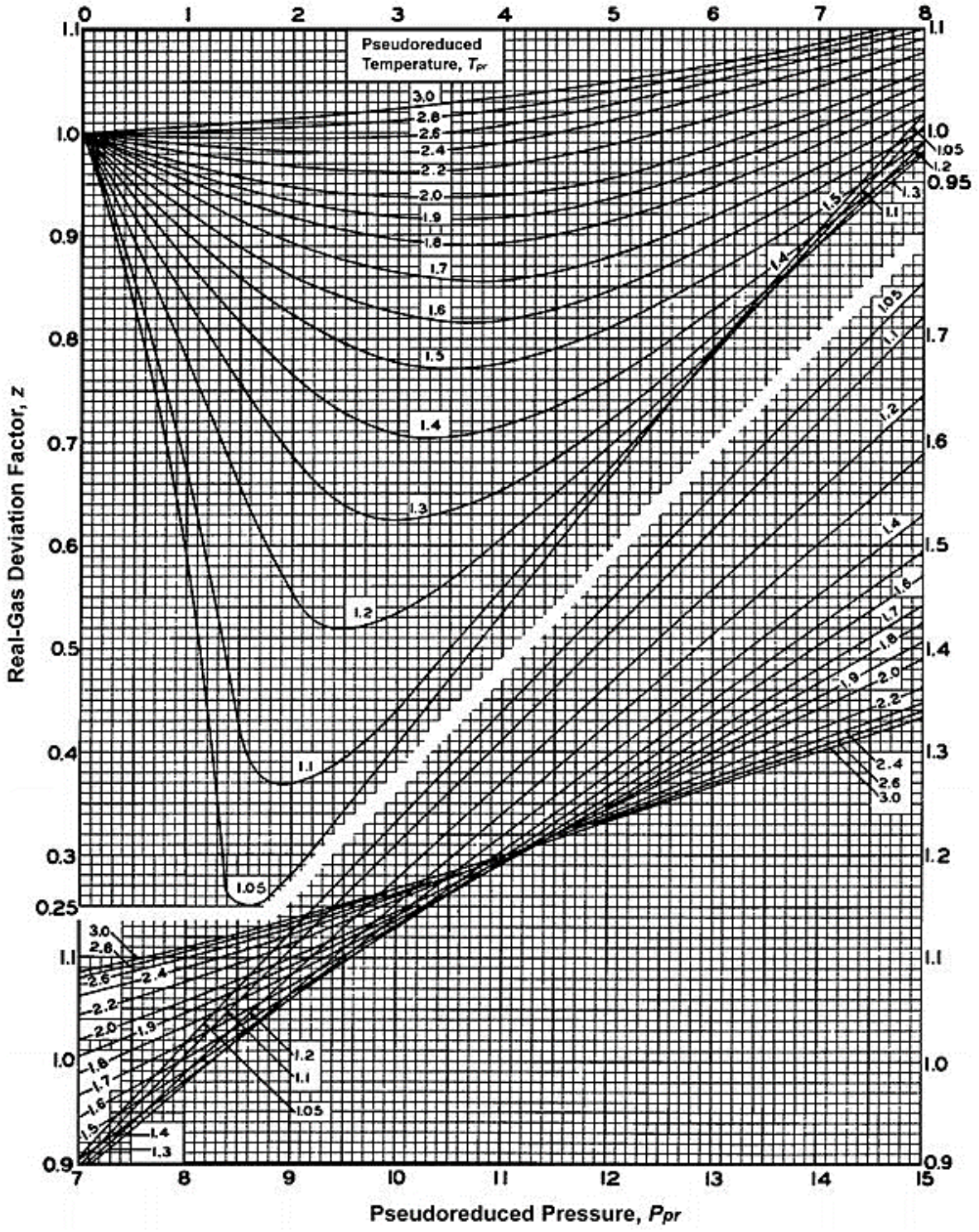

Figure 8: *Gas deviation factor chart by Standing and Katz.*

Note. Adapted from *Standing and Katz's compressibility factor chart* by Journal of Petroleum Exploration and Petroleum Technology, 2015, Springer (https://link.springer.com/article/10.1007/s13202-015-0209-3/figures/2). CC by 4.0

$$T''_{pc} = \frac{T'_{pc} - (227.2)\gamma_{N_2} - (1165)\gamma_{H_2O}}{\left(1 - \gamma_{N_2} - \gamma_{H_2O}\right)} + T_{pc,cor} \quad (29)$$

$$p''_{pc} = \frac{p'_{pc} - (493.1)\gamma_{N_2} - (3200)\gamma_{H_2O}}{\left(1 - \gamma_{N_2} - \gamma_{H_2O}\right)} + p_{pc,cor} \quad (30)$$

Where $T_{pc,cor}$ is the temperature correction for H_2O and N_2 content; $p_{pc,cor}$ is the pressure correction for H_2O and N_2 content; T''_{pc} is the corrected pseudocritical temperature; p''_{pc} is the corrected pseudocritical pressure; T'_{pc} is the corrected pseudocritical temperature for H_2S and CO_2; p'_{pc} is the corrected pseudocritical pressure for H_2S and CO_2; γ_{N_2} is the mole fraction of nitrogen gas; and γ_{H_2O} is the mole fraction of water vapor.

2.4.2 Apparent Molecular Weight

A gas mixture is composed of diverse gas compounds with different molecular weights. Therefore, an apparent molecular weight is to be calculated for the mixture. This is given by the sum of the product between the mole fraction of the ith component in the gas mixture and the molecular weight of that component as expressed by Equation 31.

$$M_a = \sum_{i=1} y_i M_i \quad (31)$$

Where M_a is the apparent molecular weight of the gas mixture, lb/lbmol (Lee & Wattenbarger, 1996).

2.4.3 Gas Specific Gravity

Gas specific gravity is given by the ratio of the densities of the gas and air measured at the same conditions of temperature and pressure. These conditions are standard conditions of $p_{sc} = 14.7$ psia and $T_{sc} = 60$ °F.

$$\gamma_g = \frac{\rho_g}{\rho_{air}} \quad (32)$$

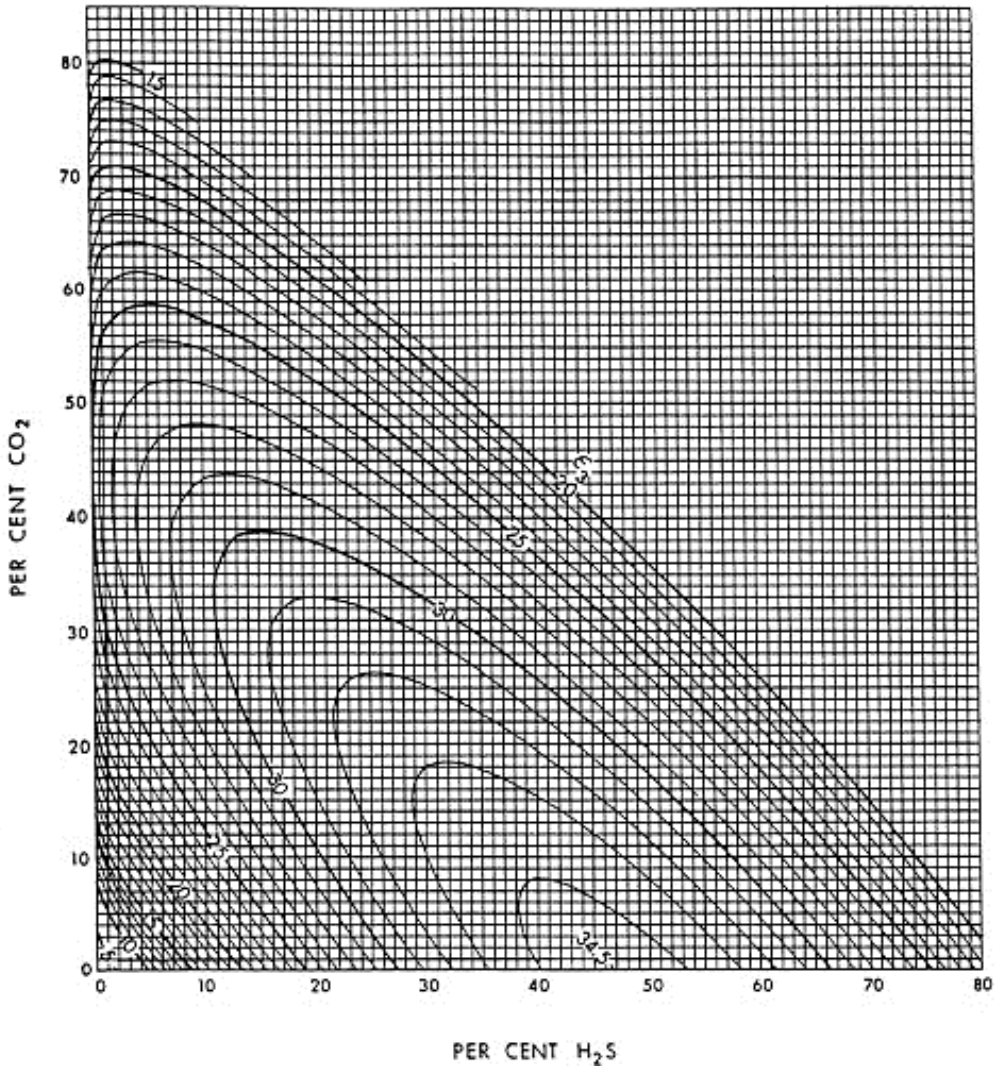

Figure 9: *ξ factor adjustments for pseudocritical properties.*

Note. Adapted from *Pseudocritical property corrections for H_2S and CO_2* (p. 8) by J. Lee & R. A. Wattenbarger, 1996, Society of Petroleum Engineers.

At standard conditions gases behave as ideal gases. Thus, the equation of state for ideal gases can be implemented and expressed as in Equation 33.

$$\gamma_g = \frac{\frac{p_{sc}M_a}{RT_{sc}}}{\frac{p_{sc}M_{air}}{RT_{sc}}} = \frac{M_a}{M_{air}} = \frac{M_a}{28.96} \qquad (33)$$

Where γ_g is the specific gravity of the gas (the specific gravity of air is equal to 1); ρ_g and ρ_{air} are the gas and air densities measured at standard conditions; M_a is the apparent molecular weight of the gas mixture; and M_{air} is the apparent molecular weight of the air equal to 28.96 lb/lbmol (Ahmed, 2019).

2.4.4 Gas Density

The density of a gas mixture can be expressed in terms of ideal gases and the apparent molecular weight of the mixture.

$$\rho_g = \frac{pM_a}{RT} \quad (34)$$

Gas density can also be calculated in terms of real gases and specific gravity.

$$\rho_g = \frac{pM_a}{ZRT} \quad (35)$$

$$\rho_g = \frac{p(M_{air}\gamma_g)}{ZRT} \quad (36)$$

Where ρ_g is the gas density, lb/ft^3; p is the absolute pressure, psia; and T is the absolute temperature, °R (Wang & Economides, 2009). Figure 10 shows how the density of gas increases with pressure (El-Banbi, Alzahabi, & El-Maraghi, 2018).

2.4.5 Gas Compressibility

Gas compressibility, also known as isothermal gas compressibility, is defined as the change of volume per unit volume as pressure is changed isothermally.

$$c_g = -\frac{1}{V}\left(\frac{\partial V}{\partial p}\right)_T \quad (37)$$

Where c_g is the isothermal coefficient of gas compressibility, 1/psi (Tiab, 2000).

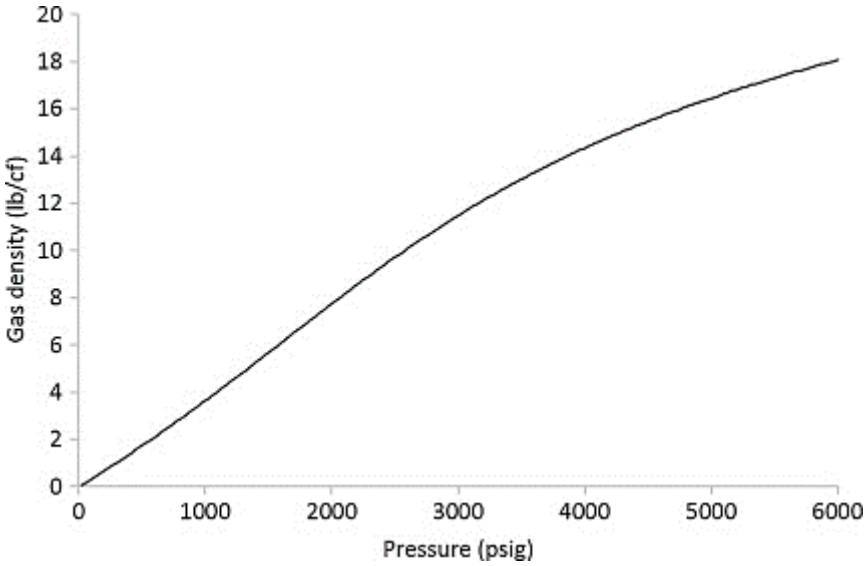

Figure 10: *Gas density as a function of pressure.*

Note. Adapted from *Gas density* by A. El-Banbi, A. Alzahabi & A. El-Maraghi, 2018, ScienceDirect (https://www.sciencedirect.com/topics/engineering/gas-density)

Gas compressibility can also be expressed in terms of Z-factor by implementing the real gas EOS.

$$c_g = \frac{1}{p} - \frac{1}{Z}\left(\frac{\partial Z}{\partial p}\right)_T \quad (38)$$

For ideal gases $Z = 1$ and $\left(\frac{\partial Z}{\partial p}\right) = 0$. Therefore, gas compressibility is inversely proportional to pressure (Ahmed, 2019).

$$c_g = \frac{1}{p} \quad (39)$$

Gas compressibility is an important property to differentiate gas from oil. At high pressures, where hydrocarbon gases behave as real gases, the gas compressibility is smaller than that of the ideal gas, since Z-factor increases as pressure increases. Therefore, gas compressibility values are similar to liquid compressibility values (Lyons, 1996). Figure 11 shows how gas compressibility is very high at low pressures and gas expansion occurs occupying large volumes (El-Banbi, Alzahabi, & El-Maraghi, 2018).

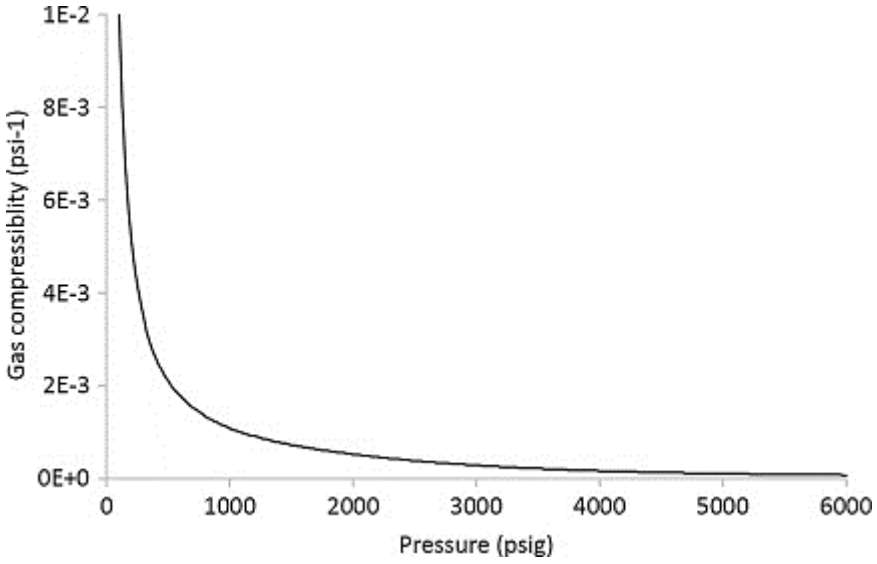

Figure 11: *Isothermal gas compressibility as a function of pressure.*

Note. Adapted from *Gas compressibility* by A. El-Banbi, A. Alzahabi & A. El-Maraghi, 2018, ScienceDirect (https://www.sciencedirect.com/topics/engineering/gas-compressibility)

2.4.6 Gas Formation Volume Factor

The gas formation volume factor is the relationship between the volume of gas at reservoir conditions and the volume of gas at standard conditions of 14.7 psia and 60 °C.

$$B_g = \frac{V_{rc}}{V_{sc}} \quad (40)$$

Where B_g is the formation volume factor of gas, ft^3/scf^3. Equation 40 can also be expressed by substituting the volume with the real gas EOS as indicated by Equation 41. Figure 12 shows how the gas formation volume factor varies with pressure (El-Banbi, Alzahabi, & El-Maraghi, 2018).

$$B_g = \frac{p_{sc}}{T_{sc}} \frac{ZT}{p} \quad (41)$$

Gas expansion factor can be calculated with the reciprocal of B_g. Where E_g is in terms of scf^3/ft^3 (Ahmed, 2007).

$$E_g = \frac{1}{B_g} \quad (42)$$

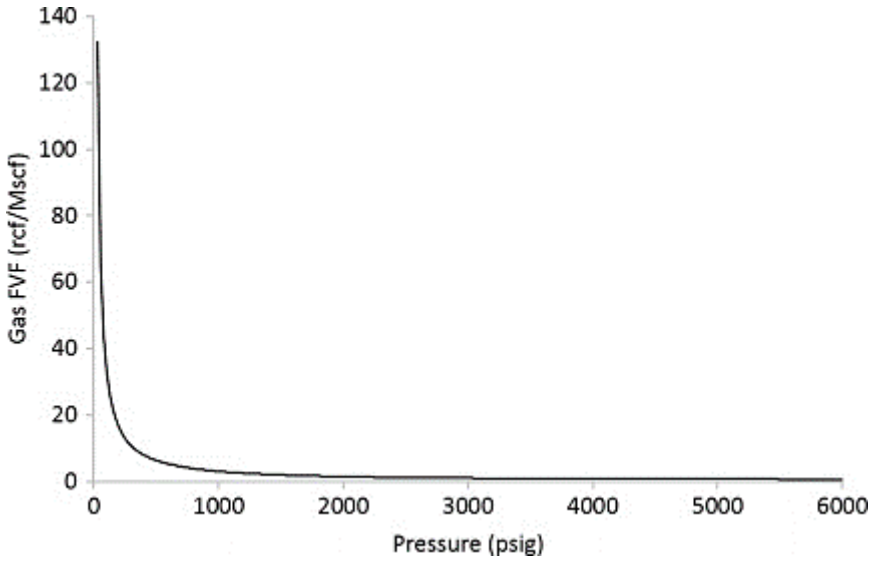

Figure 12: *Gas formation volume factor as a function of pressure.*

Note. Adapted from *Gas formation volume factor* by A. El-Banbi, A. Alzahabi & A. El-Maraghi, 2018, ScienceDirect (https://www.sciencedirect.com/topics/engineering/formation-volume-factor)

2.4.7 Gas Viscosity

Fluid viscosity is a measure of the resistance to flow. The lower the resistance, the lower the viscosity. This is a feature of gases since a common value of viscosity for a reservoir gas is $\mu_g = 0.025\ cp$ whereas for a light oil is $\mu_o = 1\ cp$ (Dake, 2001). Gas viscosity is a function of pressure, temperature, and gas composition, $\mu_g(p, T, y_i)$. It is estimated by correlations or charts for sweet gases. If corrections for impurities in the gas mixture have been done during Z-factor or gas density calculations, then the viscosity of the gas mixture can also be calculated with accuracy (Lee & Wattenbarger, 1996). Figure 13 shows how gas viscosity increases with pressure.

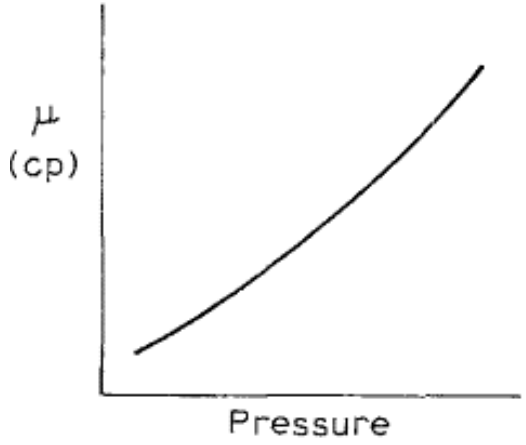

Figure 13: *Gas viscosity as a function of pressure.*

Note. Adapted from *(a) Gas viscosity and (b) compressibility as functions of pressure* (p. 479) by L. P. Dake, 2001, Elsevier.

2.5 Reservoir Rock Properties

The properties of the rock are determined by using well logs or through laboratory measurements on rock samples. These laboratory measurements on the rock samples are subdivided into two analysis: the routine core analysis (RCAL) which aims to determine the basic rock properties such as porosity, permeability, and saturation of fluids, that are useful for the determination of the volume of producible hydrocarbons; and the special core analysis (SCAL) which aims to evaluate more representative data of the reservoir such as relative permeabilities, capillary pressure, and wettability, that helps to predict the fluid flow in the reservoir during the production stage (Alyafei, 2021).

2.5.1 Porosity

Porosity is the ratio between the pore volume and the total volume of the rock.

$$\emptyset = \frac{V_{void}}{V_{Total}} = \frac{V_{Total} - V_{matrix}}{V_{Total}} \quad (43)$$

Where $\emptyset$ is the porosity expressed by percentage or fraction units; V_v is the pore volume given by the void spaces of the rock, ft^3; V_T is the total volume of the rock, ft^3; V_m is the matrix

volume or volume of the grains, ft^3. Porosity is seen as the ability of the rock to store fluids and can range from 5% to 40%. Porosity ranges of homogeneous rocks such as sandstones can vary between 20 and 35%, if sandstones are compacted, they can have values of 15 or 20%, and for more compacted rocks such as limestones, the porosity values are between 5 and 20%. Porosity is classified into primary and secondary porosities. Primary porosity occurs when the rock is formed, and secondary porosity occurs after that due to other geological processes that induces fractures. Effective porosity is usually used instead of total or absolute porosity to account for the effective and interconnected pore space for the flow of fluids (Alyafei, 2021).

2.5.2 Permeability

Permeability is an intrinsic rock property that represents the effectiveness of the transmission of fluids through the interconnected rock spaces. This is given by the Darcy's law. Equation 44 represents the Darcy's law for a horizontal linear system.

$$v = \frac{q}{A} = -\frac{k}{\mu}\frac{dp}{dl} \quad (44)$$

Where v is the apparent or Darcy's velocity, cm/s; q is the flow rate, cm^3/s; A is the cross-sectional area cm^2; k is the absolute permeability that accounts for the presence of a single-phase fluid in the rock, darcy; μ is the fluid viscosity, cp; and $\frac{dp}{dl}$ is the pressure gradient, atm/cm.

Klinkenberg effect is used when dealing with gases, since permeability to gases is shown to be higher than the permeability to liquids due to the surface contact between the walls of the rock and the fluid, known as the slip flow. Equation 45 expresses the average pressure of the porous medium, as this average pressure increases the permeability will decrease (Paris de Ferrer, 2009).

$$\bar{p} = \frac{p_1 + p_2}{2} \quad (45)$$

By extrapolating the permeability values on a straight line as a function of $^1/_{\bar{p}}$ as seen on Figure 14 until reaching the point $^1/_{\bar{p}} = 0$, infinite pressure, permeability appears to be equal to the permeability to liquids. This can be expressed by Equation 46.

$$k_a = k\left(1 + \frac{b}{\bar{p}}\right) \quad (46)$$

Where k_a is the permeability to gas, k is the permeability to liquids, $\bar{p}$ is the average pressure, and b is a constant factor which is a function of the radius of capillaries and may be small for high permeable porous formations and large for less permeable ones (Klinkenberg, 1941).

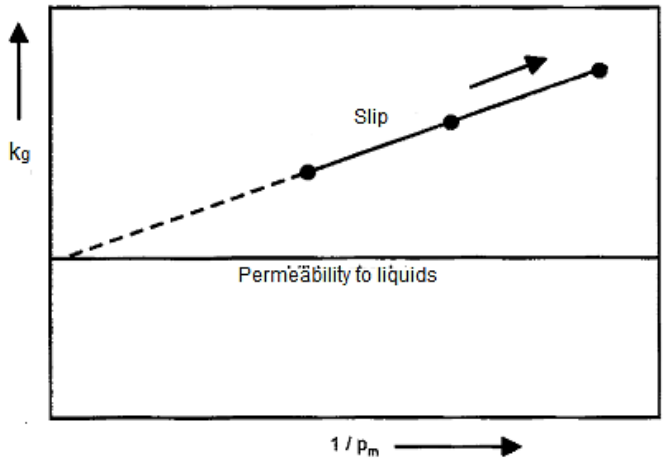

Figure 14: *Permeability to gas by Klinkenberg effect.*

Note. Adapted from *Medidas de permeabilidad al gas mostrando el efecto klinkenberg* (p. 259) by Magdalena Paris de Ferrer, 2009, Self-published

Despite that horizontal permeability, k_h, is of the great importance to the flow of hydrocarbons, this property may not be equal in all directions ($k_h \neq k_v \neq k_z$). This characteristic is known as anisotropy. Perpendicular directions to the parallel flow along the bedding planes are of important consideration when dealing with injection of gas or water, or gas segregation. This flow restriction can be interpreted by transmissibility as expressed by Equation 47 (Archer & Wall, 1986).

$$T = \frac{kA}{L} = \frac{q\mu}{\Delta p} = \frac{kh}{\mu} \quad (47)$$

Where T is transmissibility, md·ft/cp; a permeability or thickness increase, or viscosity decrease, will lead to an improvement of the fluid transmissibility in the reservoir. Another important concept is the flow capacity, kh, which is important during buildup and drawdown tests. The proportionality of $q \propto kh$ expresses that a high permeable formation of small thickness would have an equal production as a less permeable formation of larger thickness. This indicates the ability of the formation to fluid flow (Lyons, 1996).

For a heterogeneous system, and average permeability is calculated to represent a homogeneous one. If the reservoir is stratified with layers of different permeabilities and thicknesses, the flow rates are parallel to the bedding planes and the pressure drop is constant, a horizontal average permeability is used as determined by Equation 48.

$$\bar{k} = \frac{\sum_{i=0}^{n} k_i h_i}{\sum_{i=0}^{n} h_i} \quad (48)$$

Where k_i is the permeability for each layer, cp; and h_i is the thickness of each layer, ft. If permeability varies laterally in the reservoir, with a constant flow rate and thickness, and the pressure drop varies at each lateral bed, an average permeability is determined by Equation 49 for a fluid that flows in series.

$$\bar{k} = \frac{\sum_{i=0}^{n} L}{\sum_{i=0}^{n} \left(\frac{L_i}{k_i}\right)} \quad (49)$$

Where L_i is the length of each lateral bed, ft; and k_i is the permeability for each bed, md (Archer & Wall, 1986).

2.5.3 Fluid Saturation

Fluid saturation is defined as the volume of fluid present in the pore space of the rock as expressed by Equation 50.

$$S_{fluid} = \frac{V_{fluid}}{V_{void}} \quad (50)$$

If the pores of the rock are filled with more than one fluid, for instance gas, oil, and water, saturation is expressed by Equation 51 (Alyafei, 2021).

$$\frac{V_g + V_o + V_w}{V_{void}} = S_g + S_o + S_w = 1 \quad (51)$$

2.5.4 Formation Compressibility

Rock compressibility is important during the prediction of the reservoir performance when it is producing. Since as the fluids are produced, the pore volume exerted by the fluid pressure decreases, and so does porosity, and results in rock compaction. Therefore, the rock compressibility or formation compressibility is the result of the changes in pore volume with changes of compaction pressure.

$$c_f = -\frac{1}{V_p}\left(\frac{dV_p}{dp}\right)_T = \frac{1}{\emptyset V_b}\frac{\partial(\emptyset V_b)}{\partial p} = \frac{1}{\emptyset}\frac{\partial \emptyset}{\partial p} \quad (52)$$

Where c_f is the isothermal rock compressibility, 1/psi.

In case of natural depletion of hydrocarbons, dp does not cause great changes in V_p, and the effect of formation compressibility can be neglected (Alyafei, 2021). An example of this natural depletion occurs when developing gas reservoirs, since the gas is produced by using the natural pressure of the reservoir, making the pressure to decline. One of the consequences of reservoir pressure decrease may be the influx of water from a connecting aquifer, inducing reservoir compaction (Hagoort, 1988).

Considering the compressibility of the formation and compressibility of the fluids in the reservoir, the concept of total compressibility is used as expressed by Equation 53, which the best way to determine its value is through PTA tests.

$$c_t = c_g S_g + c_o S_o + c_w S_w + c_f \quad (53)$$

For gas reservoirs total compressibility is given by Equation 54. In this case, the value of the total compressibility is very close to that of gas compressibility (Guo, Sun, & Ghalambor, 2008).

$$c_t = c_g S_g + c_f \quad (54)$$

Effective compressibility values are used when performing gas reservoirs, rather than gas compressibility only. If the reservoir is abnormally pressured, the effective compressibility will be several times larger than the gas compressibility due to the expansion of gas and water and formation compressibility. Thereby, total compressibility will be expressed by Equation 55 (Ahmed, 2019).

$$c_t = 1 - \frac{(c_f + c_w S_{wi})(p_i - p)}{1 - S_{wi}} \quad (55)$$

2.5.6 Relative Permeability

The relative permeability to any fluid (gas, oil, water) is defined as the ratio between the effective permeability of that fluid to the absolute permeability of the porous medium.

$$k_{r,g} = \frac{k_g}{k} \quad (56)$$

$$k_{r,o} = \frac{k_o}{k} \quad (57)$$

$$k_{r,w} = \frac{k_w}{k} \quad (58)$$

If the reservoir contains more than one mobile fluid phase, the relative permeability is the key factor for controlling the production of such phases. Relative permeability is a function of fluid saturation and is dependent on heterogeneity and wettability (Satter & Iqbal, 2016).

In systems of two-phase fluids, one acts as the wetting phase and the other as the non-wetting phase. The endpoint values are the important points in relative permeability curves,

which represent the endpoint saturations (Hagoort, 1988). For instance, in a two-phase system where water is the wetting phase and the hydrocarbon is the non-wetting phase, the residual saturation of the non-wetting fluid is reached at the maximum water saturation point, $S_{w_{max}}$, and the irreducible saturation of the wetting phase is represented by the minimum water saturation point, $S_{w_{min}}$. Figure 15 shows a gas-oil system representing the drainage and imbibition processes. During drainage, from the critical gas saturation, S_{g_c}, at which the gas becomes mobile in the reservoir, the gas (non-wetting phase) displaces the oil phase until reaching the maximum gas saturation, $S_{g_{max}}$. This can be due to a gas drive mechanism. During the imbibition process, the gas is displaced from the maximum gas saturation, $S_{g_{max}}$, until reaching a residual gas saturation, S_{g_r}. This is due to oil displacement or water influx from an aquifer (the wetting phase) (Archer & Wall, 1986).

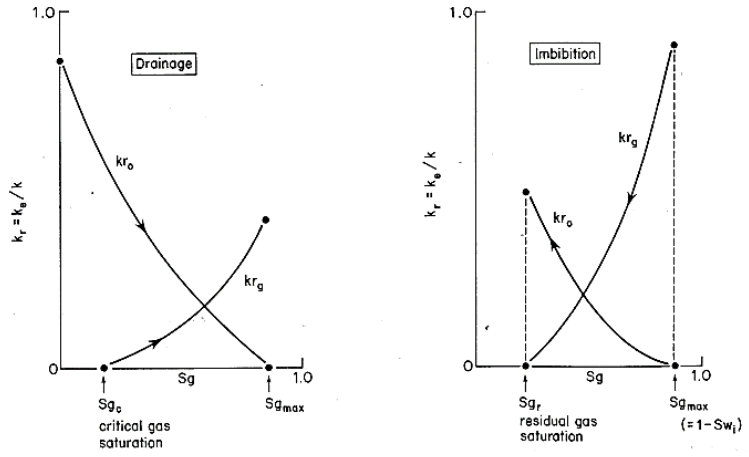

Figure 15: *Relative permeability curves for a gas-oil system during drainage and imbibition processes.*

Note. Adapted from *Gas-oil relative permeability* (p. 103) by J. S. Archer & C. G. Wall, 1986, Graham and Trotman Ltd.

2.5.7 Capillary Pressure

The effect of a liquid rising or falling in a capillary tube is known as capillarity. The water rises in the capillary tube is the surface is water-wet, due to the interfacial tension, and falls if another immiscible fluid is the wetting phase. The pore throats of the rock act as capillary tubes. Capillary pressure and interfacial tension are useful to estimate reservoir fluid saturations.

$$p_c = \frac{2\sigma cos\theta}{r} \quad (59)$$

Where p_c is the capillary pressure, Pa; σ is the interfacial tension that exists between two immiscible fluids, N/m; θ is the contact angle between the surface of the rock and the fluid, degrees; and r is the radius of the pore, m.

Capillary rise is given by Equation 60. It is defined as the height of the wetting phase above the free water level (FWL).

$$h = \frac{2\sigma cos\theta}{\rho_w g r} = \frac{p_c}{\rho_w g} \quad (60)$$

Where h is the capillary rise, m; ρ_w is the density of water, kg/m^3; and g is the gravity acceleration 9.81 m/s^2.

Capillary pressure is then defined as the pressure difference between two immiscible fluids where one is the non-wetting phase and the other the wetting phase.

$$p_c = p_{nw} - p_w \quad (61)$$

Where p_c is the capillary pressure, Pa; p_{nw} is the pressure of the non-wetting phase, Pa; and p_w is the pressure of the wetting phase, Pa (Alyafei, 2021).

In a two-phase system of gas and water, the pressure in the gas will be higher than the pressure in the water. This is due to the interfacial tension between both fluids, and it is known as capillary pressure. Since the non-wetting phase is represented by gas and the wetting phase by water, Equation 61 can be expressed as:

$$p_c = p_g - p_w \quad (62)$$

Where p_g is the pressure of the gas phase, Pa; and p_w is the pressure of the water phase, Pa. Capillary pressures are represented as a function of the water saturation (Hagoort, 1988).

The capillary pressure across the interface of a gas-water system can be expressed in terms of the densities of the two fluids as:

$$p_c = (\rho_w - \rho_g)gh \quad (63)$$

Thus, capillary rise is defined as:

$$h = \frac{p_c}{(\rho_w - \rho_g)g} \quad (64)$$

Where ρ_w is the density of water, kg/m^3; and ρ_g is the gas density, kg/m^3 (Alyafei, 2021).

Capillary pressure decreases if the pore radius is large, as in high permeable rocks. It is useful for the determination of the original fluid contacts and the transition zones, as well as for describing the fluid flow through the fractures and matrix of fractured reservoirs (Fanchi J. R., 2002).

Capillary pressure is a function of the water saturation. If rocks have different permeability, porosity, and pore sizes, the Leveret J-function, $J(S_w)$ is used to account for the rock properties and water saturation. The Leveret J-function, $J(S_w)$, determined by laboratory measurements is given by Equation 65.

$$J(S_w) = \frac{p_c}{\sigma cos\theta}\sqrt{\frac{k}{\emptyset}}\Bigg|_{lab} \quad (65)$$

After $J(S_w)$ has been determined, the capillary pressure can be evaluated at reservoir conditions as expressed by Equation 66 (Fanchi J. R., 2006).

$$p_c = \frac{\sigma cos\theta}{\sqrt{k/\emptyset}} J(S_w)\Bigg|_{res} \quad (66)$$

Figure 16 shows the capillary pressure curves in dimensionless units for a gas-water system in a sandstone. During drainage, the rock is initially fully saturated with water, the wetting phase, after the gas overcomes the entry capillary pressure, since the water is strongly attached to the rock pores due to capillary forces, the gas starts to displace water until the water is at the irreducible water saturation, S_{wi}, when is no longer mobile. The high gas pressure applied is at this point. During imbibition, the water displaces the gas, and the gas saturation decreases until reaching the residual gas saturation ,S_{gr}, where bubbles of gas are trapped immobile in the pore spaces of the rock. This process can be due to the water influx from an aquifer after the gas has been produced. The flatter the capillary pressure curve, the higher the uniformity of the pore-size distribution. It is worth mentioning that the FWL can be chosen as the reference level, since at this point the pressure of the gas and water are equal, and thus the capillary pressure is equal to zero (Hagoort, 1988).

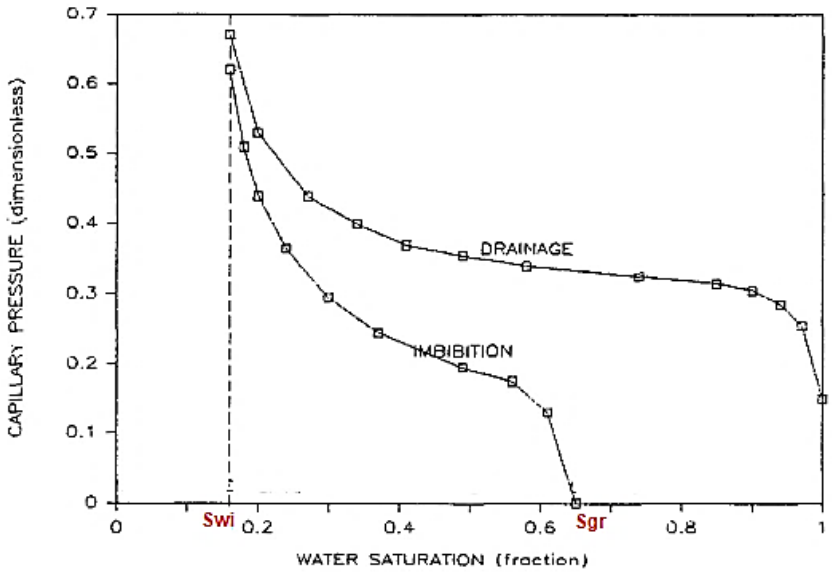

Figure 16: *Capillary pressure curves of a gas-water system.*

Note. Adapted from *Capillary pressure curves* (p. 21) by J. Hagoort, 1988, Elsevier.

Chapter 3. Fundamental Concepts of PTA for Gas Wells

Gas well test analysis is performed to determine reservoir parameters such as permeability by thickness, initial pressure, reservoir heterogeneities, reservoir size or drainage area, distances to boundaries or aquifer existence, and to estimate the near-wellbore conditions such as skin factor. The information from flow-pressure transient tests and conditions from production/injection wells is used for reservoir evaluation and characterization and to predict reservoir performance and future production. The first method used in the history of gas well testing analysis was the four-point method, which on a log-log plot the square of the average reservoir pressure minus the square of the well flowing pressure was plotted against the gas flow rate. The maximum flow rate is read at a well flowing pressure equal to zero. Now, other methods that include isochronal tests are used to determine the flow features of gas wells. Well test data can be obtained from all the life of a gas well and regularly pressure measurements help in reservoir models tuning (Chaudhry, 2003).

Two scenarios exist from a producing well if analyzing the output signal from a well given an input signal that is known. If a well is producing at a constant flow rate and the pressure response is recorded, this case will be known as pressure transient analysis (PTA). If the well is producing at a constant-well flowing pressure and the flow rate is measured, the case will be known as rate transient analysis (RTA) (Escobar, 2018).

3.1 Types of Pressure Transient Tests

Well testing is performed in all the stages of the productive life of an oil or gas field to measure reservoir characteristics such as formation pressure, permeability, and skin through the flow of formation fluids. For instance, during the exploration stage, well tests are useful to determine if the low production rates are due to natural permeability or skin factor, and to estimate the reservoir size. During the development stage, stimulation treatments can be planned and designed, the length and conductivity of the formation fractures can be estimated,

and the fluid contacts can be determined. During production, the data recovered from well tests is used for history matching of the actual production against the one predicted by numerical simulation (Schlumberger, 2013).

3.1.1 Drill Steam Tests (DSTs)

DSTs are conducted in the primary stage of the reservoir in exploration and appraisal wells. In addition to DSTs, wireline formation tests (WFTs) are also conducted at this stage and provide data about reservoir properties and behavior, as well as fluid samples. The tool is placed in the drill string and the formation characteristics are estimated by shorts sequences of open-to-flow and shut-in operations (Horne, 1990).

3.1.2 Pressure Drawdown and Buildup Tests

Pressure tests such as drawdown (DD) and buildup (BU) are conducted during the primary production of the reservoir (see Figure 17). A drawdown test is conducted by producing the well, after a shut-in period until the well has reached stabilization, at a constant rate while the downhole pressure is measured against time. This test can provide information about the reservoir limit boundary. The disadvantage is that it is difficult to reach the condition of constant flow rate. A buildup test is conducted when the well is shut-in after a period of production. The condition of constant flow rate is reached since the flow rate is equal to zero. The static downhole pressure is measured as the pressure builds up as a function of time, and the average reservoir pressure can be obtained. Its disadvantage is that the production is lost during shut in (Sylvester, Bibobra, & Ogbon, 2015) and (Escobar, 2018).

3.1.3 Injection and Falloff Tests

Other pressure tests including injection test and falloff, are run in secondary and enhanced recovery projects (see Figure 18). An injection test is similar to a drawdown test, yet the flow rate recorded is from the injected fluid. A falloff test records the period at which the

injection finishes. It is similar to a buildup test and provides information about mobility and presence of front boundaries (Sylvester, Bibobra, & Ogbon, 2015).

3.1.4 Interference Tests

To conduct an interference test, two or more wells are involved. One of the wells is open to production for a period of time and the transient pressure disturbance is monitored in the adjacent well. They define the hydraulic communication between the wells and are conventionally used during secondary and enhanced recovery projects. They can also be used to determine heterogeneities and directional permeabilities in unconventional reservoirs (Satter & Iqbal, 2016).

3.1.5 Multilayered Tests

Additional tests, such as multilayered tests are run over the life of a reservoir. The information obtained concerns the properties of each layer, the vertical and directional permeability, and boundaries (Sylvester, Bibobra, & Ogbon, 2015).

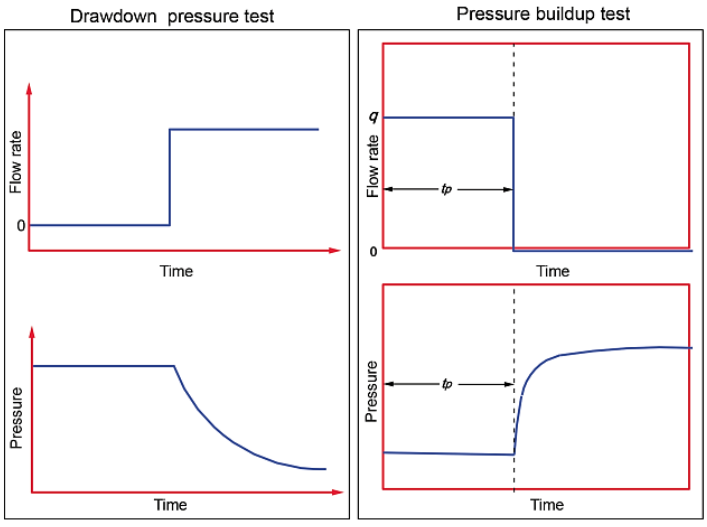

Figure 17: *Drawdown (DD) and buildup (BU) tests representation.*

Note. Adapted from *Schematic representation of pressure drawdown and pressure buildup tests* (p. 6) by F. H. Escobar, 2017, IntechOpen.

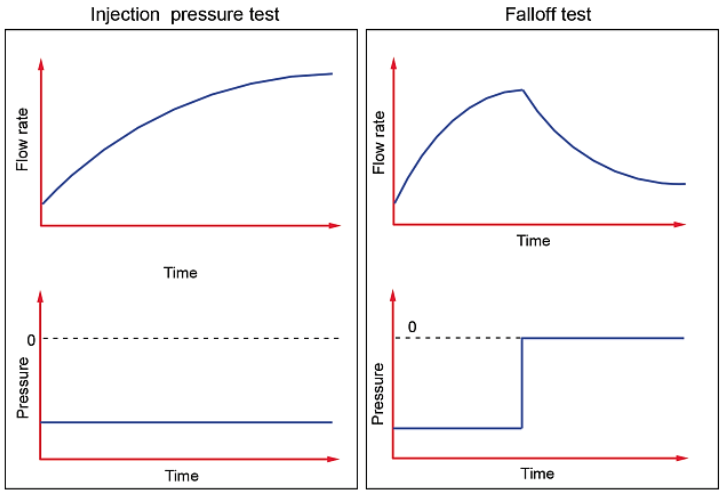

Figure 18: *Injection and falloff tests representation.*

Note. Adapted from *Injection pressure test (left) and falloff test (right)* (p. 6) by F. H. Escobar, 2017, IntechOpen.

3.2 Deliverability Tests

Deliverability tests are conducted in gas wells. Flow-after-flow, isochronal and modified isochronal tests, and single-point tests, are examples of gas deliverability tests (Lee & Wattenbarger, 1996) with the aim of determining gas wells productivity and the inflow performance relationship (IPR), by evaluating the absolute open flow potential (AOF) that is better used for the performance of gas wells than the productivity index (PI) (Schlumberger, 2006).

In flow-after-flow tests, also known as backpressure or four-point tests (Figure 19) a well flows at a constant rate for a certain period, then the rate is increased and flows constantly for a second period; this repeats for three or four rates until reaching pressure stabilization, this indicates a flow from the external boundaries of the drainage area (Schlumberger, 2013). In a single-point test, the well flows at a unique rate util the bottomhole pressure stabilizes (Lee & Wattenbarger, 1996). In an isochronal test (Figure 20), the well flows at a first rate for a certain period and then is set to shut-in for pressure buildup. Then, the well is open to flow at a second rate for the same period and is shut-in for a period longer than the previous one. This is repeated

for three or flow rates with the last rate extended until the stabilization conditions are reached. The modified isochronal test (Figure 21) follows the same approach as the isochronal test, the difference lies on the periods of shut-in, that are all the same, except for the last rate that corresponds to an extended flowing period until reaching stabilization conditions (Guo & Ghalambor, 2005).

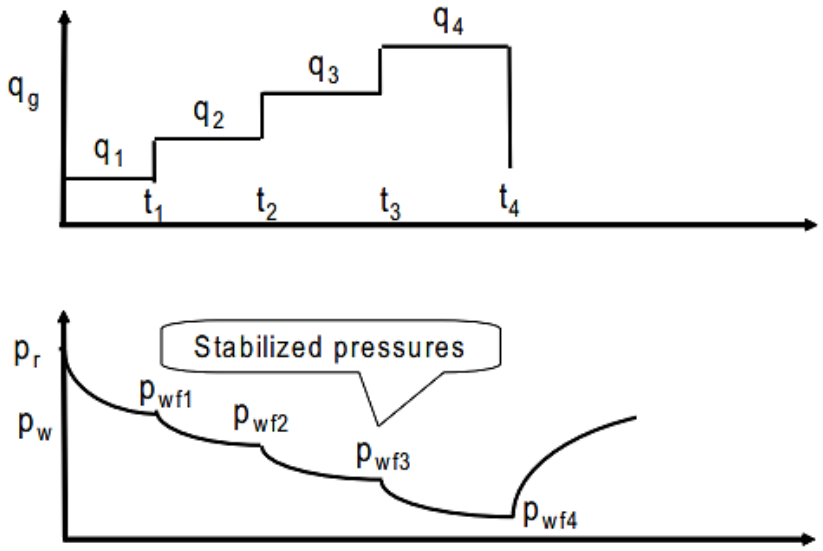

Figure 19: *Flow-after-flow test.*

Note. Adapted from *Sequence of flow after flow test* (p. 58) by Boyun Guo & Ali Ghalambor, 2005, Gulf Publishing Company.

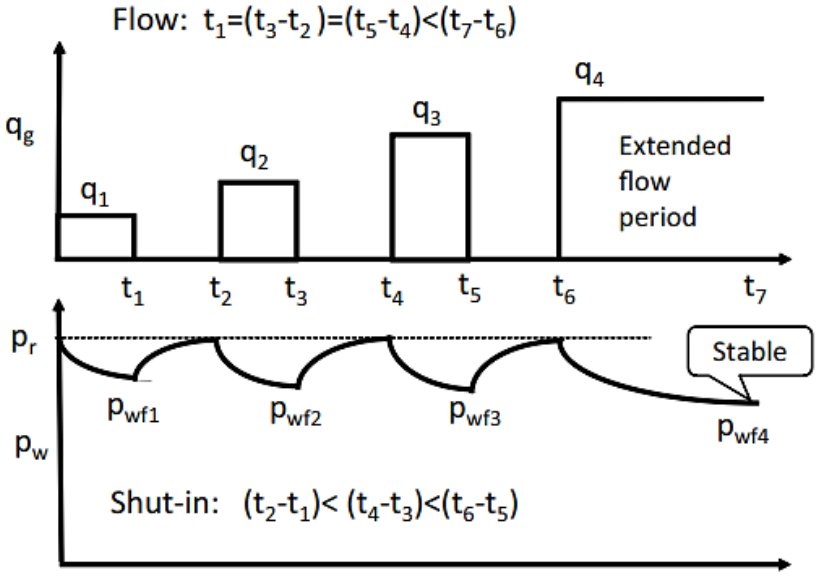

Figure 20: *Isochronal test.*

Note. Adapted from *Sequence of isochronal test* (p. 60) by Boyun Guo & Ali Ghalambor, 2005, Gulf Publishing Company.

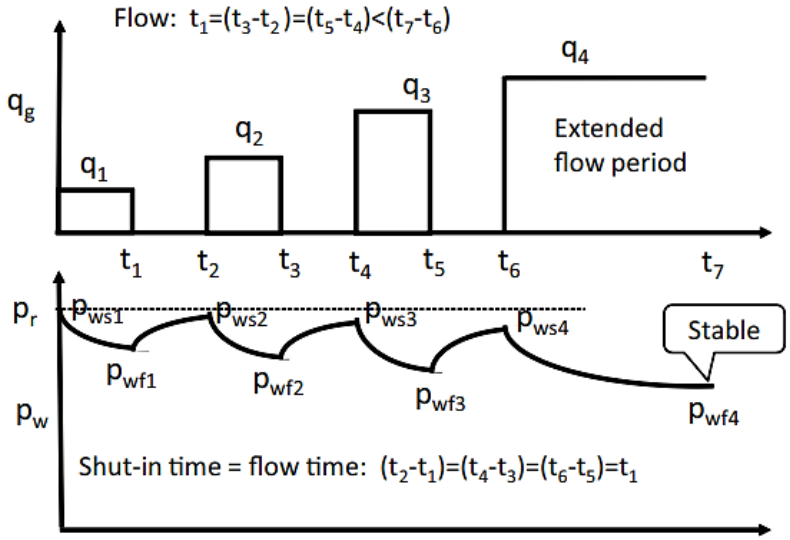

Figure 21: *Modified isochronal test.*

Note. Adapted from *Sequence of modified isochronal test* (p. 62) by Boyun Guo & Ali Ghalambor, 2005, Gulf Publishing Company.

3.3 Reservoir Characteristics

The equations used to analyze pressure transient tests depend on the characteristics of the reservoir. Therefore, some aspects should be considered such as the type of fluids in the reservoir either compressible or slightly compressible fluids; the number of phases of the fluid, like single phase or multiphase; the reservoir geometry, for instance radial flow, linear or spherical flow; and the hydraulic flow regime, such as steady-state, transient, or pseudosteady-state flow (Ahmed & McKinney, 2005).

In steady-state flow conditions the pressure is constant everywhere in the reservoir with respect to time as expressed by Equation 67. This can be due to the water influx from an aquifer connected that is giving support to the reservoir.

$$\frac{\partial p}{\partial t} = 0 \qquad (67)$$

In transient flow the change of pressure with time depends on space and time expressed by Equation 68. During transient flow conditions, the well is opened to produce at a constant flow rate to create a pressure disturbance that moves in radial direction from the well through the reservoir. Consequently, a pressure drop will be observed at the well. Figure 22 shows the conditions of transient flow where the reservoir size appears to be infinite, the reservoir pressure behavior does not change and remains equal to the initial pressure ($p = p_i$), as long as the effect of boundaries is not present yet ($r \neq r_e$). This flow condition is important for the performance of pressure transient tests and the solution to the diffusivity equation.

$$\frac{\partial p}{\partial t} = f(x, y, z, t) \qquad (68)$$

After transient conditions, pseudosteady-state flow occurs and the change of pressure with respect to time is constant as described by Equation 69. This flow condition is characterized by the presence of boundaries like a sealing fault. Consequently, the reservoir pressure will change to an average reservoir pressure ($p = \bar{p}$) that is lower than its initial pressure p_i. Figure 23 shows the three flow regimes plotted with respect to pressure and time (Smith, 1990).

$$\frac{\partial p}{\partial t} = constant \qquad (69)$$

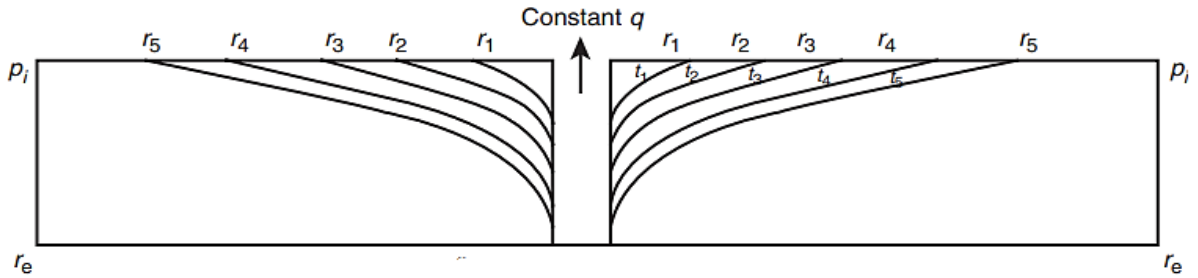

Figure 22: *Transient flow conditions at constant rate.*

Note. Adapted from *Pressure disturbance as a function of time* (p. 1/16) by Tarek Ahmed & Paul D. McKinney, 2005, Elsevier.

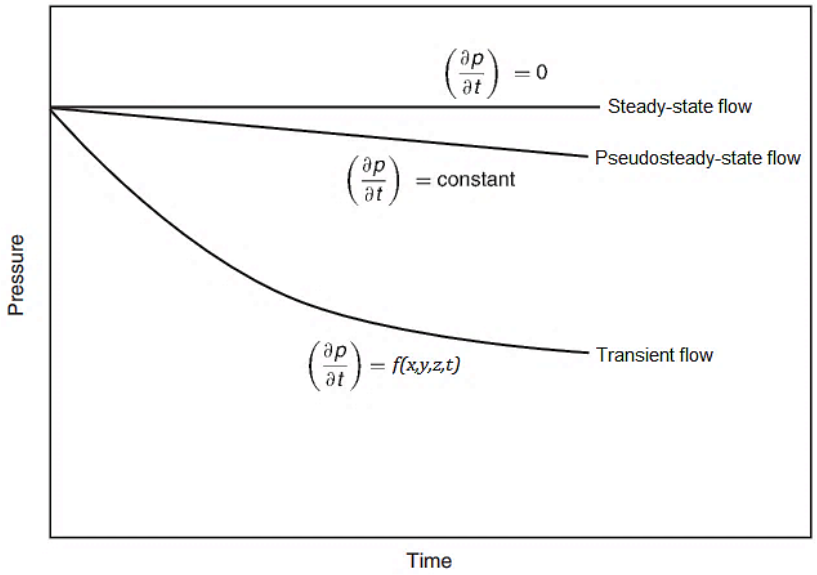

Figure 23: *Flow regimes on a pressure vs time plot.*

Note. Adapted from *Flow regimes* (p. 1/4) by Tarek Ahmed & Paul D. McKinney, 2005, Elsevier.

3.4 The Diffusivity Equation for Gas Flow

The diffusivity equation can be considered as the basis for the analysis of pressure transient tests that describes the pressure response in the reservoir due to an initial disturbance such as the change of flow rate, and which is used to solve the problems associated with fluid flow in porous media (Smith, 1990). It is the result of the combination of three equations: the Darcy's law, the law of conservation of mass, and the equation of state (EOS) for the definition of fluid compressibility (Lee, 1982).

The development of the diffusivity equation for compressible fluids such as gases differs from the one for slightly compressible fluids in the implementation of the EOS and the assumptions about fluid properties. Since for liquids the viscosity is constant, the isothermal

fluid compressibility is assumed constant, then the total compressibility is also assumed constant. This is not case for modelling gas behavior, the viscosity is no longer constant but depends on pressure and temperature, the compressibility is strongly pressure dependent, and the EOS for real gases must be introduced. Permeability is assumed constant, but in the case of wet gases or condensation in the reservoir the permeability may be pressure dependent, and at low pressures Klinkenberg effect should be considered (Ikoku, 1984).

Therefore, the pseudo-pressure function for real gases can be used as an accurate solution that accounts for certain pressure-dependent gas properties, such as viscosity, without limiting pressure ranges. This is defined by:

$$m(p) = 2\int_{p_0}^{p} \frac{p}{\mu Z} dp \qquad (70)$$

Where $m(p)$ is the gas pseudo-pressure with units psi^2/cp which is a function of pressure, temperature, and gas composition; μ is the gas viscosity, cp; Z is the gas compressibility factor; and p_0 is the low base pressure, psi (Al-Hussainy, Ramey Jr., & Crawford, 1966).

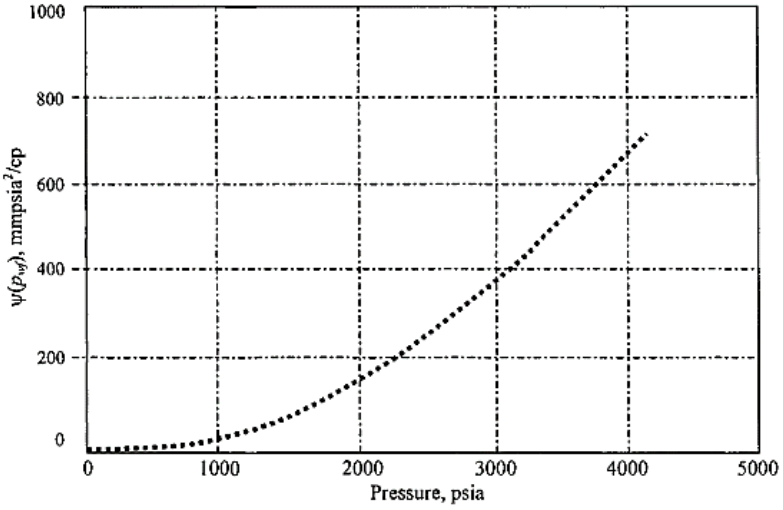

Figure 24: *Pseudopressure function.*

Note. Adapted from *$\psi - p$ curve-Example 5-2* (p. 256) by Amant U. Chaudhry, 2003, Elsevier.

For gas condensate reservoirs, a multiphase pseudopressure function can be used. This considers the molar density of the liquid and gas phases and the use of relative curves:

$$m(p) = \int_{p_0}^{p} \left(\rho_o \frac{k_{ro}}{\mu_o} + \rho_g \frac{k_{rg}}{\mu_g} \right) dp \quad (71)$$

Where $m(p)$ is the pseudopressure function, psi/cp (Bourdet, 2002).

The Darcy's law for a horizontal radial system with laminar flow is given by:

$$v = -\frac{q}{A} = \frac{k}{\mu} \frac{\partial p}{\partial r} \quad (72)$$

Where A is the cross-sectional area of a cylinder:

$$A = 2\pi r h \quad (73)$$

From the law of conservation of mass, the continuity equation can be defined by:

$$\frac{1}{r} \frac{\partial}{\partial r} (r \rho v) = -\frac{\partial}{\partial t} (\rho \emptyset) \quad (74)$$

Where $\emptyset$ is the porosity; ρ is the density, lb/ft^3; and v is the fluid velocity, ft/day.

The EOS corresponds to the density for real gases as determined by Equation 35:

$$\rho_g = \frac{p M_a}{ZRT} \quad (35)$$

The total compressibility is given by:

$$c_t = c_g + c_f \quad (75)$$

Where c_g is the isothermal compressibility for real gases as determined by Equation 38:

$$c_g = \frac{1}{p} - \frac{1}{Z} \left(\frac{\partial Z}{\partial p} \right)_T \quad (38)$$

And c_f is the formation compressibility defined by Equation 76.

$$c_f = \frac{1}{V_p} \frac{\partial V_p}{\partial p} = \frac{1}{\emptyset V_b} \frac{\partial (\emptyset V_b)}{\partial p} = \frac{1}{\emptyset} \frac{\partial \emptyset}{\partial p} \quad (76)$$

The generalized diffusivity equation for real gases with radial flow can be expressed by a nonlinear partial differential equation as:

$$\frac{1}{r}\frac{\partial}{\partial r}\left(\frac{p}{\mu Z}r\frac{\partial p}{\partial r}\right)=\frac{\mu c_t \emptyset}{k}\frac{p}{\mu z}\frac{\partial p}{\partial t} \quad (77)$$

Where the diffusivity constant or hydraulic diffusivity is determined by:

$$\eta=\frac{\mu c_t \emptyset}{k} \quad (78)$$

Since $\frac{p}{\mu Z}$ and μc_t are not constant, yet very pressure-dependent, Equation 77 can be rearranged in terms of the pseudopressure function as:

$$\frac{1}{r}\frac{\partial}{\partial r}\left(r\frac{\partial m(p)}{\partial r}\right)=\left(\frac{\mu c_t \emptyset}{k}\right)\frac{\partial m(p)}{\partial t} \quad (79)$$

Equation 79 can be applied under the assumptions of a homogeneous and isotropic reservoir with constant permeability and compressibility, radial flow exists, the fluid is in a single phase and obeys the law of real gases, the Darcy's law applies (laminar flow), gravity effects are neglected, and isothermal conditions exist (Lee, Rollins, & Spivey, 2003).

For multiphase flow in gas-condensate reservoirs, Equation 79 can be expressed as:

$$\frac{1}{r}\frac{\partial}{\partial r}\left(r\frac{\partial m(p)}{\partial r}\right)=\left(\frac{c_t \emptyset}{\lambda_t}\right)\frac{\partial m(p)}{\partial t} \quad (80)$$

Where λ_t is the total mobility given by the sum of the individual mobilities of the fluid phases:

$$\lambda_t=\frac{k_g}{\mu_g}+\frac{k_o}{\mu_o}+\frac{k_w}{\mu_w} \quad (81)$$

And c_t is the total compressibility determined by Equation 53.

$$c_t=c_g S_g+c_o S_o+c_w S_w+c_f \quad (53)$$

It should be noticed that the effective permeability to each phase is the result of the product of the absolute permeability and the relative permeability to that fluid and this depends on saturation, viscosity is a pressure-dependent property, and fluid saturation is a function of time. Equation 80 can be applied under the assumptions that the system is radial, Darcy's law applies,

the reservoir is isotropic and homogeneous, isothermal conditions exist, and capillary and gravitational forces are neglected (Chaudhry, 2003).

3.4.1 Solution to the Diffusivity Equation

The solution to the diffusivity equation for gas wells implies that a set of initial and boundary conditions must be first defined. The initial condition refers to have a reservoir pressure at any location equal to the initial reservoir pressure when the production begins. The inner boundary condition is at the well interface, the flow rate must be constant, this means that constraints of skin or wellbore storage effects may be considered. The outer boundary condition refers to the reservoir extent: if the reservoir behaves as infinite-acting, no boundaries are found; if the reservoir has a sealing fault, a no-flow boundary is identified; and if the reservoir pressure remains constant, an active aquifer is connected (Schlumberger, 2006).

In pressure transient analysis, the radial diffusivity equation can be solved by the constant-terminal-rate solution, in which the production rate is constant $q = constant$ and the pressure at the well is recorded p_{wf}. This solution uses the Ei-function and the pressure drop in dimensionless configuration p_D (Ahmed & McKinney, 2005).

The Ei-function solution, also known as the line-source solution, was proposed by Matthews and Russell (1967) as a solution to the diffusivity equation for an infinite-acting reservoir. This represents the well as a line-source where the wellbore radius is approximated to zero $(r_w \rightarrow 0)$. In transient flow, the initial condition is to have a uniform reservoir pressure $p(r, 0) = p_i$ at $(t = 0)$. The inner boundary condition is to have a constant-rate production, where the rate $q \propto \frac{\partial p}{\partial r} = constant$ at $r = r_w$. The outer boundary condition refers to an infinite-acting reservoir (IARF), where the reservoir during radial flow behaves as if it is infinite in size and not influenced by boundaries, and the reservoir pressure at any time approaches the initial reservoir pressure $p(r \rightarrow \infty, t) = p_i$ (Lee, Rollins, & Spivey, 2003).

By using the Boltzmann transformation, the equation of the line-source solution to the diffusivity equation can be expressed by Equation 82 (Chaudhry, 2003).

$$m(p_D) = -\frac{1}{2}Ei\left(-\frac{{r_D}^2}{4t_D}\right) \quad (82)$$

The condition to apply the line-source solution is determined by Equation 83 in oilfield units.

$$\frac{(3.975 \times 10^5)\emptyset\mu c_t {r_w}^2}{k} < t < \frac{948\emptyset\mu c_t {r_e}^2}{k} \quad (83)$$

This condition means that at times exceeding the limit t value, the behavior of the reservoir as infinite-acting is no longer considered due to the boundaries effect.

The Ei function, can be approximated for values of $x \leq 0.01$ to:

$$Ei(-x) = \ln(1.781x) \quad (84)$$

Where Ei is the exponential integral and x is the argument given in oilfield units by:

$$x = -\frac{{r_D}^2}{4t_D} = -\frac{948\emptyset\mu c_t r^2}{kt} \quad (85)$$

If the value of the argument is $x > 0.01$, the value of $Ei(-x)$ can be obtained from data registered in tables and substituted in the line-source solution. If $x > 10$, the Ei function is considered zero. Since the behavior of the flow is influenced by the pressure drop near the wellbore, the bottomhole pressure at $r = r_w$ can be expressed by the logarithmic approximation for $x \leq 0.01$ (Lee, Rollins, & Spivey, 2003).

Dimensionless variables are used during the analysis of well tests. They should be defined to extend the solution to the diffusivity equation in dimensionless pressure drop.

The dimensionless pseudopressure can be determined by Equation 86 in gasfield units.

$$m(p_D) = \frac{m(p_i) - m(p_{wf})}{\left(\frac{1422 q_{sc} T}{kh}\right)} \quad (86)$$

Where $m(p_D)$ is the dimensionless pressure; k is the permeability, md; h is the thickness, ft; q_{sc} is the gas flow rate, Mscf/day; $m(p_i)$ is the initial pseudopressure, psia^2/cp; and $m(p_{wf})$ is the bottomhole pseudopressure, psia^2/cp. (Dake, 1978)

$$r_D = \frac{r}{r_w} \quad (87)$$

Where r_D is the dimensionless radius and it is equal to 1 at $r = r_w$.

$$r_{eD} = \frac{r_e}{r_w} \quad (88)$$

$$t_D = \frac{0.000264kt}{\emptyset \mu c_t {r_w}^2} \quad (89)$$

$$t_{DA} = \frac{0.000264kt}{\emptyset \mu c_t A} = t_D \frac{{r_w}^2}{A} = t_D \frac{{r_w}^2}{\pi {r_e}^2} \quad (90)$$

Where t_D is the dimensionless time; t_{DA} is the dimensionless time in terms of the drainage area; A is the reservoir area, ft^2; r_e is the radius of the reservoir, ft; $\emptyset$ is the porosity of the formation, %; c_t is the total compressibility of the system, 1/psi; r_w is the wellbore radius, ft; and t is the time, hours (Horne, 1990).

The dimensionless variables can be substituted in the diffusivity equation. Therefore, the line-source solution can be expressed in terms of dimensionless variables (Dake, 1978).

$$\frac{1}{r_D} \frac{\partial}{\partial r_D} \left(r_D \frac{\partial m(p_D)}{\partial r_D} \right) = \frac{\partial m(p_D)}{\partial t_D} \quad (91)$$

If the wellbore pressure is evaluated ($r_D = 1, t_D$), then:

$$m(p_D) = \frac{1}{2} \ln(t_D + 2.25) \quad (92)$$

Where:

$$r_D = \frac{r}{r_w} = \frac{r_w}{r_w} = 1 \quad (93)$$

For an infinite-acting radial flow conditions ($r_D = \infty$), p_D is a function of t_D, and for $t_D \geq 100$, the line-source solution can also be expressed by Equation 92. If the reservoir is finite, p_D is a function of t_D and r_D. Therefore, for $\frac{t_D}{{r_{eD}}^2} > 25$, the dimensionless pressure drop solution for a finite reservoir is given by Equation 94 (Ahmed & McKinney, 2005).

$$m(p_D) = \frac{1}{2}\ln\left(\frac{t_D}{{r_D}^2} + 2.25\right) \quad (94)$$

Where:

$$r_D = \frac{r}{r_w} = \frac{r_e}{r_w} \quad (95)$$

Therefore, the constant-terminal-rate solution to the diffusivity equation for gases can be expressed by Equation 96, in which the gas flow rate q_{sc} is evaluated at standard conditions of $p_{sc} = 14.7$ psia and $T_{sc} = 60$ °F.

$$m(p_{wf}) = m(p_i) - \frac{1422 q_{sc} T}{kh} \times \frac{1}{2}\left[\ln 2.25\left(\frac{0.000264kt}{\emptyset \mu c_t {r_w}^2}\right)\right] \quad (96)$$

In transient conditions for $t_D > 100$, the dimensionless pseudopressure is expressed as:

$$m(p_D) = \frac{1}{2}\ln(t_D + 2.25) \quad (97)$$

Equation 97 can also be expressed as:

$$m(p_{wf}) = m(p_i) - \left(\frac{1637 q_{sc} T}{kh}\right)\left[log\left(\frac{kt}{\emptyset \mu c_t {r_w}^2}\right) - 3.23\right] \quad (98)$$

The dimensionless pseudopressure is then given by:

$$m(p_D) = 1.151 \log(t_D + 2.25) \quad (99)$$

Where p_{wf} is the bottomhole pressure, psi; p_i is the initial reservoir pressure, psi; $q_{g,sc}$ is the gas flow rate at standard conditions, Mscf/day; T is the reservoir temperature, °R; k is the permeability, md; h is the thickness, ft; $\emptyset$ is the porosity; r_w is the wellbore radius, ft; c_t is the

total compressibility estimated at p_i, 1/psi; μ is the gas viscosity estimated at p_i, cp; and t is the time, hours (Dake, 1978).

The diffusivity equation solved for gas wells must include the apparent skin, also called pseudo-skin, since the gas flow near the wellbore occurs at high velocities that causes an additional pressure drop due to turbulence effects. Therefore, the apparent skin factor describes both the wellbore damage due to skin effect and the non-Darcy flow due to turbulence effects. This is defined by Equation 100.

$$s' = s + Dq_{sc} \quad (100)$$

The skin factor, s, is referred to the wellbore damage caused by the operations of drilling or completion, which leads to a reduction of the formation permeability near the wellbore called the skin zone, and subsequently an additional pressure reduction in the formation. The skin factor can be expressed as:

$$s = \left[\frac{k}{k_{skin}} - 1\right] ln\left(\frac{r_{skin}}{r_w}\right) \quad (101)$$

If the skin factor is $s > 0$, there is wellbore damage; if it is $s < 0$, a stimulation treatment or hydraulic fracture has been implemented; and if the skin factor is $s = 0$, no damage exists near the wellbore (ERCB, 1975). The pressure drop due to skin can be expressed as:

$$\Delta p_s = \Delta p_{actual} - \Delta p_{zero\ skin} \quad (102)$$

Where Δp_s is the additional pressure drop due to skin effect; Δp_{actual} is the pressure drop if skin exists in the zone near the wellbore; and $\Delta p_{zero\ skin}$ is the pressure drop if no skin would be present (Lee, Rollins, & Spivey, 2003).

The concept of flow efficiency is sometimes used to estimate the theoretical flow rate if the skin were removed (Horne, 1990).

$$FE = \frac{m(p_i) - m(p_{wf}) - m(\Delta p_{skin})}{m(p_i) - m(p_{wf})} \quad (103)$$

Where Δp_{skin} is the pressure drop due to skin (Ikoku, 1984).

The non-Darcy coefficient is represented by D, and the product Dq_{sc} is the rate-dependent skin. As the fluid flow is moving radially to the wellbore the flow velocity increases, and turbulent flow is observed affecting the response of the well. This causes an additional pressure drop, which is known as the non-Darcy flow due to turbulence effects. This effect is added to the Darcy's flow equation, replacing it, and giving rise to the Forchheimer's equation:

$$\frac{\partial p}{\partial r} = \frac{\mu}{k} v + \beta \cdot \rho \cdot v^2 \quad (104)$$

Where β is the turbulence factor which is a function of permeability and porosity $\beta(k, \emptyset)$. The non-Darcy flow can be handled by using the rate-dependent skin Dq_{sc} or by numerical modelling introducing the Forchheimer's equation (Houzé, Viturat, & Fjaere, 1988-2020).

Finally, by introducing the apparent skin to the diffusivity equation for gas wells in transient conditions, the solution is determined by:

$$m(p_{wf}) = m(p_i) - \frac{1422 q_{sc} T}{kh} \times \frac{1}{2}\left[\ln 2.25 \left(\frac{0.000264 kt}{\emptyset \mu c_t {r_w}^2}\right) + 2s'\right] \quad (105)$$

Or expressed as:

$$m(p_{wf}) = m(p_i) - \left(\frac{1637 q_{g,sc} T}{kh}\right)\left[log\left(\frac{kt}{\emptyset \mu c_t {r_w}^2}\right) - 3.23 + 0.87 s'\right] \quad (106)$$

And the dimensionless pseudopressure as a function of time can be expressed by Equation 107 (Lee, Rollins, & Spivey, 2003).

$$m(p_D) = \frac{1}{2}\ln(t_D + 2.25) + s + Dq_{sc} \quad (107)$$

Pressure transient ends when the effects of the boundaries are present, and pseudosteady-state conditions begin. After reaching this condition the pressure change is constant over time. Therefore, the solution to the diffusivity equation leads to the definition of

a new boundary condition. Since the reservoir is no longer infinite-acting, the radius is at the outer boundary, $r = r_e$, no-flow boundary (Terry & Rogers, 2015).

$$m(p_D) = \frac{1}{2}\ln 2.25\left(\frac{A}{C_A r_w{}^2}\right) + 2\pi\left(\frac{kt}{\emptyset\mu c_t A}\right) + s' \quad (108)$$

Where A is the drainage area, ft^2; and C_A is the reservoir shape factor. The product $\emptyset\mu A$ indicates the pore volume (Dake, 1978).

For a circular radial system with a drainage area equal to $A = \pi r^2$ and shape factor equal to $C_A = 31.62$, the solution for gas flow under pseudosteady-state conditions considering the apparent skin factor is given by Equation 109.

$$m(p_{wf}) = m(\bar{p}) - \left(\frac{1422 q_{sc} T}{kh}\right)\left[ln\left(\frac{r_e}{r_w}\right) - 0.75 + s'\right] \quad (109)$$

Where $\bar{p}$ is the average reservoir pressure, psi; q_{sc} is the gas flow rate at standard conditions, Mscf/day; and T is the reservoir temperature, °R.

For steady-state conditions Equation 110 is given (Ahmed & McKinney, 2005). In steady-state conditions the change in pressure with time is zero and a new boundary condition is determined for the solution to the diffusivity equation. This is known as constant-pressure boundary, since at time t the pressure at the external boundary is equal to the initial reservoir pressure ($p = p_i$) at $(r = r_e)$ (Lee, Rollins, & Spivey, 2003).

$$m(p_{wf}) = m(p_i) - \left(\frac{1422 q_{g,sc} T}{kh}\right)\left[ln\left(\frac{r_e}{r_w}\right) - 0.5 + s'\right] \quad (110)$$

3.5 Wellbore Storage

Due to the fact that the flowing rate of a well is controlled at surface, at the wellhead, the effects of wellbore storage may affect the constant flowing rate from the formation, q_f, since the wellbore, q_w, is also contributing to the production due to the storage effect. Wellbore storage can be caused by the expansion of the fluid or by the change of the fluid level in the wellbore. When a well is open to production, the pressure in the well will drop, and this will

cause that the fluid expands in the wellbore. Therefore, the initial period of production will be due to the fluid occupying the wellbore volume. If the wellbore is filled with the fluid before producing, at the time the well is open to flow the liquid level in the wellbore will change and will fall and combine with the production from the formation, contributing to the total production from the well; this depends mainly on the position of the packer and its effect is small. The total production at surface can be expressed as:

$$q = q_f + q_w \quad (111)$$

Where q_f is the production from the formation and q_w is the production from the wellbore (Horne, 1990).

If wellbore storage is attributed to the expansion of the fluids, wellbore storage can be represented by Equation 112.

$$C = \frac{\Delta V_{wb}}{m(p_i) - m(p_{wf})} = V_{wb} c_{wb} \quad (112)$$

Where C is the wellbore storage coefficient, for gas wells, MCF/psi; ΔV_{wb} is the change of the fluid volume in wellbore, MCF; $m(p_i) - m(p_{wf})$ is the pressure drop, psi^2/cp; V_{wb} is the total fluid volume in the wellbore, ft^3; and c_{wb} is the compressibility of the fluid in the wellbore 1/psi. In case of gas wells, due to the large compressibility of the fluid, fluid expansion will highly contribute to the storage effect.

The dimensionless wellbore storage coefficient is usually preferred to estimate the duration of the effects of wellbore storage. This can be expressed by Equation 113.

$$C_D = \frac{5.615C}{2\pi h \emptyset c_t {r_w}^2} = \frac{0.8936C}{h \emptyset c_t {r_w}^2} \quad (113)$$

Pure wellbore storage effect occurs at early time (Bourdet, Ayoub, & Plrard, 1989), the wellbore pressure during wellbore storage can be expressed in dimensionless terms.

$$p_D = \frac{t_D}{C_D} \quad (114)$$

Equation 114 expressed in logarithmic form gives:

$$\log(p_D) = \log(t_D) - \log(C_D) \quad (115)$$

A plot with the $\log(p_i - p_{wf})$ vs $\log(\Delta t)$ will result in a unit slope $\frac{C_D p_D}{t_D} = 1$ that is of a great aid to identify wellbore storage effects at early transient flow (Lee, 1982). The end of wellbore storage effects can be determined at:

$$t_D > (60 + 3.5s)C_D \quad (116)$$

Where s is the skin factor (Ahmed & McKinney, 2005); and the pressure response for the IARF is given by:

$$p_D = \frac{1}{2}\left[ln\left(\frac{t_D}{C_D}\right) + 0.81 + lnC_D e^{2s}\right] \quad (117)$$

Where $C_D e^{2s}$ represents the condition of the well with wellbore storage and skin (Bourdet, Ayoub, & Plrard, 1989).

3.6 Radius of Investigation

The distance that a pressure disturbance has reached in the reservoir after a flow rate change in a well is known as the radius of investigation, r_i. The radius of investigation is a function of the formation and fluid properties, and the elapsed time after the flow rate change. When producing a well, the pressure transient propagates into the reservoir. First, the pressure decreases at wellbore level, then as the flow time increases, the pressure at other distances r into the reservoir decreases as well. Therefore, for a certain flow time t, the pressure transient or pressure disturbance reaches a certain distance r_i, which is the radius of investigation determined by Equation 118 in consistent units.

$$r_i = \sqrt{\frac{kt}{948\emptyset\mu c_t}} \quad (118)$$

Where r_i is the radius of investigation, m; assuming a homogeneous, cylindrical, and isotropic reservoir.

The radius of investigation is useful to understand the shape of pressure buildup curves. For instance, at early flow times the buildup curve is affected by skin and wellbore storage effects; and at long times the shape of the buildup curve may change due to boundaries or heterogeneities reached by the radius of investigation.

From Equation 118, the time t necessary to test a well to investigate the formation properties at a distance r in the reservoir is given by Equation 119.

$$t = \frac{948\emptyset\mu c_t {r_i}^2}{k} \quad (119)$$

Where r_i can be assumed twice the proposed value for safety reasons.

Hence, the time to reach stabilization expressed by Equation 120, represents the beginning of pseudosteady-state flow in which the pressure disturbance reaches the boundaries at $r_i = r_e$ (Lee, 1982).

$$t_s = \frac{948\emptyset\mu c_t {r_e}^2}{k} \quad (120)$$

3.7 Superposition

Superposition is seen as the sum of the individual components that take part to a total system. Therefore, the sum of individual solutions to the diffusivity equation for one well, can be the solution to the diffusivity equation in case of multiple wells. The effects of multiple wells, boundaries, rate change and pressure change on the solution to the diffusivity equation for transient flow can be handled by superposition (Ahmed & McKinney, 2005). Multiple wells and boundaries are addressed by applying superposition in space, while rate and pressure changes are solved by superposition in time.

3.7.1 Multiple Wells

Reservoirs are produced by more than one well. If each of these wells produces at a different constant rate q, the bottomhole pressure p_{wf} in one well is affected by its own production and the production of the other wells. Therefore, the pressure drop Δp in that well is equal to the sum of the individual pressure drops due to the other wells. Figure # shows a system with three wells A, B, and C. The pressure drop in well A due to wells B and C is expressed by Equation 121.

$$(p_i - p_{wf})_A = (p_i - p_{wf})_A + (p_i - p_{wf})_B + (p_i - p_{wf})_C \quad (121)$$

By developing Equation 121, the pressure drop in well A would be given by Equation 122 (Lee, Rollins, & Spivey, 2003).

$$\begin{aligned} \Delta m(p)_{Total\ at\ well\ A} &= \left(\frac{1637 q_{sc} T}{kh}\right)\left[log\left(\frac{kt}{\emptyset \mu c_t {r_w}^2}\right) - 3.23 + 0.87s\right] \\ &- \left(\frac{711 q_{sc} T}{kh}\right)\left[\mathrm{Ei}\left(-\frac{948 \emptyset \mu c_t {r_{AB}}^2}{kt}\right)\right] \\ &- \left(\frac{711 q_{sc} T}{kh}\right)\left[\mathrm{Ei}\left(-\frac{948 \emptyset \mu c_t {r_{AC}}^2}{kt}\right)\right] \end{aligned} \quad (122)$$

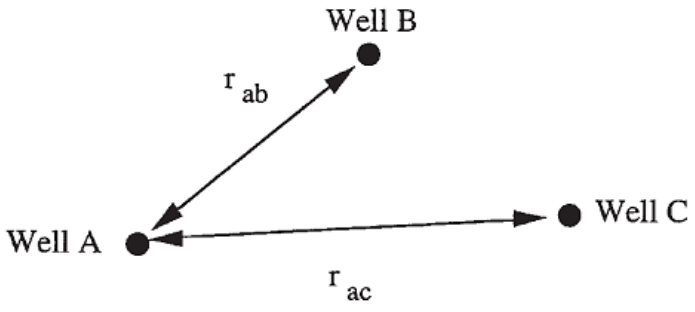

Figure 25: *System of Multiple Wells.*

Note. Adapted from *Wellbore pressure in a multiwell system* (p. 18) by John Lee, John B. Rollins, & John P. Spivey, 2003, Society of Petroleum Engineers.

The pressure drop or pressure drawdown in well A is calculated by using the logarithmic approximation of the Ei-function, since the pressure drop is because of its own production (r_w). The pressure drops in the other wells are calculated by using the Ei-function solution, since larger distances are considered (r) (Smith, 1990). Additionally, the skin factor, s, is added to the to calculation of the pressure drop in well A, as the damaged zone near well A affects the pressure evaluation. However, the damaged zones of the other wells do not affect the evaluation of the pressure at well A (Lee & Wattenbarger, 1996).

Superposition to solve the effects of multiple wells is used in interference tests, in which one of the wells is an observation well with no flowing rate, and the interference produced by the other wells is measured in the observation well. Additionally, if a new well is to be drilled in the field, the pressure in this well can be predicted by applying this concept (Chaudhry, 2003).

3.7.2 Boundary Effects

No-flow boundaries or sealing faults can be addressed by superposition using the method of images. This method states that an imaginary well is located at the same distance r from the boundary as the actual producing well, and that it is producing at the same rate as the actual well (Lee, Rollins, & Spivey, 2003). This is represented on Figure 26. Therefore, the pressure can be evaluated by considering the effects of the boundary as if it is the imaginary well located at a distance $2r$. This can be expressed by Equation 123, where the pressure drop at the actual well is the sum of the pressure drop caused by its own production, and the pressure drop of the image well (Ahmed, 2019).

$$\left(p_i - p_{wf}\right)_{actual} = \left(p_i - p_{wf}\right)_{actual} + \left(p_i - p_{wf}\right)_{image} \quad (123)$$

This can be developed to give Equation 124 (Ahmed & McKinney, 2005).

$$\Delta m(p)_{Total} = \left(\frac{1637 q_{actual} T}{kh}\right)\left[log\left(\frac{kt}{\emptyset \mu c_t {r_w}^2}\right) - 3.23 + 0.87s\right] - \left(\frac{711 q_{image} T}{kh}\right)\left[\mathrm{Ei}\left(-\frac{948 \emptyset \mu c_t (2L)^2}{kt}\right)\right] \quad (124)$$

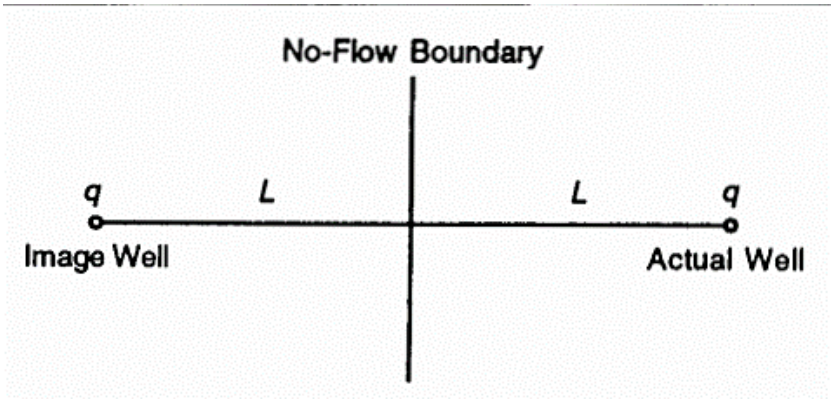

Figure 26: *Boundary effects by an image well.*

Note. Adapted from *Image-well technique for a well near a no-flow boundary* (p. 101) by John Lee & Robert A. Wattenbarger, 2003, Society of Petroleum Engineers.

3.7.3 Variable-Rate History

For producing wells with variable flow rates, the sum of each pressure change due to each changing flow rate will result in the total pressure change in the well. This can be expressed by Equation 125, in which the pressure in the producing well p_{wf} is due to three variable rates q_1, q_2, q_3 for a time t, as represented on Figure 27 (Smith, 1990).

$$\left(p_i - p_{wf}\right)_T = \left(p_i - p_{wf}\right)_{q_1 - 0} + \left(p_i - p_{wf}\right)_{q_2 - q_1} + \left(p_i - p_{wf}\right)_{q_3 - q_2} \quad (125)$$

The concept of superposition in space and time can be applied to fields with multiple wells producing with multiple rates (Lee, 1982). By further developing the concept in the previous equation, Equation 126 is given (Ahmed & McKinney, 2005).

$$\Delta m(p)_{Total} = \left(\frac{1637 q_1 T}{kh}\right)\left[log\left(\frac{kt}{\emptyset \mu c_t {r_w}^2}\right) - 3.23 + 0.87s\right]$$
$$+ \left(\frac{1637(q_2 - q_1)T}{kh}\right)\left[log\left(\frac{k(t - t_1)}{\emptyset \mu c_t {r_w}^2}\right) - 3.23 + 0.87s\right] \quad (126)$$
$$+ \left(\frac{1637(q_3 - q_2)T}{kh}\right)\left[log\left(\frac{k(t - t_2)}{\emptyset \mu c_t {r_w}^2}\right) - 3.23 + 0.87s\right]$$

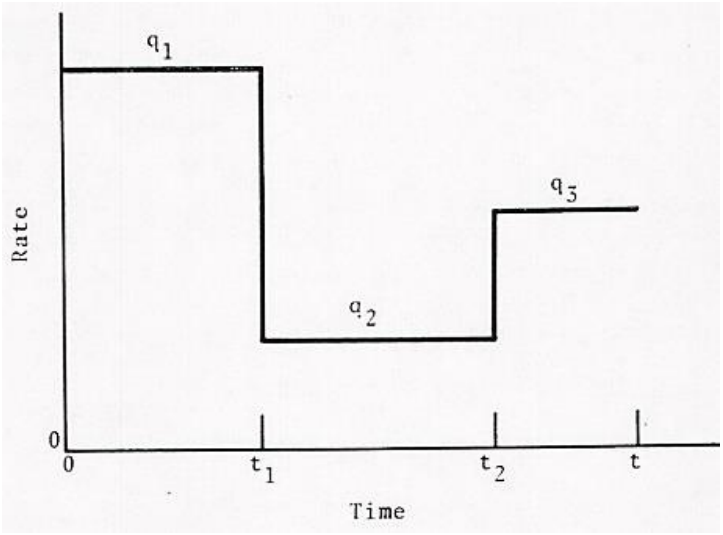

Figure 27: *Variable-Rate History.*

Note. Adapted from *Rate history of a variable rate well* (pp. 2-63) by James T. Smith, 1990, Self-published.

3.8 The Analysis of Deliverability Tests

Conventional deliverability tests require at least one stabilized flowing condition. At this point there is no longer change in pressure with time, the transient regime reaches a no-flow boundary and pseudosteady-state conditions are observed. During this regime, the average pressure $\bar{p}$ decreases linearly, and $\mu\ c_t$ changes as a function of $\bar{p}$. At this point the radius of investigation has reached the external radius of the reservoir, and the stabilization time can be determined (Lee & Wattenbarger, 1996). Recalling Equation 120:

$$t_s = \frac{948\emptyset\mu c_t {r_e}^2}{k} \quad (120)$$

Rawlins and Schellhardt (1935) presented an empirical equation to analyze gas well deliverability and determine the AOF potential of the well. Assumming radial flow and in terms of pseudopressure function, this equation known as the backpressure equation is expressed as:

$$q_{sc} = C\left[m(\bar{p}) - m(p_{wf})\right]^n \quad (127)$$

Equation 127 can be expressed in logarithmic form as:

$$log(q_{sc}) = log(C) + n\{log\left[m(\bar{p}) - m(p_{wf})\right]\} \quad (128)$$

Where q_{sc} is the gas flow rate at standard conditions, Mscf/day; C is the performance coefficient, Mscf/day/psi^2/cp; and n is the exponent that indicates if the flow is turbulent (0.5) or laminar (1), the range is $0.5 < n < 1$.

The plot of $log\left[m(\bar{p}) - m(p_{wf})\right]$ vs $log(q_{sc})$ (see Figure 28) will give a straight line with slope $1/n$, from which the exponent n can be calculated.

The performance coefficient C can be calculated by:

$$C = \frac{q_{sc}}{\left[m(\bar{p}) - m(p_{wf})\right]^n} \quad (129)$$

The absolute open flow (AOF) potential is the volume of gas that would be produced per day is the pressure against the sand face would be a base pressure such as the atmospheric pressure (14.7 psi). The AOF can be read from the plot or calculated by Equation 130.

$$q_{sc,AOF} = C[m(\bar{p}) - m(p_{base})]^n \quad (130)$$

Where $m(p_{base})$ is in terms of a base pressure, such as the atmospheric pressure; and $q_{sc,AOF}$ is the theoretical rate (AOF) at the base pressure, Mscf/day (Lee & Wattenbarger, 1996).

Houpeurt (1959) developed theoretical quadratic equations to evaluate the deliverability of a gas well from the radial diffusivity equation. The equation in transient conditions is determined by:

$$m(p_s) - m(p_{wf}) = 1637\frac{T}{kh}\left(log\frac{k\Delta t}{\emptyset\mu c_t {r_w}^2} - 3.23 + 0.87s\right)q_{sc} + 1422\frac{T}{kh}D{q_{sc}}^2 \quad (131)$$

Where p_s is the stabilized bottomhole pressure, which is equal to the initial pressure for new reservoirs, and lower than the initial pressure for reservoirs already developed. The quadratic expression of this equation is given by:

$$\Delta m(p) = a(t)q_{sc} + b{q_{sc}}^2 \quad (132)$$

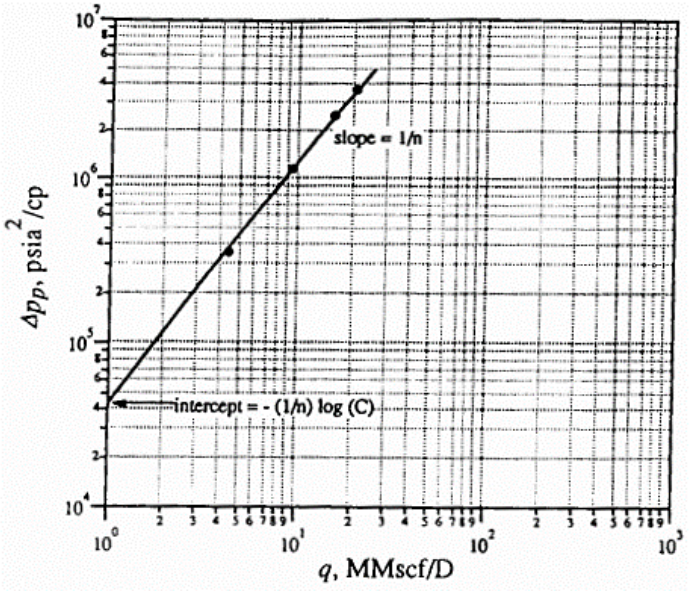

Figure 28: *The empirical relationship of Rawlins and Schellhardt (1935).*

Note. Adapted from *Analysis-Example 7.1* (p. 173) by John Lee & Robert A. Wattenbarger, 2003, Society of Petroleum Engineers.

In pseudosteady-state conditions, the equation is expressed as:

$$m(\bar{p}) - m(p_{wf}) = 1637\frac{T}{kh}\left(log\frac{A}{C_A {r_w}^2} + 0.85 + 0.87s\right)q_{sc} + 1422\frac{T}{kh}D{q_{sc}}^2 \quad (133)$$

Where $\bar{p}$ is the average pressure. The quadratic expression for the pseudosteady-state regime is given by:

$$\Delta m(p) = aq_{sc} + b{q_{sc}}^2 \quad (134)$$

A plot on Cartesian coordinates of $\frac{m(\bar{p})-m(p_{wf})}{q_{sc}}$ vs q_{sc} will exhibit a best-fit line with points at higher rates from which the values of a (intercept) and b (slope) can be obtained (Lee & Wattenbarger, 1996).

$$a = \left(\frac{\Delta m(p)}{q}\right)_1 - bq_1 \quad (135)$$

$$b = \frac{\left(\frac{\Delta m(p)}{q}\right)_2 - \left(\frac{\Delta m(p)}{q}\right)_1}{q_2 - q_1} \quad (136)$$

The AOF can be determined by solving the quadratic equation in pseudosteady-state flow regime (Bourdet, 2002).

$$q_{sc,AOF} = \frac{-a + \sqrt{a^2 + 4b[m(\bar{p}) - m(p_{base})]}}{2b} \quad (137)$$

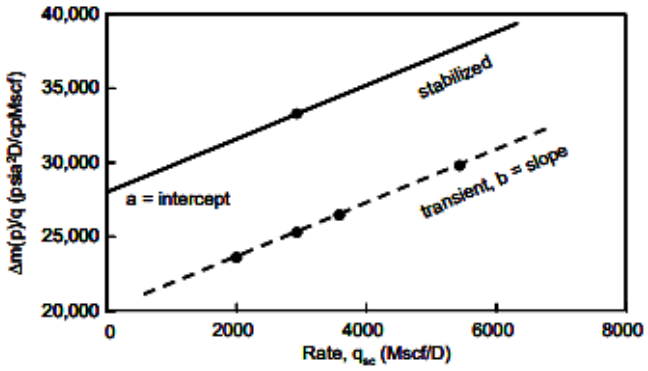

Figure 29: *Houpeurt plot.*

Note. Adapted from *Deliverability plot for an isochronal or a modified isochronal test. Linear scale, pseudo-pressure method* (p. 315) by Dominique Bourdet, 2002, Elsevier.

3.9 Analysis of Pressure Drawdown Tests

3.9.1 The semilog approach

Production of gas wells occurs normally under variable flow rates or at constant wellhead pressure (Tiab, 2000). To conduct a drawdown test, the well is previously shut-in to have a uniform pressure throughout the reservoir, then the well is open to produce at a constant rate. During the flow period the bottomhole pressure is measured as a function of time. Permeability, skin, and reservoir volume can be evaluated from drawdown tests (Lee, 1982). The diffusivity equation for gas flow under transient conditions producing at a single constant rate is used to describe the pressure drawdown in the wellbore:

$$m(p_{wf}) = m(p_i) - \left(\frac{1637 q_{sc} T}{kh}\right)\left[log\left(\frac{kt}{\emptyset \mu c_t {r_w}^2}\right) - 3.23 + 0.87 s'\right] \quad (138)$$

Where μ and c_t are evaluated at the initial reservoir pressure. By rearranging Equation 138 to the equation of the straight line $m(p_{wf}) = b + mt$:

$$m(p_{wf}) = m(p_i) - \left(\frac{1637 q_{sc} T}{kh}\right)\left[log\left(\frac{k}{\emptyset \mu c_t {r_w}^2}\right) - 3.23 + 0.87 s'\right] - \left(\frac{1637 q_{g,sc} T}{kh}\right) log\ t$$

A plot of $m(p_{wf})$ vs $log\ t$ (see Figure 30) will allow to estimate the permeability k from the slope of the line m, and to obtain the apparent skin s'.

$$m = \frac{1637 q_{sc} T}{kh} \quad (139)$$

$$s' = s + D q_{sc} = 1.151\left[\frac{m(p_i) - m(p_{wf})_{t=1h}}{m} - log\left(\frac{k}{\emptyset \mu c_t {r_w}^2}\right) + 3.23\right] \quad (140)$$

Where $m(p_{wf})_{t=1h}$ is obtained from the straight line of the semilog plot or is extrapolated if necessary (Lee & Wattenbarger, 1996).

The pseudopressure drop due to the apparent skin effect is given by Equation 141, and the flow efficiency is expressed by Equation 103 (Ikoku, 1984).

$$m(\Delta p_{skin}) = 0.87|m|s' \quad (141)$$

$$FE = \frac{m(p_i) - m(p_{wf}) - m(\Delta p_{skin})}{m(p_i) - m(p_{wf})} \quad (103)$$

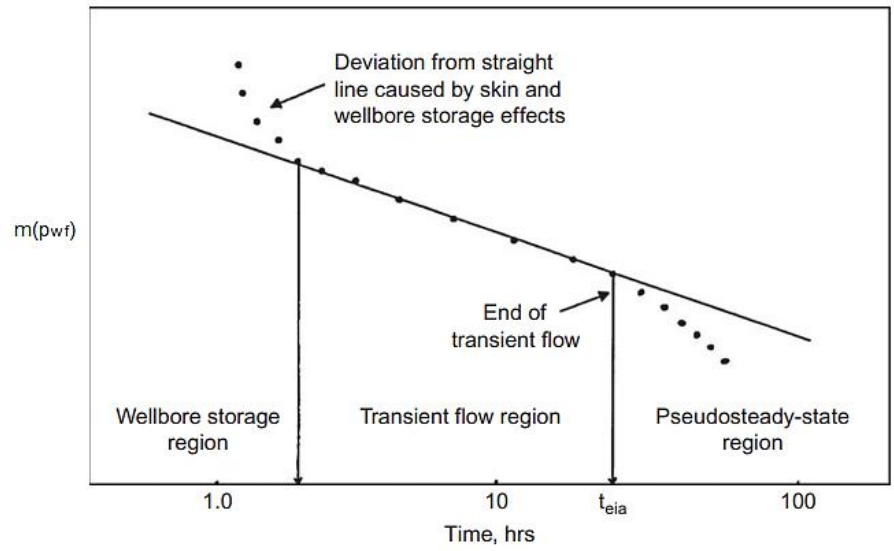

Figure 30: *Semilog plot of drawdown tests.*

Note. Adapted from *Semilog plot of pressure drawdown data* (p. 434) by Tarek Ahmed, 2019, Elsevier.

This assumes that the non-Darcy flow coefficient is constant. However, it depends on gas viscosity, since the viscosity of the gas changes as a function of pressure, and the pressure near the wellbore decreases (Lee, Rollins, & Spivey, 2003). Due to the fact that the apparent skin factor s' comprises the mechanical skin s and the rate-dependent skin Dq_{sc}, the drawdown test of a gas well must have at least two flow rates to differentiate both skins (Dake, 1978).

$$s_1' = s + Dq_{sc1} \quad (142)$$

$$s_2' = s + Dq_{sc2} \quad (143)$$

As an alternative, a plot of s' vs q_{sc} will give a straight line from which the non-Darcy coefficient D is obtained from the slope, and the skin factor s is obtained from the intercept on $q_{sc} = 0$ (Chaudhry, 2003).

For a gas well with a production history of variable rates in transient conditions, the method of superposition in time is applied. Therefore,

$$\frac{m(p_i) - m(p_{wf})}{q_n} = m' \sum_{j=1}^{n} \left[\frac{(q_j - q_{j-1})}{q_n} log(t_n - t_{j-1}) \right] + m' \left[log\left(\frac{k}{\emptyset \mu c_t {r_w}^2} \right) - 3.23 + 0.87 s' \right] \quad (144)$$

A plot on Cartesian coordinates of the pseudopressure function $\frac{m(p_i) - m(p_{wf})}{q_n}$ vs the time rate function $\sum_{j=1}^{n} \frac{(q_j - q_{j-1})}{q_n} log(t_n - t_j)$ will give a straight line with slope m', from which the flow capacity kh can be determined, or if the formation thickness h is known, the permeability k can be estimated:

$$m' = \frac{1637T}{kh} \quad (145)$$

Where $m(p_i)$ is the initial pseudopressure, psia^2/cp; $m(p_{wf})$ is the bottomhole pressure at t_n, psi^2/cp; q_n is the last of n production rates, Mscf/day; t_n is the cumulative flowing time for n flow periods at constant rate, hours; and t_j is the time of rate change, hours (Lee & Wattenbarger, 1996).

The apparent skin ${s_n}'$ due to the flow rate q_n can be determined by:

$${s_n}' = s + Dq_n = 1.151 \left[\frac{1}{m'} \left(\frac{m(p_i) - m(p_{wf})}{q_n} \right) - \log\left(\frac{k}{\emptyset \mu c_t {r_w}^2} \right) + 3.23 \right] \quad (146)$$

If the drawdown test is long enough to reach pseudosteady-state conditions (boundary-dominated flow), the equation can be expressed as:

$$\frac{m(p_i) - m(p_{wf})}{q_{sc}} = \frac{\Delta m(p)}{q_{sc}} = \frac{711T}{kh}\left(\ln 2.25\frac{A}{C_A {r_w}^2} + s\right) + \left[\frac{2.356T}{\mu c_t \emptyset Ah}\right]t \quad (147)$$

Equation 147 can be rearranged to a linear equation $\frac{\Delta m(p)}{q_{sc}} = b + mt$. A plot on Cartesian coordinates of $\frac{\Delta m(p)}{q_{sc}}$ vs t will exhibit a straight line from which the slope m and intercept b can be obtained. The drainage volume can be obtained from the slope (Ahmed & McKinney, 2005).

$$m_{pss} = \frac{-2.356T}{\mu c_t \emptyset Ah} \quad (148)$$

$$b_{pss} = \frac{711T}{kh}\left(\ln\frac{2.25A}{C_A {r_w}^2} + s\right) \quad (149)$$

By including the non-Darcy flow coefficient and applying the principle of superposition in time, the equation can be expressed as:

$$\frac{m(p_i) - m(p_{wf_n}) - D{q_n}^2}{q_n} = \frac{2.356T}{\mu c_t \emptyset Ah}\sum_{j=1}^{n}\frac{q_j}{q_n}\Delta t_j + \frac{711T}{kh}\left(ln\frac{2.25A}{C_A {r_w}^2} + s\right) \quad (150)$$

A plot of $\frac{m(p_i) - m(p_{wf_n}) - D{q_n}^2}{q_n}$ vs $\sum_{j=1}^{n}\frac{q_j}{q_n}\Delta t_j$ will form a straight line from which m_{pss} and b_{pss} can be obtained. Since $D{q_n}^2$ should be known, an approximation can be obtained from:

$$m(p_i) - m(p_{wf}) = \frac{711 q_{sc} T}{kh}\left(ln\frac{2.25A}{C_A {r_w}^2} + s\right) + D{q_{sc}}^2 \quad (151)$$

Which can be expressed as:

$$m(p_i) - m(p_{wf}) = Bq_{sc} + D{q_{sc}}^2 \quad (152)$$

Where p_i is assumed to be equal to $\bar{p}$; B is the Darcy coefficient, and D is the non-Darcy flow coefficient. Therefore, the plot of $\frac{m(p_i) - m(p_{wf_n})}{q_n}$ vs q_n will give a straight line with slope D and intercept B. The value of the slope D can be modified or decreased until reaching a linear plot of $\frac{m(p_i) - m(p_{wf_n}) - D{q_n}^2}{q_n}$ vs $\sum_{j=1}^{n}\frac{q_j}{q_n}\Delta t_j$ (Dake, 1978).

3.10 Analysis and Interpretation of Pressure Buildup Tests

Buildup tests allow to determine the pressure buildup in the wellbore with time when the well is shut in. This pressure transient test is useful for the determination of the static pressure of the reservoir, formation permeability, extent of the skin zone, and the effects of heterogeneities and boundaries such as faults, interference between wells, and reservoir limits. Buildup tests are conducted by firstly flowing the well at a constant rate for a production time t_p until reaching stabilization. The bottomhole pressure is measured at t_p, and the well is shut in for a time elapsed Δt (Lee, 1982). The bottomhole pressure during the buildup is measured as a function of time (Ahmed & McKinney, 2005).

The analysis of a pressure buildup is based on the method of superposition in time. The first drawdown is caused by a constant flowing rate and the second drawdown by a constant rate equal to zero. Despite the fact that superposition is applied for single-phase fluids and slightly compressibles, the method can also be applied to gas flow (Reynolds, Bratvold, & Ding, 1987). The superposition of the two solutions gives a single equation known as the Horner equation (Horner, 1951). For gas flow, the Horner equation can be expressed for an infinite-acting reservoir as:

$$m(p_{ws}) = m(p_i) - \left(\frac{1637 q_{sc} T}{kh}\right)\left[log\left(\frac{t_p + \Delta t}{\Delta t}\right)\right] \quad (153)$$

Where $m(p_{ws})$ is the bottomhole shut-in pressure.

A plot of $m(p_{ws})$ vs $log\left(\frac{t_p+\Delta t}{\Delta t}\right)$ will form a straight line with a negative slope m from which permeability can be calculated. This is known as Horner plot (see Figure 31) and the shape of the buildup data at early time may be affected by wellbore storage and skin. The straight line can be extrapolated to a Horner time equal to 1 to estimate the extrapolated pressure p^* that is equal to the initial reservoir pressure for a new well. (Terry & Rogers, 2015).

$$m = \frac{-1637 q_{sc} T}{kh} \quad (154)$$

The apparent skin can be calculated from:

$$s' = s + Dq_{sc} = 1.151 \left[\frac{m(p_{1\,hour}) - m(p_{wf})_{\Delta t=0}}{|m|} - log\left(\frac{k}{\emptyset \mu c_t {r_w}^2}\right) + 3.23 \right] \quad (155)$$

Where $m(p_{1\,hour})$ is the pseudopressure value obtained from the straight line at 1 hour or extrapolated if necessary, and $m(p_{wf})_{\Delta t=0}$ is the bottomhole pseudopressure measured just before shut in (Ahmed & McKinney, 2005).

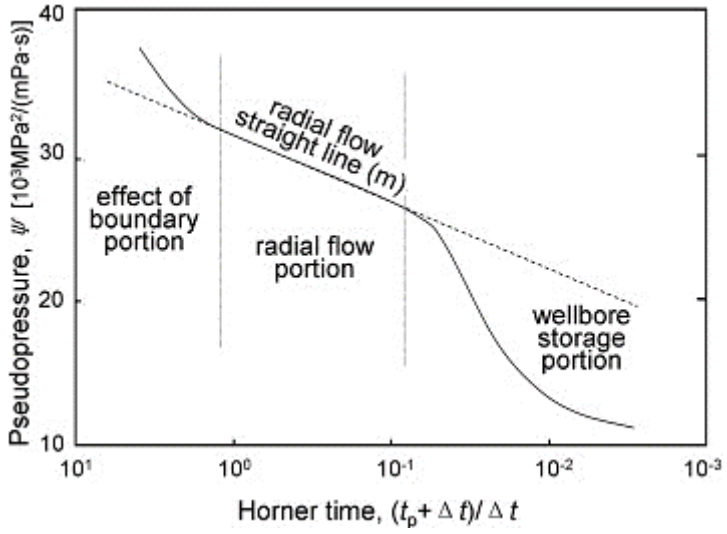

Figure 31: *Horner plot.*

Note. Adapted from *Another Horner pressure buildup curve* by HuiNong Zhuang, 2013, ScienceDirect (https://www.sciencedirect.com/topics/engineering/ horner-plot)

For a well producing long enough to reach pseudosteady-state conditions before shutting in, the Horner method used for an infinite-acting reservoir is no longer applied, it requires to correct the false pressure p^* (Hasan & Kabir, 1983) after reaching the boundaries, the pressure decreases throughout the reservoir. Although the slope of the Horner plot is still used to determine the formation permeability (Lee, 1982). For finite-acting or bounded reservoirs, other methods such as the MDH method, the Ramey-Cobb method, the MBH

method, and the Dietz method can be implemented for the analysis of the late-transient data, to correct the false pressure p^*, and to estimate the average reservoir pressure $\bar{p}$ (Ahmed & McKinney, 2005).

The MDH method assumes that the flowing period is long enough to reach pseudosteady-state regime $t_p \gg \Delta t$. Then, $t_p + \Delta t \cong t_p$. Therefore, the Horner equation is modified to form the MDH equation:

$$m(p_{ws}) = m(p_i) - \left(\frac{1637 q_{sc} T}{kh}\right)\left[log\left(\frac{t_p}{\Delta t}\right)\right]$$

$$m(p_{ws}) = m(p^*) - mlog(t_p) + mlog(\Delta t) \quad (156)$$

A plot of $m(p_{ws})$ vs $log(\Delta t)$ will exhibit a straight line with a positive slope m of equal value as the Horner slope, from which permeability can be calculated. Since the intercept is given by $m(p^*) - mlog(t_p)$, the reservoir pseudopressure at shut-in time $\Delta t = 1\, hour$ can be calculated by using Equation 157 (Escobar, 2018).

$$m(p_{ws}) = m(p_{1\,hour}) + mlog(\Delta t) \quad (157)$$

To evaluate the average reservoir pressure $\bar{p}$, the knowledge of the reservoir shape and drainage area must be known. For instance, for a circular reservoir the shape factor is equal to $C_A = 31.62$ and the drainage area can be calculated as $A = \pi r^2$. If the reservoir configuration is different, then the shape factor C_A must be first evaluated and the drainage area A can be determined from the slope m_{pss} of the semilog analysis of the drawdown data given by Equation 148. The most widely used method is the MBH method and it proposes that at a given dimensionless producing time t_{pDA} based on the drainage area can be used to estimate the dimensionless MBH pressure $P_{D,MBH}$ from a MBH chart (Ahmed & Meehan, 2012).

$$t_{pDA} = \left[\frac{0.0002637k}{\emptyset \mu c_t A}\right] t_p \quad (158)$$

Using the pseudopressure approach for gases:

$$m(\bar{p}) = m(p^*) - \frac{|m|}{2.303} p_{D,MBH} \quad (159)$$

3.11 Log-Log Type-curves

To obtain a better interpretation of the pressure transient data, type-curves are used with the conventional drawdown and buildup methods. Type-curves are represented on log-log plots of dimensionless variables based on the flow solutions (see Figure 32) (Ahmed & McKinney, 2005). Therefore, a match of the actual response of the reservoir should be found with a type-curve by superposing the actual plot of the transient data with the type-curve plot (Agarwal, Al-Hussainy, & Ramey, 1970).

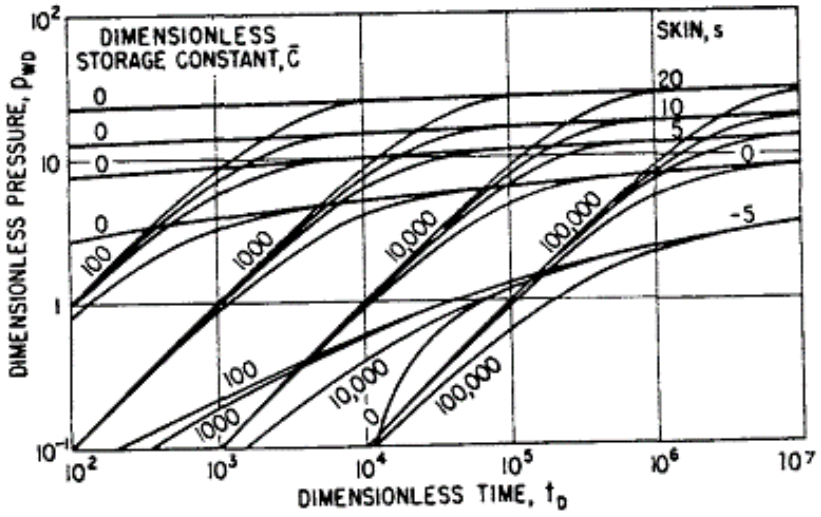

Figure 32: *Type-curves graph.*

Note. Adapted from p_{wD} *vs* t_D *for infinite radial system with storage and skin effect* (p. 286) by Ram G. Agarwal, Rafi Al-Hussainy & H.J. Ramey, Jr., 1970, Society of Petroleum Engineers Journal (https://doi.org/10.2118/2466-PA)

The use of the pseudotime function in conjunction with the pseudopressure function for the analysis of gas well tests with the use of type-curves is of great importance to account for the effects of the data distorted by wellbore storage effects during the early-transient period

(Lee & Wattenbarger, 1996). The pseudotime function was introduced by Agarwal (1979) to deal with the gas viscosity and the total compressibility variations with pressure and time.

$$t_a = \int_0^t \frac{dt}{\mu c_t} \quad (160)$$

Where t_a is the real gas pseudotime function, hour-psia/cp.

The dimensionless variables for gas flow are described by Equations 161 and 162.

$$m(p_D) = \frac{m(p_i) - m(p_{wf})}{\left(\frac{1422 q_{sc} T}{kh}\right)} \quad (161)$$

$$t_D = \frac{0.000264kt}{\emptyset \mu c_t {r_w}^2} \quad (162)$$

By taking the logarithm of the dimensionless variables:

$$log[m(p_D)] = log\left[m(p_i) - m(p_{wf})\right] + log\left(\frac{kh}{1422 q_{sc} T}\right) \quad (163)$$

And

$$log(t_D) = log(t) + log\left(\frac{0.000264k}{\emptyset \mu c_t {r_w}^2}\right) \quad (164)$$

This suggests that a plot of $log\left[m(p_i) - m(p_{wf})\right]$ vs $\log(t)$, that represents the actual data, will have the same shape as the plot of $log[m(p_D)]$ vs $\log(t_D)$, the theoretical type-curve, with a vertical shift given by $log\left(\frac{kh}{1422 q_{sc} T}\right)$ and a horizontal shift of $log\left(\frac{0.000264k}{\emptyset \mu c_t {r_w}^2}\right)$ from which reservoir properties can be estimated (Horne, 1990).

On the other hand, if the line-source solution to the diffusivity equation is considered to model the pressure response of the wellbore, then the type-curve will be given by plotting $log[m(p_D)]$ vs $\log\left(\frac{t_D}{{r_D}^2}\right)$.

Where:

$$\log\left(\frac{t_D}{{r_D}^2}\right) = \log(t) + log\left(\frac{0.000264k}{\emptyset \mu c_t r^2}\right) \quad (165)$$

Therefore, the type-curve matching between the actual data and the theoretical type-curve will occur at the match points given by Equations 166 and 167, from which the reservoir parameters including kh and $\emptyset c_t$ can be estimated (Ahmed & McKinney, 2005).

$$log\left(\frac{m(p_D)}{m(p_i)-m(p_{wf})}\right)_{MP} = log\left(\frac{kh}{1422q_{sc}T}\right) \quad (166)$$

And

$$log\left(\frac{t_D/{r_D}^2}{t}\right)_{MP} = log\left(\frac{0.000264k}{\emptyset\mu c_t r^2}\right) \quad (167)$$

To account for the effects of wellbore storage and skin during the early-transient period, Gringarten et al. (1979) presented a new type-curve, which for wellbore storage the dimensionless pressure for gas flow is expressed as:

$$m(p_D) = \frac{t_D}{C_D} \quad (168)$$

Where C_D is the dimensionless wellbore storage coefficient. By expressing Equation 168 in a logarithmic form:

$$log[m(p_D)] = log\,(t_D) - log(C_D) \quad (169)$$

Therefore, a plot of $log[m(p_D)]$ vs $log\,(t_D)$ will give a straight line of unit slope that represents wellbore storage. The radial flow at the end of wellbore storage is determined by:

$$m(p_D) = \frac{1}{2}\left[ln\left(\frac{t_D}{C_D}\right) + ln(2.25) + ln(C_D e^{2s})\right] \quad (170)$$

A plot of $log[m(p_D)]$ vs $log\left(\frac{t_D}{C_D}\right)$, as shown on Figure 33, exhibits the conditions of the well given by $C_D e^{2s}$, and the beginning of the radial flow to approximately one and a half log cycle after the end of wellbore storage effects. The time at which this effect ends can be determined by:

$$t_D > (60 + 3.5s)C_D \quad (171)$$

The type-curve matching for a drawdown test plotted as $log[m(p_i) - m(p_{wf})]$ vs $\log(t)$ will occur at the following match points determined by Equation 172 and Equation 173 (Ahmed & Meehan, 2012).

$$log\left(\frac{m(p_D)}{m(p_i) - m(p_{wf})}\right)_{MP} = log\left(\frac{kh}{1422 q_{sc} T}\right) \quad (172)$$

And

$$log\left(\frac{t_D/C_D}{t}\right)_{MP} = log\left(\frac{0.0002951k}{\mu C}\right) \quad (173)$$

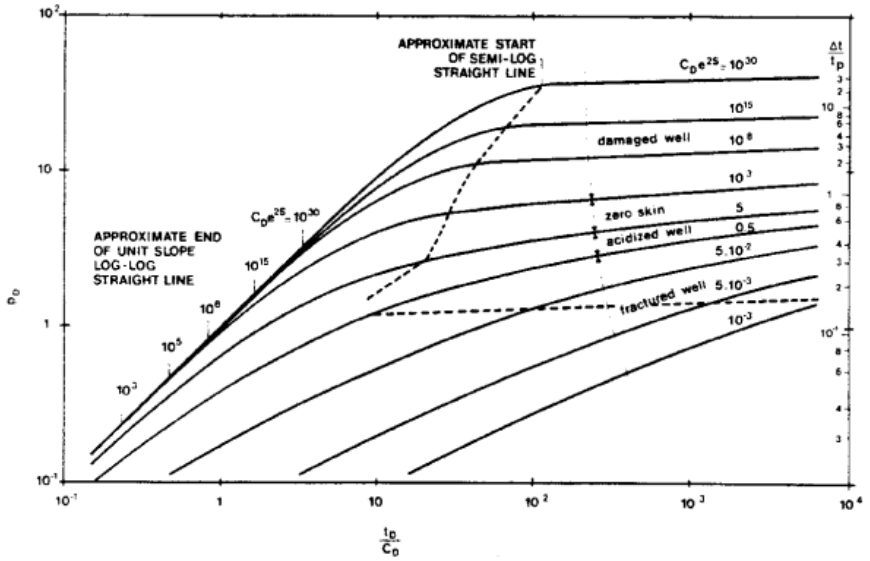

Figure 33: *Type-curves accounting for wellbore storage and skin effects.*

Note. Adapted from *New type-curve for wellbore storage and skin effects* (p. 13) by Alain C. Gringarten, Dominique Bourdet, Pierre A. Landel and Vladimir J. Kniazeff, 1979, Society of Petroleum Engineers of Aime (https://doi.org/10.2118/8205-MS)

Agarwal (1980) introduced an equivalent time Δt_e for the analysis of buildup tests with the aim to consider the effects of short producing times t_p in comparison with the shut-in time

Δt. Additionally, the real gas pseudotime function is used to consider the changing gas properties with pressure. If these changes are small, then the real time t is used.

$$\Delta t_{ae} = \frac{t_{ap} \times \Delta t_a}{t_{ap} + \Delta t_a} \quad (174)$$

Therefore, the shut-in time Δt should be replaced by Δt_{ae}. The type-curve matching of a buildup test plotted as $log\left[m(p_i) - m\left(p_{wf}\right)\right]$ vs $log(\Delta t_{ae})$, will occur at the following match points:

$$log\left(\frac{m(p_D)}{m(p_i) - m\left(p_{wf}\right)}\right)_{MP} = log\left(\frac{kh}{1422 q_{sc} T}\right) \quad (175)$$

And

$$log\left(\frac{t_D/C_D}{\Delta t_{ae}}\right)_{MP} = log\left(\frac{0.0002951k}{\mu C}\right) \quad (176)$$

To calculate the dimensionless wellbore storage coefficient C_D, the value of C can be estimated by selecting a point from the unit slope. The skin factor is obtained by applying Equation 177 (Lee, Rollins, & Spivey, 2003).

$$s = \frac{1}{2} ln\left(\frac{C_D e^{2s}}{C_D}\right) \quad (177)$$

3.12 The Pressure Derivative Method

Bourdet et al. (1983) introduced a new type-curve known as the pressure derivative type-curve for a well with wellbore storage and skin in a homogeneous reservoir. The pressure derivative is given by:

$$\Delta p' = \frac{dp}{d \ln \Delta t} = \Delta t \frac{dp}{dt} \quad (178)$$

Where Δt is the elapsed time at which the test period begins, either a producing time for a drawdown test or a shut-in time for a buildup test. A plot of log $\Delta p'$ vs log Δt is considered for pressure analysis. In terms of dimensionless variables, the pressure derivative is expressed as:

$$p'_D = \frac{d(p_D)}{d\ln(t_D/C_D)} \quad (179)$$

During the period of pure wellbore storage, Δp and $\Delta p'$ are equal, as shown on Figure 34. Therefore, for a real gas flow:

$$\Delta m(p') = \Delta m(p) = \frac{q_{sc}B_g}{24C}\Delta t \quad (180)$$

And in terms of dimensionless variables:

$$m(p'_D) = \frac{d[m(p_D)]}{d\ln(t_D/C_D)} = 1 \quad (181)$$

This suggests that a plot of $m(p'_D)(t_D/C_D)$ vs (t_D/C_D) on log-log coordinates will form a straight line of unit slope as shown on Figure 34. For the infinite-acting radial flow (IARF) period, the pressure change is expressed by the constant terminal rate solution in transient conditions given by Equation 182.

$$\Delta m(p) = m(p_i) - m(p_{wf}) = \frac{1422q_{sc}T}{kh} \times \frac{1}{2}\left[\ln 2.25\left(\frac{0.000264k\Delta t}{\emptyset\mu c_t {r_w}^2}\right) + 2s'\right] \quad (182)$$

From the equation of the radial flow at the end of wellbore storage effects, the pressure derivative is constant as represented by Figure 35.

$$m(p_D) = \frac{kh[m(p_i) - m(p_{wf})]}{1422q_{sc}T} = \frac{1}{2}\left[\ln\left(\frac{t_D}{C_D}\right) + \ln(2.25) + \ln(C_D e^{2s})\right] \quad (183)$$

$$\Delta m(p') = \frac{711q_{sc}T}{kh} \quad (184)$$

In dimensionless terms, the pressure derivative is expressed as:

$$m(p'_D) = \frac{d[m(p_D)]}{d\ln(t_D/C_D)} = 0.5 \quad (185)$$

A plot of $m(p'_D)\,(t_D/C_D)$ vs (t_D/C_D) on log-log coordinates will form a horizontal line at which the IARF will show a stabilization at 0.5 (see Figure 35).

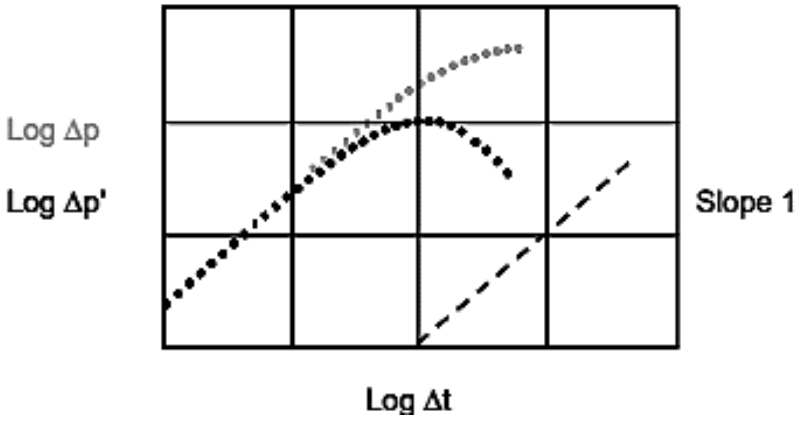

Figure 34: *Pressure and pressure derivative during wellbore storage period.*

Note. Adapted from *Pressure and derivative responses on log-log scales. Wellbore storage* (p. 37) by Dominique Bourdet, 2002, Elsevier.

As seen on Figure 36, the pressure derivative method is useful for the identification of flow regimes. At early time, the period dominated by wellbore storage effect is represented by the straight line with slope equal to 1; at late time, the IARF reaches stabilization represented by the horizontal line; and the hump that represents the transition from the wellbore-storage dominated flow and the radial flow, is used to estimate the skin factor from $C_D e^{2s}$. Thus, a match of the type-curves will occur at these two flow regimes (Bourdet, 2002).

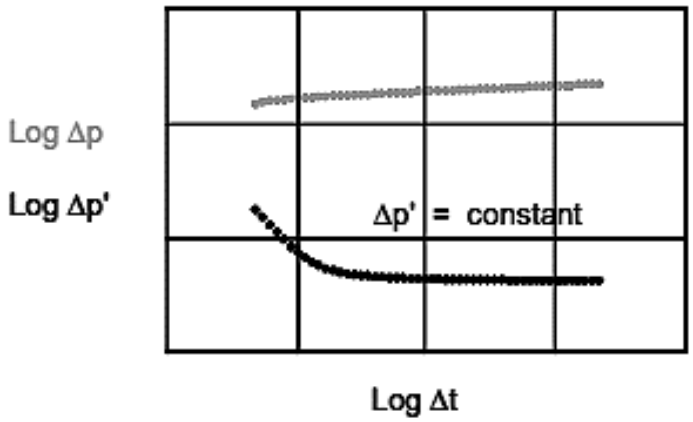

Figure 35: *Pressure and pressure derivative during the IARF period.*

Note. Adapted from *Pressure and derivative responses on log-log scales. Radial flow* (p. 37) by Dominique Bourdet, 2002, Elsevier.

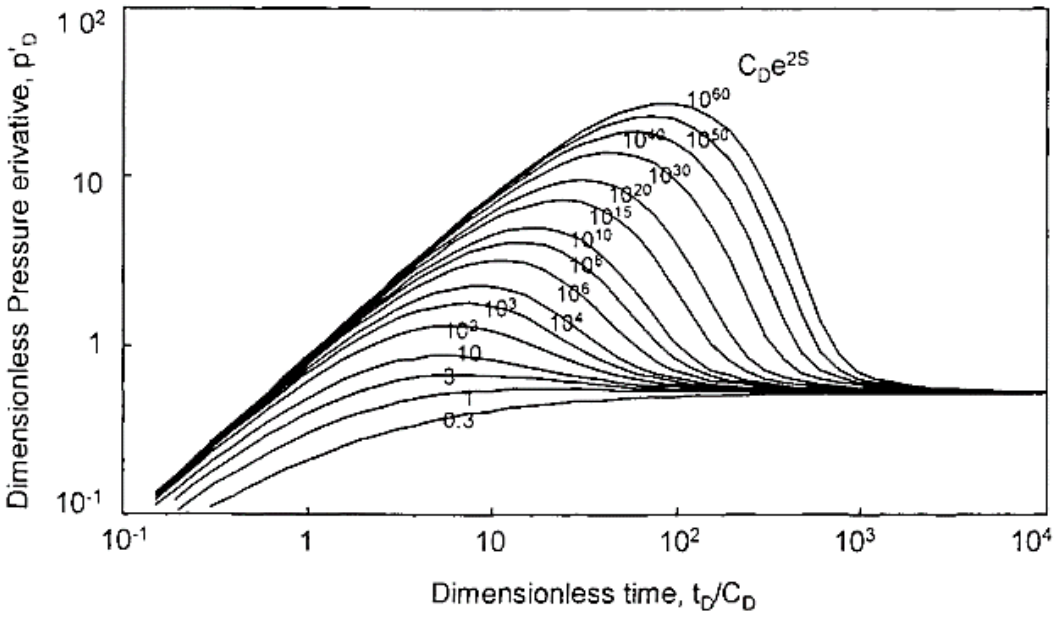

Figure 36: *Pressure Derivative Type-Curve.*

Note. Adapted from "*Well with wellbore storage and skin, homogeneous reservoir" Derivative of type-curve* (p. 38) by Dominique Bourdet, 2002, Elsevier.

For the analysis of drawdown tests using the pressure derivative type-curve, the pressure change Δp and the pressure derivative $\Delta p'$ are plotted as a function of the elapsed time Δt_a on log-log coordinates. This elapsed time corresponds to the drawdown period, i.e., the producing time t_a (Chaudhry, 2003).

$$\Delta m(p) = m(p_i) - m(p_{wf}) = \frac{1422 q_{sc} T}{kh} \times \frac{1}{2}\left[\ln 2.25\left(\frac{0.000264 k t_a}{\emptyset \mu c_t {r_w}^2}\right) + 2s'\right] \qquad (186)$$

The pressure derivative is with respect to the logarithm of the producing time, then:

$$\Delta m(p') = \frac{d\Delta m(p)}{d \ln t_a} = \frac{711 q_{sc} T}{kh} \qquad (187)$$

Where $m(p_{wf})$ is the bottomhole flowing pseudopressure as a function of the producing time t_a (Lee, Rollins, & Spivey, 2003).

For the analysis of buildup tests, the pressure change Δp and the pressure derivative $\Delta p'$ are plotted as a function of the elapsed time Δt_a on log-log coordinates. This elapsed time corresponds to the buildup period, i.e., the shut-in time Δt_a (Chaudhry, 2003).

$$\Delta m(p) = m(p_{ws}) - m(p_{wf}) = \frac{1422 q_{sc} T}{kh} \times \frac{1}{2}\left[\ln 2.25\left(\frac{0.000264 k \Delta t_a}{\emptyset \mu c_t {r_w}^2}\right) + 2s'\right] \quad (188)$$

Where $m(p_{ws})$ is the shut-in pseudopressure and $m(p_{wf})$ is the bottomhole flowing pseudopressure at $\Delta t_a = 0$ (Lee, Rollins, & Spivey, 2003).

For a single constant production rate followed by a shut-in time, the pressure derivative is with respect to the Horner time, then:

$$\Delta m(p') = \frac{d\Delta m(p)}{d \ln\left(\frac{t_{ap} + \Delta t_a}{\Delta t_a}\right)} = \frac{711 q_{sc} T}{kh} \quad (189)$$

As regards the short producing times t_{ap}, the pressure derivative is with respect to the equivalent time or Agarwal time:

$$\Delta m(p') = \frac{d\Delta m(p)}{d \ln\left(\frac{t_{ap} \times \Delta t_a}{t_{ap} + \Delta t_a}\right)} = \frac{711 q_{sc} T}{kh} \quad (190)$$

In case of several flowing periods, the method of superposition in time for multiple rates is applied. The pressure derivative will be then with respect to the superposition time (Houzé, Viturat, & Fjaere, 1988-2020).

Deviations from the transient flow regime on log-log plots or semilog plots, may be due to heterogeneities or presence of boundaries that cause the pressure response to behave in a different manner. Figure 37 represents how the response of a drawdown test may be at different times. At early-times, deviations from the assumption of the radial flow are due to the effects of wellbore storage. After these effects, heterogeneities may be present such as skin or damage due to partial penetration of the well and fractures. Then, after identifying these effects, the

pressure response of radial flow or IARF is present. Finally, at late time the effects of boundaries may be felt (Ahmed & McKinney, 2005).

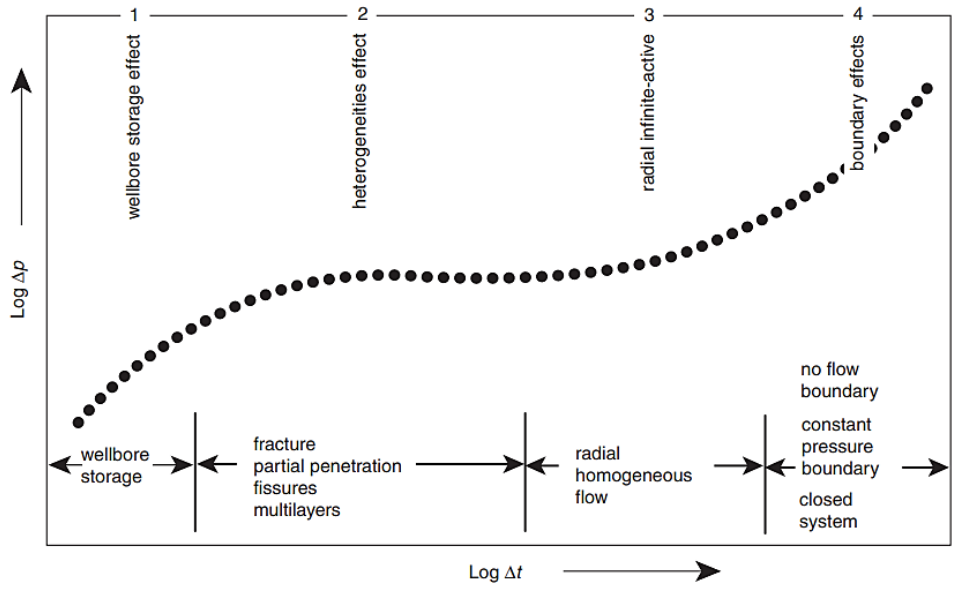

Figure 37: *Log-log plot of Δp vs Δt.*

Note. Adapted from *Log-log plot of a typical drawdown* (p. 1/79) by Tarek Ahmed, 2005, Elsevier.

Chapter 4. Interpretation Models

The interpretation model consists of three components of the flow regime that dominates at different times during the flow period (Gringarten, 2012). These flow regimes are summarized in Table 4.

Table 4: *Flow regime components of the interpretation model.*

Note. Adapted from Components of the well test interpretation model by Alain C. Gringarten (2012), The Way Ahead (https://jpt.spe.org/twa/well-test-analysis-practice).

Near-Wellbore Effects	**Reservoir Behavior**	**Boundary Effects**
Wellbore Storage	Homogeneous	No-Flow Boundaries
Skin	Heterogeneous	Constant-Pressure Boundary
Fractures	Double Porosity	Leaky Boundaries
Partial Penetration	Double Permeability	
Horizontal Well	Composite	
Early Times	**Middle Times**	**Late Times**

4.1 Analysis of Early-Time Data

During the early-time period, the inner boundary conditions dominate the flow behavior and regime. These effects are felt near the wellbore and valuable information about this region can be obtained (Gringarten, 2012).

4.1.1 Wellbore Storage and Skin

On a pressure and pressure derivative plot, wellbore storage and skin are identified at early time. The wellbore storage effect is characterized by exhibiting a straight line of unit slope on the log-log plot (see Figure 38). On the same plot, a hump can be observed during the transition from wellbore storage effects and IARF, the maximum of this hump indicates the

presence of skin. If no maximum is observed, the wellbore is not damaged (Ahmed & McKinney, 2005).

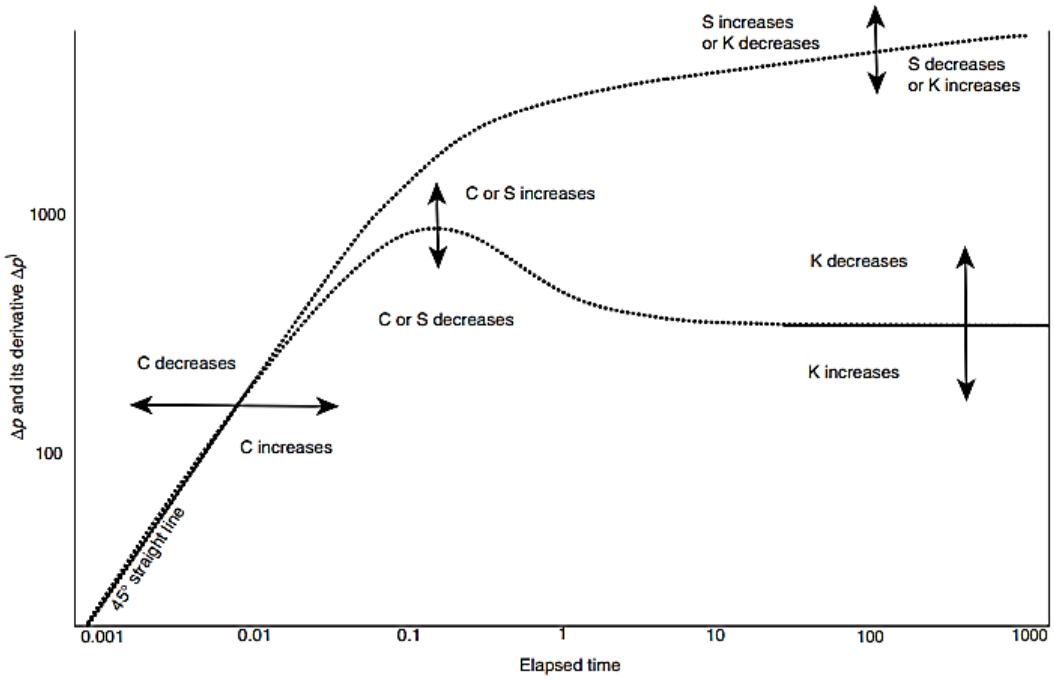

Figure 38: *Identification of wellbore storage and skin.*

Note. Adapted from Δ*p and its derivative vs. elapsed time* (p. 1/80) by Tarek Ahmed, 2005, Elsevier.

4.1.2 Partial Penetration

Reservoir fluids may flow through a well thickness that is smaller than the net reservoir thickness. A well can be partially penetrated to avoid the production of gas from the top in an oil reservoir, or to avoid the production of water from the bottom if an aquifer is present. On the other hand, an unexpected partial penetration may occur if impermeable zones exist in the reservoir. Nonetheless, reservoir's vertical permeability can be estimated by testing a well with partial penetration. Figure 39 shows the evolution of the flowing condition through a partially penetrated well. Immediately after a well is open to production, radial flow occurs around the perforated interval, this may not be observed if wellbore storage effects are present. During this

flow regime the skin and the flow capacity kh_p of the perforated interval can be estimated. As the perturbation develops vertically, spherical flow occurs, and an important parameter that can be evaluated is reservoir anisotropy (k_v/k_h). When the perturbation reaches the net reservoir thickness, the flow regime is radial, and the parameters such as reservoir flow capacity kh and overall skin s_{ov} can be determined.

$$s_{ov} = s_p + s\left(\frac{h}{h_p}\right) \quad (191)$$

Where s_{ov} is the overall skin that results of the well skin and the effects of partial perforation; s_p is the partial penetration skin; s is the well skin; h is the net reservoir thickness, ft; and h_p is the thickness of the perforated interval, ft (Bourdarot, 1998).

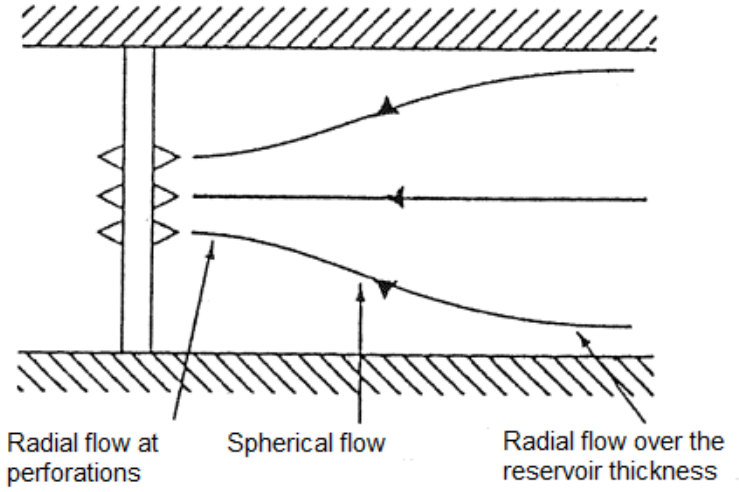

Figure 39: *Effects of partial penetration.*

Note. Adapted from *Fig. 15.4* (p. 195) by Gilles Bourdarot, 1998, Éditions Technip and Institut Français du Pétrole.

4.2 Analysis of Middle-Time Data

After the effects of the inner boundary conditions, the infinite-acting radial flow (IARF) period occurs. During this period the basic reservoir parameters are identified, and the system behavior can result in a homogeneous or heterogeneous reservoir. A homogeneous reservoir is

characterized by having a porous medium described by average rock properties. On the other hand, a heterogeneous reservoir may be composed of fissures and fractures or may be a multilayered system (Ahmed & McKinney, 2005).

4.2.1 Double-Porosity Reservoirs

Naturally fractured reservoirs are heterogeneous reservoirs that consist of fissures or natural fractures that depending on their size can form interconnected channels or a porous block. The porous block has a high storage capacity of the reservoir fluids but low permeability, whereas the fissures have a high permeability but low storage capacity. These reservoirs are characterized by having matrix permeabilities around 0.1 md and porosities not more than 10%. Fracture porosity is the responsible of the high productivity of some wells since the total volume of the reservoir fluids are contained in the fractures. An average value of fracture porosity is 0.5% (Da Prat, 1990). The behavior of these reservoirs is known as double-porosity since the matrix $\emptyset_m$ and the fissure system $\emptyset_f$ correspond to a primary and secondary porosity respectively. The main contribution of fluids to the well is given by the fissure system due to its high permeability, and this is recharged with fluids by the matrix system that acts as the source (Ahmed & McKinney, 2005).

Two important parameters that describe the behavior of double-porosity reservoirs are the storativity ratio ω given by Equation 192, which describes the flow capacity between the fractures and the reservoir system, and the interporosity flow λ given by Equation 193, which describes how easily the fluids can be exchanged between the matrix and the fractures.

$$\omega = \frac{(\emptyset V c_t)_f}{(\emptyset V c_t)_f + (\emptyset V c_t)_m} \quad (192)$$

$$\lambda = \alpha {r_w}^2 \frac{k_m}{k_f} \quad (193)$$

Where α represents the influence of the geometry of the matrix blocks on the fluid exchanges between matrix and fractures.

$$\alpha = \frac{4n(n+2)}{{r^2}_{matrix}} \quad (194)$$

As represented on Figure 40, there are three flow periods that characterize fractured reservoirs. The first period is described by the fissure system, here the fluid starts to flow from the fractures and the reservoir behaves as if it is homogeneous, characterized by a first stabilization flow. The second period represents the transition in which the fluid contribution is made by the matrix. The third period corresponds to the fluid flow from the matrix and the fractures, the reservoir behaves as if it is homogeneous again and a second stabilization flow is observed (Bourdarot, 1998).

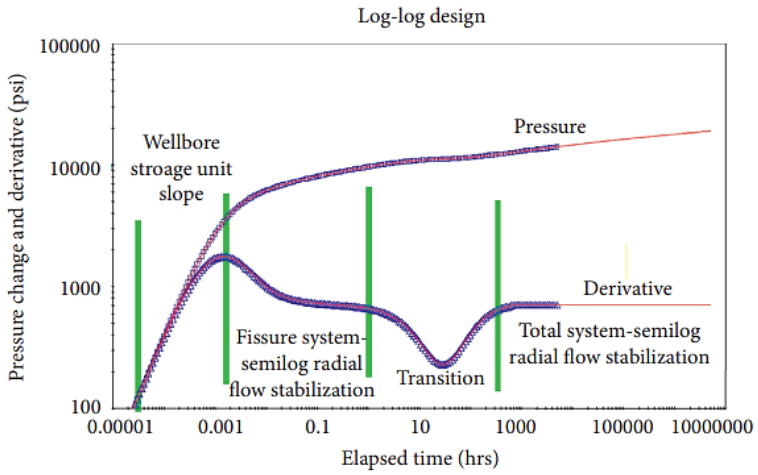

Figure 40: *Identification model of a naturally fractured reservoir.*

Note. Adapted from *Pressure and derivative log-log curve in dual-porosity reservoirs* (p. 3) by Mohsen Safari-Beidokhti, et al., 2021, Mathematical Problems in Engineering.

4.2.2 Double-Permeability Reservoirs

Multilayered reservoirs are characterized by having superposed layers with different characteristics. A system with two layers may communicate between them in a vertical

crossflow, while the fluids flow horizontally in each of the layer into the well. The total flow capacity $(\mathrm{kh})_{\mathrm{Total}}$ of the system is equal to the sum of the flow capacity $(\mathrm{kh})_{\mathrm{i}}$ of each of the layers. Additionally, the total reservoir capacity $(\emptyset \mathrm{c_T h})_{\mathrm{Total}}$ is equal to the sum of the capacity $(\emptyset \mathrm{c_T h})_{\mathrm{i}}$ of each of the layers. The parameters that help to describe the behavior of multilayered reservoirs are the storativity ratio ω given by Equation 195, which describes the contrast of the capacity between the two layers; the mobility ratio κ given by Equation 196, which describes the contrast of the transmissivity between the two layers; and the interlayer crossflow coefficient λ given by Equation 197, which describes how easily the fluids can be exchanged between the two layers (Bourdarot, 1998).

$$\omega = \frac{(\emptyset c_T h)_1}{(\emptyset c_T h)_{Total}} \quad (195)$$

$$\kappa = \frac{(kh)_1}{(kh)_{Total}} \quad (196)$$

$$\lambda = \frac{{r_w}^2}{(kh)_{Total}} \frac{2}{2\frac{h'}{k_z{}'} + \frac{h_1}{k_{z1}} + \frac{h_2}{k_{z2}}} \quad (197)$$

Where the subscript 1 refers to the layer 1, assuming it has the higher permeability zones, while the subscript 2 refers to the layer 2 with the lower permeability zones. If $\kappa = 1$, the behavior corresponds to a double-porosity response. If $\lambda = 0$, there is no crossflow between the layers. Therefore, the interlayer crossflow coefficient is a function of the vertical permeability k_z. The thickness h' and the vertical permeability $k_z{}'$ correspond to the wall or screen between the layer 1 and the layer 2 (Bourdet, 2002). Figure 41 represents the model response of a double-permeability reservoir.

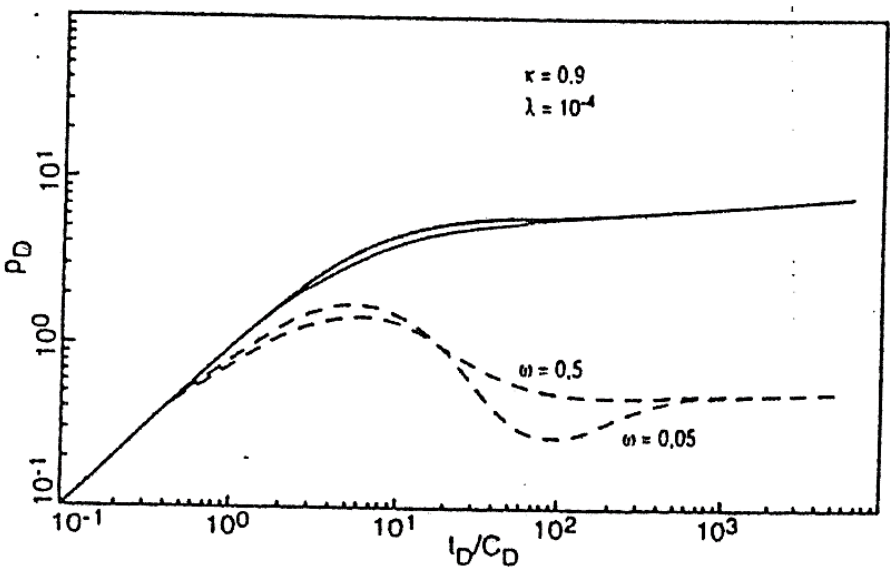

Figure 41: *Identification model of a double-permeability reservoir.*

Note. Adapted from *Fig. 14.2* (p. 185) by Gilles Bourdarot, 1998, Éditions Technip and Institut Français du Pétrole.

4.2.3 Composite Reservoirs

A composite reservoir is a heterogeneous reservoir that is divided into two regions. The dividing boundary may be radial or linear, and each region is characterized by having different mobilities and storativities (Schlumberger, 2006). The parameters that describe the behavior of a composite reservoir model are mobility M, expressed by Equation 198, and storativity F, expressed by Equation 199. Figure 42 represents the behavior of a radial composite reservoir (Bourdet, 2002).

$$M = \frac{(k/\mu)_1}{(k/\mu)_2} \qquad (198)$$

$$F = \frac{(\emptyset c_t)_1}{(\emptyset c_t)_2} \qquad (199)$$

Where the subscripts 1 and 2 corresponds to the region 1 and region 2 respectively.

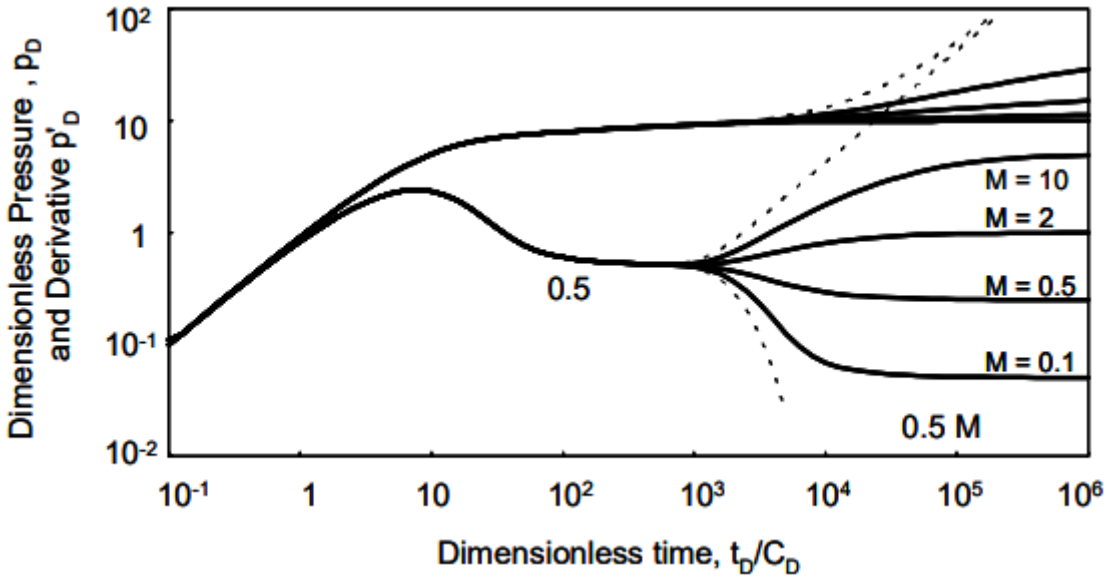

Figure 42: *Identification model of a radial composite reservoir.*

Note. Adapted from *Log-log plot of radial composite responses, changing mobility and constant storativity.* p_D *versus* $t_D/C_D 1$. (p. 184) by Dominique Bourdet, 2002, Elsevier.

4.3 Analysis of Late-Time Data

As the transient pressure reaches farther into the reservoir, the influence of the outer boundaries affects the transient response at the well (Lee, Rollins, & Spivey, 2003). As Table 4 indicates, the outer boundaries may be described as no-flow boundaries, characterized by impermeable barriers; constant-pressure boundaries, characterized by an aquifer adjacent to the reservoir; and leaky boundaries (Satter & Iqbal, 2016).

4.3.1 No-Flow Boundaries

This condition refers to faults or impermeable barriers that influence the pressure transient response. As there is not an external pressure at the boundary that supports the reservoir pressure, a large pressure change is observed at the well (Satter & Iqbal, 2016).

According to G. Bourdarot (1998), no-flow boundaries can be characterized by sealing faults, intersecting faults, channels, and closed reservoirs. A linear sealing fault, as well as unconformities or change in facies, indicate a no-flow boundary condition. The pressure drop

at the well can be obtained by implementing the method of images. At late time, the pressure drops faster once the fault is reached. The time at which the fault is reached can be used to determine the radius of investigation. Figure 43 shows the characteristics of the pressure-derivative curve when a sealing fault is present, the level of the derivative is doubled from an initial stabilization at 0.5 to a second one at 1.

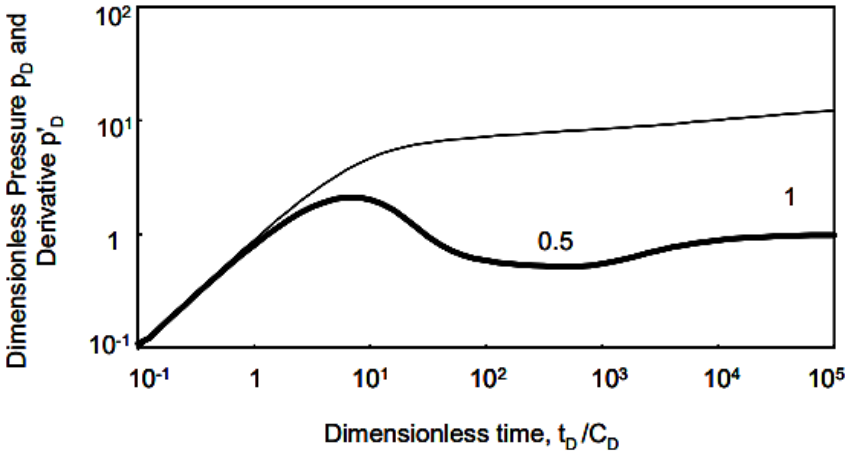

Figure 43: *Identification model of a homogeneous reservoir with a sealing fault.*

Note. Adapted from *Pressure and derivative responses fora well with wellbore storage near one sealing fault in a homogeneous reservoir. Log-log scales,* p_D *versus* t_D/C_D. by (p. 206) Dominique Bourdet, 2002, Elsevier.

Intersecting faults can be characterized by two intersecting boundaries with an angle between them defined as the ratio of the slopes of the straight lines on a semilog plot as expressed by Equation 200.

$$\theta = 2\pi \frac{m_1}{m_2} \qquad (200)$$

Figure 44 indicates the presence of two intersecting faults represented by a pressure-derivative curve with an initial stabilization at 0.5 going to a second stabilization at π/θ. The smaller the angle, the longer the time to reach the second stabilization. If the angle is much smaller, the faults are considered parallel; thus, a channel behavior.

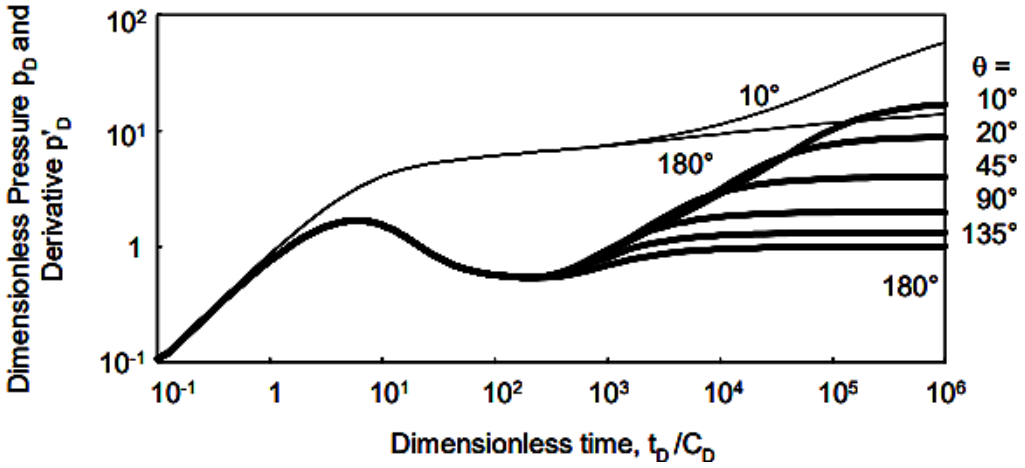

Figure 44: *Identification model of a homogeneous reservoir with two intersecting faults.*

Note. Adapted from *Pressure and derivative responses for a well with wellbore storage near two intersecting sealing faults in a homogeneous reservoir. Log-log scales,* p_D *versus* t_D/C_D. (p. 221) by Dominique Bourdet, 2002, Elsevier.

Channels can be classified as infinite channels or bounded channels. An infinite channel has two parallel no-flow linear boundaries, which can be two sealing faults or a channel deposit. A bounded channel refers to a third boundary that indicates the end of the channel, which can be identified by using the method of images. The representation of a channel behavior involves having a well located at a distance d from one of the boundaries, and the boundaries separated by a distance l. The characteristic behavior of a channel when the two faults are reached by the transient response is the presence of linear flow. Therefore, the pressure-derivative curve will show a straight line with a slope of $1/2$ at late time, as indicated on Figure 45. In case of a bounded reservoir, the slope of the straight line is doubled.

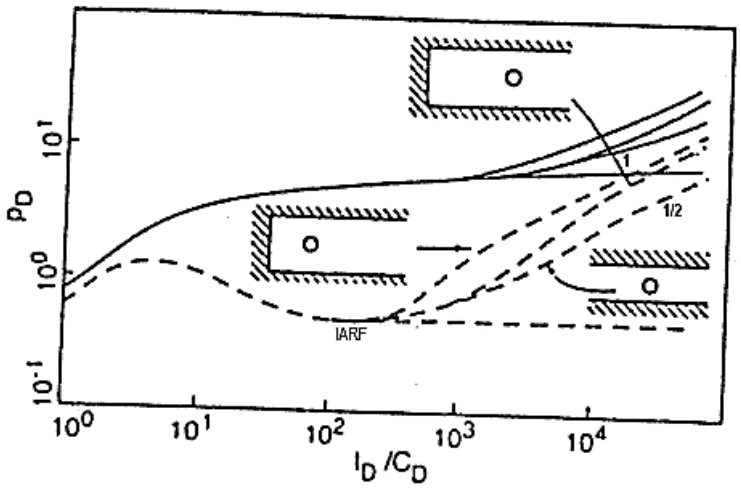

Figure 45: *Reservoir model identification with an infinite and a bounded channel.*

Note. Adapted from *Fig. 8.7* (p. 112) by Gilles Bourdarot, 1998, Éditions Technip and Institut Français du Pétrole.

A closed reservoir is limited by no-flow boundaries such as sealing faults. Two cases can be observed when all the boundaries are reached. During drawdown, pseudosteady-state flow will appear after the transient flow in the IARF, the shape of the transition between these two flow regimes depends on the position of the well in the limited area and on the shape of the drainage area. During the pseudosteady-state flow, the drainage area can be calculated, and as the pressure decreases linearly with time, the pressure derivative curve is characterized by having a straight line with a slope of 1, as represented on Figure 46. On the other hand, during buildup, the pressure will reach stabilization becoming uniform and constant in the drainage area, and the average pressure can be obtained. Figure 46 shows the pressure-derivative curve going downwards to zero when the average pressure is being reached.

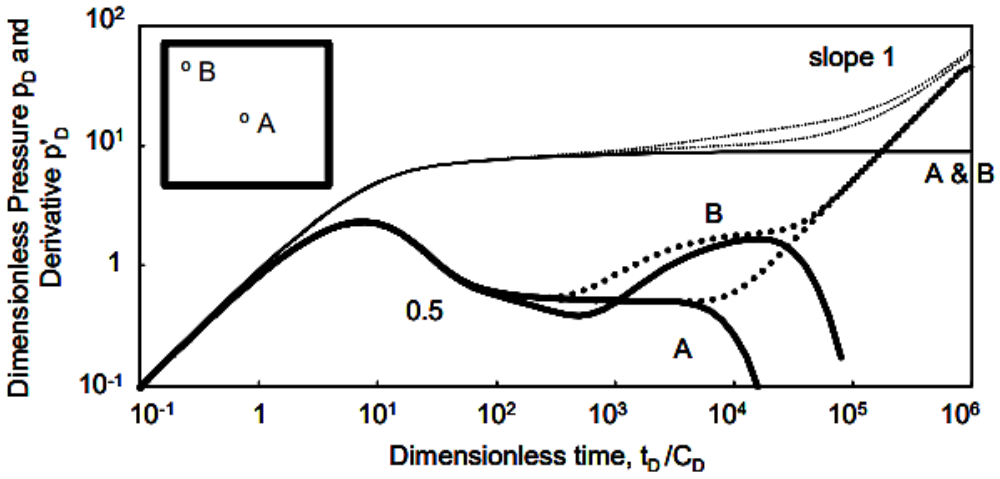

Figure 46: *Identification model of a closed reservoir during buildup and drawdown.*

Note. Adapted from *Pressure and derivative responses for a well with wellbore storage in a closed square homogeneous reservoir. Log-log scales,* p_D *versus* t_D/C_D. (p. 226) by Dominique Bourdet, 2002, Elsevier.

4.3.2 Constant-Pressure Boundaries

A constant-pressure boundary refers to a reservoir with an adjacent active aquifer. The pressure change diminishes due to the strong water influx that supports the reservoir pressure (Satter & Iqbal, 2016). The pressure will stabilize to the value at which the constant-pressure boundary condition is reached. Figure 47 shows the pressure-derivative curve going downwards with a negative unit slope straight line. The distance to the boundary can be calculated once the boundary condition is observed on the log-log plot (Schlumberger, 2006).

4.3.3 Leaky Boundaries

Leaky boundaries refer to communicating faults. The semi-permeable boundary acts as a fluid flow restriction. The fault transmissibility of the partially communicating boundary can be determined by Equation 201.

$$\alpha = \frac{k_f/w_f}{k/L} \qquad (201)$$

Where k_f and w_f refers to the permeability and thickness of the fault respectively, and L refers to the distance from the well to the fault. Figure 48 represents the response of a well near a leaky boundary with different fault transmissibility values (Bourdet, 2002).

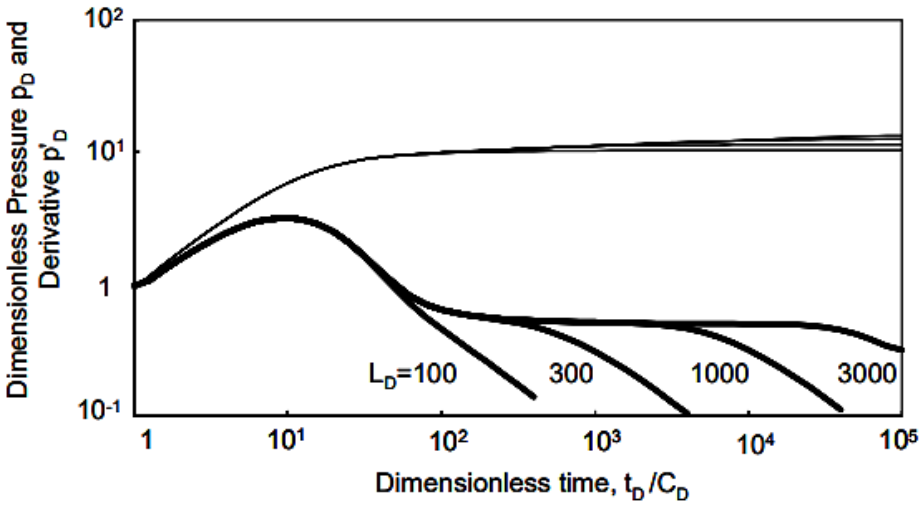

Figure 47: *Identification model of a reservoir with a constant-pressure boundary.*

Note. Adapted from *Pressure and derivative responses for a well with wellbore storage and skin near one constant pressure boundary in a homogeneous reservoir. Log-log scales,* p_D *versus* t_D/C_D (p. 240) by Dominique Bourdet, 2002, Elsevier.

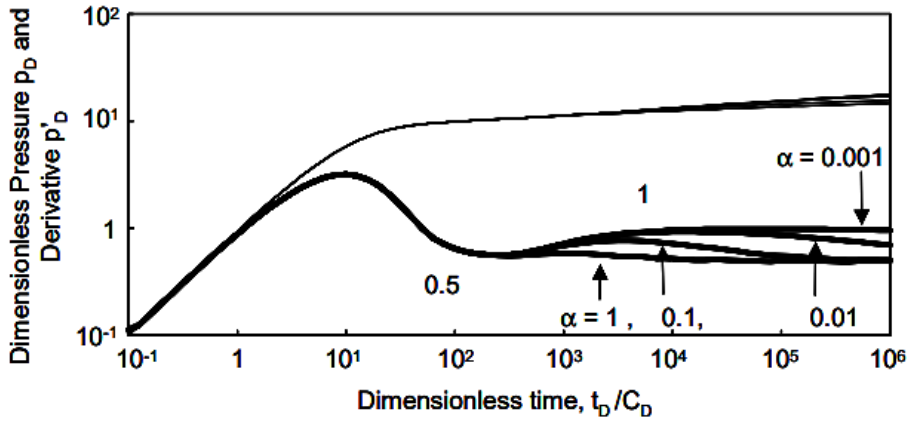

Figure 48: *Identification reservoir model for a well near a leaky boundary.*

Note. Adapted from *Pressure and derivative responses for a well with wellbore storage and skin near a semi-permeable linear boundary. Log-log scales,* p_D *versus* t_D/C_D (p. 245) by Dominique Bourdet, 2002, Elsevier.

Chapter 5. Conclusions

The current work aimed to present the different methods used to analyze the pressure transient response from gas well tests based on the properties and characteristics of gas flow in the reservoir. The study highlights the importance of considering the pressure-dependent properties of gas to perform a reliable analysis and interpretation of pressure transient testing methods. The work also described the reservoir identification models and their parameters of the flow regimes that are encountered during the flowing time in a pressure transient test. The mathematical expressions are rearranged from the mostly used oil equations to gas well applications to illustrate the main characteristics that influence the bottomhole flowing pressure measure. Additionally, further work is needed to address the gas flow in tight reservoirs and to include a numerical well testing approach that can provide new insights into reservoirs with high degree of heterogeneities and skin effects around gas wells.

References

Agarwal, R. G. (1979). "Real gas pseudo-time". A new function for pressure buildup analysis of MHF gas wells. *SPE Annual Technical Conference and Exhibition.* doi:https://doi.org/10.2118/8279-MS

Agarwal, R. G. (1980). A new method to account for producing time effects when drawdown type-curves are used to analyze pressure buildup and other test data. *SPE Annual Technical Conference and Exhibition.* doi:https://doi.org/10.2118/9289-MS

Agarwal, R. G., Al-Hussainy, R., & Ramey, H. J. (1970). An investigation of wellbore storage and skin effect in unsteady liquid flow: I. Analytical treatment. *Society of Petroleum Engineers Journal, 10*(03), 279–290. doi:https://doi.org/10.2118/2466-PA

Ahmed, T. (2007). *Equations of state and and PVT analysis: applications for improved reservoir modeling.* Gulf Publishing Company.

Ahmed, T. (2019). *Reservoir engineering handbook* (V ed.). Elsevier. doi:https://doi.org/10.1016/C2016-0-04718-6

Ahmed, T., & McKinney, P. D. (2005). *Advanced reservoir engineering.* Elsevier.

Ahmed, T., & Meehan, D. N. (2012). *Advanced reservoir management and engineering* (II ed.). Elsevier.

Al-Hussainy, R., Ramey Jr., H. J., & Crawford, P. B. (1966). The flow of real gases through porous media. *Journal of Petroleum Technology, 18*(05), 624-636. doi:https://doi.org/10.2118/1243-A-PA

Alyafei, N. (2021). *Fundamentals of reservoir rock properties* (II ed.). Self-published.

Archer, J. S., & Wall, C. G. (1986). *Petroleum engineering. Principles and practice.* Graham and Trotman Ltd.

Belhaj, H. (2016). Management of injected nitrogen into a gas condensate reservoir. *Ingeniería e Investigación, 36*(1), 52-61. doi:http://dx.doi.org/10.15446/ing.investig.v36n1.50319

Bourdarot, G. (1998). *Well testing: interpretation methods.* (B. Brown Balvet, Trans.) Éditions Technip and Institut Français du Pétrole.

Bourdet, D. (2002). *Well test analysis: The use of advanced interpretation models.* Elsevier.

Bourdet, D., Ayoub, J. A., & Plrard, Y. M. (1989). Use of pressure derivative in well-test interpretation. *SPE Formation Evaluation, 4*(02), 293-302. doi:https://doi.org/10.2118/12777-PA

Bourdet, D., Whittle, T. M., Douglas, A. A., & Pirard, Y. M. (1983). *A new set of type curves simplifies well test analysis.* Gulf Publishing Co.

Chaudhry, A. U. (2003). *Gas well testing handbook.* Elsevier.

Cord-Ruwisch, R. K. (1987). Sulfate-reducing bacteria and their activities in oil production. *Journal of Petroleum Technology, 39*(01), 97-106. doi:https://doi.org/10.2118/13554-PA

Da Prat, G. (1990). *Well test analysis for fractured reservoir evaluation* (Vol. 27). Elsevier.

Dake, L. P. (1978). *Fundamentals of reservoir engineering.* Elsevier.

Dake, L. P. (2001). *The practice of reservoir engineering (revised edition)* (I ed., Vol. 36 of Developments in Petroleum Science). Elsevier.

El-Banbi, A., Alzahabi, A., & El-Maraghi, A. (2018). Dry gases. In *PVT property correlations* (pp. 29-63). Elsevier. doi:https://doi.org/10.1016/B978-0-12-812572-4.00003-5

ERCB. (1975). *Theory and practice of the testing of gas wells* (III ed.). Energy Resources Conservation Board (ERCB).

Ertekin, T., & Ayala, L. F. (2019). *Reservoir engineering models: analytical and numerical approaches* (I ed.). New York: McGraw-Hill Education.

Escobar, F. H. (2017). Gas well testing. In H. A. Al-Megren, & R. H. Altamimi, *Advances in natural gas emerging technologies.* InTechOpen. doi:10.5772/61380

Escobar, F. H. (2018). *Novel, integrated and revolutionary well test interpretation and analysis.* IntechOpen. doi:DOI: 10.5772/intechopen.81078

Fanchi, J. R. (2002). *Shared earth modeling.* Elsevier.

Fanchi, J. R. (2006). *Principles of applied reservoir simulation* (III ed.). Elsevier.

Gringarten, A. C. (2012, June 14). *Society of Petroleum Engineers.* Retrieved from THE WAY AHEAD "Well test analysis in practice": https://jpt.spe.org/twa/well-test-analysis-practice

Gringarten, A. C., Bourdet, D., Landel, P. A., & Kniazeff, V. J. (1979). A comparison between different skin and wellbore storage type-curves for early-time transient analysis. *SPE Annual Technical Conference and Exhibition.* doi:https://doi.org/10.2118/8205-MS

Guo, B., & Ghalambor, A. (2005). *Natural gas engineering handbook* (II ed.). Gulf Publishing Company.

Guo, B., Sun, K., & Ghalambor, A. (2008). *Well productivity handbook: vertical, fractured, horizontal, multilateral, and intelligent wells* (I ed.). Houston, Texas: Gulf Publishing Company.

Hagoort, J. (1988). *Fundamentals of gas reservoir engineering* (Vol. 23). Elsevier.

Hasan, A. R., & Kabir, C. S. (1983). Pressure buildup analysis: A simplified approach. *Journal Petroleum Technology, 35*(01), 178–188. doi:https://doi.org/10.2118/10542-PA

Horne, R. N. (1990). *Modern well test analysis: a computer-aided approach.* Petroway, Inc.

Horner, D. R. (1951). Pressure build-up in wells. *Proceedings Third World Petroleum Congress*, 25-43.

Houpeurt, A. (1959). On the flow of gases in porous media. *Revue de L'Institut Francais du Petrole, 14*(11), 1468-1684.

Houzé, O., Viturat, D., & Fjaere, O. S. (1988-2020). *Dynamic data analysis* (Vol. v5.30.01). KAPPA.

Ikoku, C. U. (1984). *Natural gas reservoir engineering.* Krieger Publishing Company.

Jackson, R. R., Banerjee, R., & Thambynayagam, R. (2003). An integrated approach to interval pressure transient test analysis using analytical and numerical methods. *SPE Middle East Oil and Gas Show and Conference* (pp. SPE-81515-MS). SPE. doi:https://doi.org/10.2118/81515-MS

Klinkenberg, L. J. (1941). The permeability of porous media to liquids and gases. *Drilling and Production Practice, American Petroleum Institute*, 200-213.

Lee, J. (1982). *Well testing.* Society of Petroleum Engineers.

Lee, J., & Wattenbarger, R. A. (1996). *Gas reservoir engineering.* Society of Petroleum Engineers.

Lee, J., Rollins, J. B., & Spivey, J. P. (2003). *Pressure transient testing* (Vol. 9). Society of Petroleum Engineers.

Lyons, W. C. (1996). *Standard handbook of petroleum and natural gas engineering* (Vol. II). Butterworth-Heinemann.

Matthews, C. S., & Russell, D. G. (1967). *Pressure buildup and flow tests in wells* (Vol. 1). SPE Monograph Series.

McCain Jr, W. D. (1990). *The properties of petroleum fluids* (II ed.). Tulsa, Oklahoma: PennWell Publishing Company.

Mohamed Mansour, E., El Aily, M., & Eldin Mohamed Desouky, S. (2019). *Gases reservoirs fluid phase behavior.* IntechOpen. doi:DOI: 10.5772/intechopen.85610

Paris de Ferrer, M. (2009). *Fundamentos de ingeniería de yacimientos.* Self-published.

Pedersen, K. S., Christensen, P. L., & Shaikh, J. A. (2014). *Phase behavior of petroleum reservoir fluids* (2nd ed.). CRC Press. doi:https://doi.org/10.1201/b17887

Rawlins, E. L., & Schellhardt, M. A. (1935). *Back-pressure data on natural-gas wells and their application to production practices.* U.S. Bureau of Mines.

Reynolds, A. C., Bratvold, R. B., & Ding, W. (1987). Semilog analysis of gas well drawdown and buildup data. *SPE Formation Evaluation, 2*(04), 657–670. doi:https://doi.org/10.2118/13664-PA

Safari-Beidokhti, M., Hashemi, A., Abdollahi, R., Hematpur, H., & Esfandyari, H. (2021). Numerical well test analysis of condensate dropout effects in dual-permeability model of naturally fractured gas condensate reservoirs: Case studies in the south of Iran. *Mathematical Problems in Engineering, 2021*, 10. doi:https://doi.org/10.1155/2021/9916914

Satter, A., & Iqbal, G. M. (2016). *Reservoir Engineering. The fundamentals, simulation, and management of conventional and unconventional recoveries.* Elsevier.

Schlumberger. (2006). *Fundamentals of formation testing.*

Schlumberger. (2013). Fundamentos de las pruebas de pozos. (R. v. Flatern, Ed.) *Oilfield Review, 24*(4), 58-60.

Smith, J. T. (1990). *Pressure transient testing: design and analysis* (Vol. I). Self-published.

Sylvester, O., Bibobra, I., & Ogbon, O. N. (2015). Well test and PTA for reservoir characterization of key properties. *American Journal of Engineering and Applied Sciences, 8*(4), 638-647. doi:https://doi.org/10.3844/ajeassp.2015.638.647

Terry, R. E., & Rogers, J. B. (2015). *Applied petroleum reservoir engineering* (III ed.). Pearson Education.

Tewari, R. D., Dandekar, A. Y., & Moreno Ortiz, J. (2019). *Petroleum fluid phase behavior: characterization, processes, and applications* (1st ed.). CRC Press. doi:https://doi.org/10.1201/9781315228808

Tiab, D. (2000). *Gas reservoir engineering.* School of Petroleum and Geological Engineering, The University of Oklahoma, Oklahoma, USA.

Wang, X., & Economides, M. (2009). *Advanced natural gas engineering.* Gulf Publishing Company.

Warren, G. M. (1993). Numerical Solutions for Pressure Transient Analysis. *SPE Gas Technology Symposium* (pp. SPE-26177-MS). Calgary, Alberta, Canada: SPE. doi:https://doi.org/10.2118/26177-MS